Magnetic field effect in organic light emitting diodes

Vom Fachbereich Material- und Geowissenschaften zur Erlangung des akademischen Grades Doktor-Ingenieur (Dr.-Ing.) genehmigte Dissertation von

Dipl.-Phys. Ulrich Niedermeier, geboren am 12.01.1980 in Landshut

Januar 2010 — Darmstadt — D 17

TECHNISCHE UNIVERSITÄT DARMSTADT

ELECTRONIC e-mat MATERIALS

Magnetic field effect in organic light emitting diodes

Vom Fachbereich Material- und Geowissenschaften zur Erlangung des akademischen Grades Doktor-Ingenieur (Dr.-Ing.) genehmigte Dissertation von
Dipl.-Phys. Ulrich Niedermeier, geboren am 12.01.1980 in Landshut

1. Gutachten: Prof. Dr. Heinz von Seggern
2. Gutachten: Prof. Dr. Lambert Alff

Tag der Einreichung: 08. Oktober 2009
Tag der Prüfung: 14. Dezember 2009

Darmstadt — D 17

Zusammenfassung

Die Entdeckung einer magnetfeldabhängigen Widerstandsänderung von organischen Leuchtdioden (OLEDs) im Jahr 2003 hat großes wissenschaftliches und industrielles Forschungsinteresse hervorgerufen. Dieser “organische Magnetowiderstandseffekt” (OMR-Effekt) ist jedoch trotz bisheriger Fortschritte auf dem Gebiet der organischen Spin-Elektronik ein noch nicht vollständig geklärtes Phänomen. Die vorliegende Arbeit befasst sich daher mit der experimentellen Charakterisierung sowie mit einer möglichen theoretischen Beschreibung des OMR-Effektes und leistet damit einen Beitrag zum besseren Verständnis der mikroskopischen Vorgänge, die dem Effekt zugrunde liegen. In Messungen an OLED-Bauteilen auf Polymerbasis werden die Abhängigkeiten des OMR-Effektes von wesentlichen Parametern wie Magnetfeld, Betriebsspannung, Betriebsstrom und Temperatur untersucht. Anhand dieser Ergebnisse werden in einer kritischen Analyse bisher veröffentlichte Modellvorstellungen zum möglichen Mechanismus des OMR-Effektes bewertet. Nach dieser Analyse wird ein Konzept zur Erklärung des OMR-Effektes favorisiert, das eine magnetfeldabhängige Änderung des Spinzustandes von Elektron-Loch-Paaren als Ursache für Veränderungen im Stromfluss und der Lichtemission von OLEDs vorschlägt. Im Rahmen dieses Konzeptes können sowohl alle eigenen Ergebnisse als auch Messungen aus der Literatur erklärt werden. Eine wesentliche Erkenntnis der vorliegenden Arbeit ist darüber hinaus die Tatsache, dass sich die Größe des OMR-Effektes in den untersuchten OLED-Bauteilen durch geeignete elektrische und optische Konditionierungsprozesse erhöhen lässt. Insbesondere die elektrische Art der Konditionierung führt zu einem deutlichen Anstieg der OMR-Werte, wirkt sich zugleich aber negativ auf den Ladungstransport und die optischen Kenndaten der OLEDs aus. Diese Ergebnisse können durch Messungen zur Ladungsträgerextraktion erklärt werden, die nach einer elektrischen Konditionierung eine Zunahme der Anzahl elektronischer Fallenzustände in der Emissionsschicht der untersuchten OLEDs nahelegen. Messungen des OMR-Effektes unter Beleuchtung mit Infrarot-Strahlung sowie theoretische Überlegungen im Rahmen des Elektron-Loch-Paar-Konzeptes unterstreichen zudem den positiven Einfluss von Fallenzuständen auf den OMR-Effekt. Zum Schluss wird gezeigt, dass die Erhöhung der OMR-Werte nach elektrischer oder optischer Konditionierung durch geeignete Erwärmung der Bauteile größtenteils wieder rückgängig gemacht werden kann. Dies lässt darauf schließen, dass die Konditionierungsprozesse keine permanente Degradation der OLEDs verursachen. Als mögliche Erklärung für die Auswirkungen einer Konditionierung werden daher Änderungen der Morphologie innerhalb der Emissionsschicht der Bauteile vorgeschlagen.

Contents

1 Introduction **1**

2 Theoretical and experimental basics **5**

2.1 Basic properties of organic semiconductors 5

2.2 Fundamentals of organic light emitting diodes 6

2.2.1 Device structure 6

2.2.2 Working principle 7

2.3 Magnetic field effects in organic materials 12

2.3.1 Magnetic field effect on delayed fluorescence 13

2.3.2 Magnetic field effect on photocurrent 14

2.3.3 Magnetic field effect on device resistance and electroluminescence . . 14

2.4 Spin dynamics in organic materials 17

2.5 Most discussed models to explain the organic magnetoresistance 22

2.5.1 Bipolaron model 23

2.5.2 Exciton model 25

2.5.3 Exciton polaron interaction model 26

2.6 Experimental and measurement techniques 28

2.6.1 OLED processing 28

2.6.2 Measurement setups 30

3 Characterization of the OMR effect in OLEDs **37**

3.1 Magnetic field effect on current and luminescence 37

3.2 Influence of device architecture on OMR 42

3.2.1 Influence of emitter 42

3.2.2 Influence of cathode 45

3.2.3 Influence of hole injection layer 47

3.3 Temperature dependence of OMR 48

3.4 Influence of illumination on OMR 49

3.5 Evaluation of most discussed OMR models from literature 50

3.5.1 Evaluation of the bipolaron model 51

3.5.2 Evaluation of the exciton model 52

3.5.3 Evaluation of the exciton polaron interaction model 53

3.6 Discussion of the electron-hole pair model 54
3.6.1 General description of the electron-hole pair model 55
3.6.2 Mathematical description of the electron-hole pair model 57
3.7 Experimental verification of the electron-hole pair model 61

4 Enhancement of the OMR effect by device conditioning 67
4.1 Basic features of electrical conditioning 67
4.2 Variation of conditioning parameters 69
4.3 Influence of electrical conditioning on electro-optical device parameters . . . 70
4.4 Electrical conditioning of Alq_3 devices 72
4.5 Optical conditioning 74
4.6 Discussion of conditioning mechanism 76

5 Material modification during device conditioning 79
5.1 OMR under infrared illumination 79
5.2 Thermally stimulated current measurements 82
5.3 Photo-CELIV measurements 84

6 Reduction of the OMR effect by thermal activation 87
6.1 OMR reduction by relaxation at room temperature 87
6.2 OMR reduction by thermal annealing 88
6.2.1 Annealing after electrical conditioning 88
6.2.2 Annealing after optical conditioning 90
6.3 Electrical conditioning at low temperatures 91
6.4 Discussion of results 92

7 Conclusion and outlook 95
7.1 Conclusion 95
7.2 Outlook 97

A Calculations within the electron-hole pair model 99

List of abbreviations and symbols 103

List of figures 105

Bibliography 109

List of publications and conference contributions 115

1 Introduction

Organic semiconducting materials have attracted tremendous academic and industrial research interest over the past decades due to a potential implementation in novel applications. Thin films of organic semiconductors have successfully been used in devices such as organic light emitting diodes (OLEDs) [Tan87, Bur90, Fri99], organic field effect transistors (OFETs) [Tsu86, Sir99] and organic photovoltaic cells (OPVs) [Yu94, Bra01]. Compared to their inorganic counterparts devices based on organic semiconductors offer many advantageous features, including a possible fabrication on large, thin and even flexible substrates in processes which can be quite easy and cost-efficient. Research on OLED devices has particularly been pushed forward driven by the goal to produce highly efficient and long-term stable light sources for displays and lighting applications. The high potential of OLED devices has already been demonstrated by several industrial companies which succeeded in releasing products involving the OLED technology to the market [Son07, Kod08, Osr08]. While most research activities in the field of OLEDs have been focused on an optimization of electro-optical device parameters, only little attention has been paid to magnetic field effects in those devices for a long time. However, the history of inorganic electronics has shown that device concepts that make use of both the electric charge and the spin state of charge carriers can open up ways to completely new fields of application. In 1988 it was found that the electrical resistance of inorganic structures comprising alternating layers of magnetic and non-magnetic materials can be changed by external magnetic fields [Bai88, Bin89]. The discovery of this giant magnetoresistance (GMR) effect was a milestone in the field of inorganic spin electronics and was awarded with the Nobel Prize in Physics 2007. Nowadays, GMR devices with typical resistance changes of up to several 10 % at magnetic fields on the order of 10 mT are used in a variety of applications ranging from hard disk read-heads to magnetic field sensors in automotive environments.

Research on magnetic field effects in OLED devices is still a young research area and started in 2003 when Kalinowski *et al.* discovered that the resistance and the light output of OLEDs can be changed by the application of external magnetic fields [Kal03a]. This novel phenomenon was referred to as “organic magnetoresistance” (OMR) effect and was particularly interesting since the investigated OLED devices did not contain any ferromagnetic materials. Soon after the discovery of OMR it was reported that the effect can be observed in a number of fluorescent organic materials at room temperature and can reach values of up to 10 % at moderate magnetic fields of 10 mT [Fra04, Mer05a, Mer05b]. These initial

observations suggested that the OMR effect might be an attractive working principle for new types of low-cost magnetic field sensors in the future.
Before the OMR effect can be brought into practical application it is essential to clarify the microscopic origin of the effect and to identify ways to control the size of the effect. These tasks are particularly challenging since no satisfying explanation for the OMR effect has been provided in literature so far. Recent publications mainly focus on three theoretical models that have been proposed as potential explanations for the OMR effect in the past [Pri06, Des07a, Bob07]. However, these models have been controversely discussed since each of the proposed mechanisms is only in line with a limited number of experimental results and at the same time contradicts several other results. Additional confusion has arisen due to the fact that different research groups investigating similar device structures reported significantly different values of the OMR effect [Pri06, Des07a, Blo07, Ngu08].

It is the scope of this thesis to analyze these issues and to improve the understanding of the mechanisms that are responsible for the OMR effect. In order to achieve this goal, a comprehensive experimental characterization of the OMR effect in polymer-based OLED devices will be presented and a conceptional model for the OMR effect will be discussed which is consistent with own results and data from literature. Finally, methods will be demonstrated which can be used to actively control the size of the OMR effect in a given device structure.
To provide a systematic presentation this thesis is organized in the following way:

- Chapter 2 contains an overview of relevant basics on organic semiconductors and introduces the device structure and the working principle of OLEDs. In this context the influence of a magnetic field on spin dynamics in OLED devices will be addressed. Previous experimental and theoretical studies of magnetic field effects in general and of the organic magnetoresistance effect in particular will be reviewed. The chapter closes with a description of the OLED fabrication process and a discussion of the measurement techniques that were used to characterize the devices in this thesis.
- Chapter 3 starts with an experimental characterization of basic features of the OMR effect. Results from OMR measurements in different device structures, at different temperatures and under illumination will be presented. Based on these results and on data from literature it will be demonstrated that the theoretical models which have been discussed most intensively in recent publications regarding the OMR effect are unsatisfactory. Therefore, a different approach to explain the OMR effect by considering a previously proposed electron-hole pair model will be discussed in detail.

- Chapter 4 is devoted to the phenomenon that the OMR effect can be enhanced by appropriate device treatments. Electrically stressing a device and exposing it to highly intense light in the near-ultraviolet range will be introduced as two ways of device conditioning to increase the OMR effect in a given structure. Consequences of conditioning for the electro-optical device performance will also be addressed. Finally, a material modification induced by the conditioning procedure will be suggested.
- Chapter 5 shows further experimental evidence of the proposed material modification from chapter 4. It will be demonstrated that the OMR effect in conditioned devices can be affected by illumination with infrared light. Using different charge carrier extraction techniques it will furthermore be shown that the conditioning procedure changes the distribution of electronic states inside the active material and affects the charge carrier transport properties.
- Chapter 6 provides experimental results showing that the enhancement of the OMR effect by device conditioning is non-permanent. Thermally activated relaxation processes will be demonstrated to cause a reduction of the magnetoconductance values once the conditioning procedure has been switched off. Based on these results a possible mechanism of the material modification during conditioning and the subsequent relaxation will be suggested.
- Finally, the thesis concludes with a summary of the obtained results and provides an outlook regarding issues that need further investigations in the future.

2 Theoretical and experimental basics

This chapter reviews fundamental properties of organic semiconductors and discusses the architecture as well as the working principle of OLEDs. A special focus will be on magnetic field dependent spin dynamics in OLED devices. The organic magnetoresistance effect will be introduced and previous experimental and theoretical work on magnetic field effects will be summarized. Finally, the fabrication process of OLED devices and the measurement methods that were used in the course of this thesis will be described.

2.1 Basic properties of organic semiconductors

Organic semiconductors are unsaturated carbon compounds with alternating sequences of single and double bonds between the carbon atoms. Each carbon atom has sp^2-hybridized orbitals and can establish strong σ-bonds with neighboring atoms, which results in a highly localized electron density in the plane of the molecule. In addition, the unhybridized p_z-orbitals of neighboring atoms can overlap and form π-bonds which give rise to a delocalized π-electron system above and below the plane of the molecule. Binding π-orbitals in this system are completely filled with electrons whereas antibinding π^*-orbitals are completely empty. The π-orbital with highest energy is called the highest occupied molecular orbital (HOMO), the π^*-orbital with lowest energy is called the lowest unoccupied molecular orbital (LUMO). HOMO and LUMO in organic materials are often seen as equivalents to the edges of valence band and conduction band in inorganic semiconductors and are separated by an energy gap in the range of several eV. The existence of a variety of organic materials with energy gaps in the visible spectral range makes this class of materials especially promising for future optoelectronic applications.

In contrast to the strong interaction between neighboring atoms in a single organic molecule the interaction between neighboring molecules in an organic material in the solid state is established by rather weak van-der-Waals forces. This intermolecular coupling only results in a very small energy splitting of the involved HOMOs and LUMOs so that the principal electronic structure is not changed when organic condensed matter is formed out of single molecules. As a consequence of the weak intermolecular interaction charge carriers in organic semiconductors are localized to molecules instead of being delocalized over the entire bulk material like in the case of inorganic semiconductors. The charge carrier transport from one molecule to another is usually described by thermally activated hopping processes between the localized states [Bäs93]. The charge carrier mo-

bilities achieved in this hopping transport ($\mu \approx 10^{-6}\,\mathrm{cm}^2/\mathrm{Vs}$ for PPV [Blo01]) are typically much smaller than mobilities that result from band transport in inorganic semiconductors ($\mu \approx 1\,\mathrm{cm}^2/\mathrm{Vs}$ for amorphous silicon [Jus00a]).

Organic semiconductors are usually divided into two classes depending on their molecular weight. One class is the group of small molecule materials, which have a molecular weight of less than 1000 g/mol. These materials are usually deposited using evaporation techniques in vacuum. It was demonstrated that the use of small molecule materials in OLED devices can lead to an excellent device performance in terms of efficiency and lifetime [Rei09]. However, due to the need of complex vacuum deposition systems a large-scale device production using small molecule materials is rather expensive. The second class of organic semiconductors are polymers, which are chain-like macromolecules with high molecular weight. Polymer materials are soluble and can be deposited easily and cost-efficiently using solution-based processes like spin-coating or inkjet printing.

2.2 Fundamentals of organic light emitting diodes

In 1987 Tang and van Slyke realized the first OLED device on the basis of small molecule materials [Tan87], three years later Burroughes *et al.* reported the fabrication of the first polymer-based OLED device [Bur90]. Ever since these discoveries, extensive research has been carried out in order to understand the physical processes that occur during the operation of OLED devices. In addition, large efforts have been made to improve the device architecture and to find new materials which lead to an enhancement of the device efficiency and long-term stability.

2.2.1 Device structure

In general, an OLED device consists of a layer structure with at least one organic layer sandwiched between two electrodes. At least one of the electrodes needs to be transparent in the visible range so that light outcoupling from the device is possible.
Figure 2.1 schematically shows the architecture of an OLED device. Typically, an OLED is fabricated on a glass substrate with a thickness of less than 1 mm. A commonly used anode material is the highly transparent indium tin oxide (ITO) which is sputtered on the glass substrate. The organic layers are either deposited from solution (in the case of polymers) or thermally evaporated (in the case of small molecule materials). In polymer devices the number of layers is typically limited due to the restriction that solvents with different polarity are necessary for the deposition of consecutive layers. In small molecule OLEDs several functional layers are usually deposited in addition to the emitter layer in order to

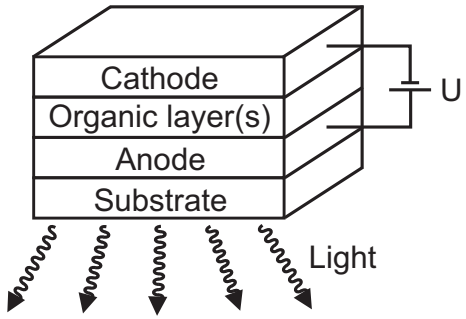

Figure 2.1:
Typical device structure of an OLED.

enhance the charge carrier injection and to control the charge carrier balance in the device. The cathode usually consists of a thin layer (< 5 nm) of a reactive metal (e.g., Ba, Ca, Mg) or a metal fluoride (e.g., LiF, CsF) followed by an Al layer. Apart from being involved in the charge carrier injection process the Al layer also protects the reactive material underneath from oxidation and improves the quality of the electrical contact to the device. Finally, the OLED can optionally be encapsulated with a glass lid to hermetically protect the organic layers and the reactive metals from a contamination by oxygen or water.

2.2.2 Working principle

The operation of an OLED device is governed by four fundamental processes:

- Injection of charge carriers from the electrodes into the organic layers
- Transport of charge carriers under the influence of an electric field
- Formation of electron-hole pairs and excitons
- Radiative decay of excitons and light emission

These processes are illustrated in figure 2.2 and will be discussed in detail in the following paragraphs.

Charge carrier injection and transport

In order to establish a current flow through an OLED device, it is necessary to inject charge carriers from the electrodes into the organic layers. During device operation in forward direction the anode is positively biased while the cathode is negatively biased. The difference in work functions between anode and cathode determines the built-in potential. To obtain a current flow electrons are injected from the cathode into the LUMO of the organic material while holes are injected from the anode into the HOMO of the organic material. The energetic barrier in the injection process is determined by the difference between the Fermi energy of the electrode material and either the ionization potential (in the case of hole injection) or the electron affinity (in the case of electron injection) of the organic

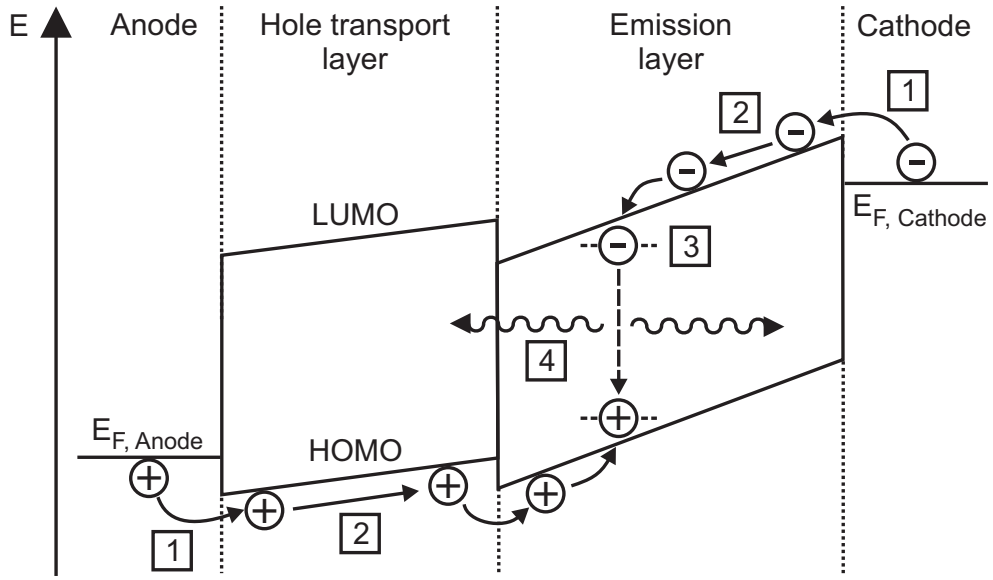

Figure 2.2: Schematic energy level diagram of a two-layer OLED device under the influence of an externally applied voltage. For simplicity the energetic states of HOMO and LUMO are treated as discrete levels. The relevant processes of charge carrier injection (1), charge carrier transport (2), exciton formation (3) and exciton decay (4) are assigned.

material. In devices with large barriers the injection efficiency is a limiting factor for the current flow since charge carriers need to overcome the injection barrier via tunneling, thermionic injection or thermionic field emission [Abk95, Ark98, Sco03]. In order to keep the injection barriers small, metals with a high work function are typically used as anode materials whereas reactive metals with a low work function or metal fluoride interlayers are typically used as cathode materials. When the injection barriers are small enough so that the current flow is not limited by the properties of the contacts and is only determined by the bulk properties of the device, the contacts are called ohmic contacts.

After injection the electrons and holes are still uncorrelated and move in the direction of the counter electrode under the influence of an electric field which is caused by the externally applied voltage. The charge carriers form negatively and positively charged polarons which correspond to localized charges of ionized molecules or conjugated segments. An electron is represented by a radical anion, a hole corresponds to a radical cation. The charge transport occurs via oxidation and reduction processes of neighboring molecules. Due to the energetic and positional disorder in the material the energy levels of HOMO and LUMO are distributed. In fact, it was shown by Bässler *et al.* that the HOMO and LUMO levels can be approximated by a density of states (DOS) with a Gaussian shape [Bäs93]. The choice of this particular shape for the DOS is supported by the observation that absorption spectra of organic materials usually have Gaussian profiles [Roc82].

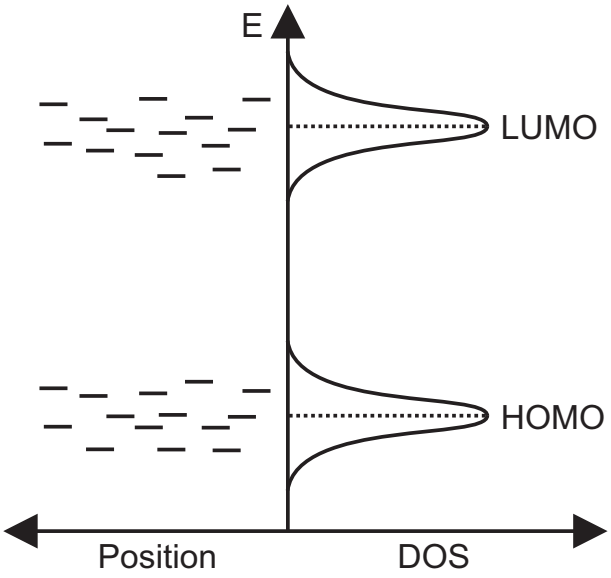

Figure 2.3:
Representation of the energy distribution of the localized states in an organic semiconductor. The density of states for the HOMO and the LUMO level is approximated by a Gaussian distribution.

Figure 2.3 schematically illustrates the electronic structure of an organic semiconductor. It was furthermore shown that charge carrier transport between localized states in disordered materials occurs via hopping processes [Bäs93]. The charge carrier mobility in these systems depends on temperature, electric field, charge carrier concentration and on the energetic and structural disorder in the organic material [Bäs93, Pas05]. It should be emphasized in this context that up to now no reports exist in literature which directly show a dependence of the charge carrier mobility on magnetic fields in charge carrier transport measurements.

Charge transport can be slowed down by trap states which are energetically located in the energy gap of the organic semiconductor [Sch04]. Charge carriers in trap states can not participate in the charge transport until they are released from their traps either by thermal activation or by energy transfer, e.g., from an excited state. Due to the fact that hopping processes in organic materials occur between strongly localized molecular sites the low-energy tail states of the DOS can be seen as intrinsic trap states for the charge carrier transport. In addition, trap states can originate from defects or impurities in the material or they can be created on purpose by doping a host material with an appropriate guest material. A convenient way of analyzing the distribution of trap states in an organic semiconductor is the measurement technique of thermally stimulated currents [Mal02] which will be introduced in section 2.6.2.

Charge carrier recombination and light emission

When charge carriers of opposite charge meet in the organic material they can form neutral electron-hole pairs (e-h pairs) which are the precursor states for excitons. A necessary condition for the formation of an e-h pair is that the distance between electron and hole

becomes smaller than the Coulomb capture radius which indicates the distance where the Coulomb energy exceeds the kinetic energy of the charge carriers [Pop82]. Even though the charge carriers in an e-h pair are coulombically bound, they initially have a large inter-charge separation distance and can be located either on different molecules or on different segments of the same molecule.
For the discussion of the organic magnetoresistance effect the spin states of e-h pairs are of central importance. Figure 2.4 depicts a schematic representation of the four different spin configurations that an e-h pair can have and shows the wavefunctions of the corresponding states [Ste89]. As it will be shown in section 2.4 these pure spin states are no eigenfunctions of the Hamiltonian which describes the e-h pair system in a stage where electron and hole are still well separated from each other. Consequently, the spin states undergo a coherent evolution in time in a process called “spin evolution” [Ste89].

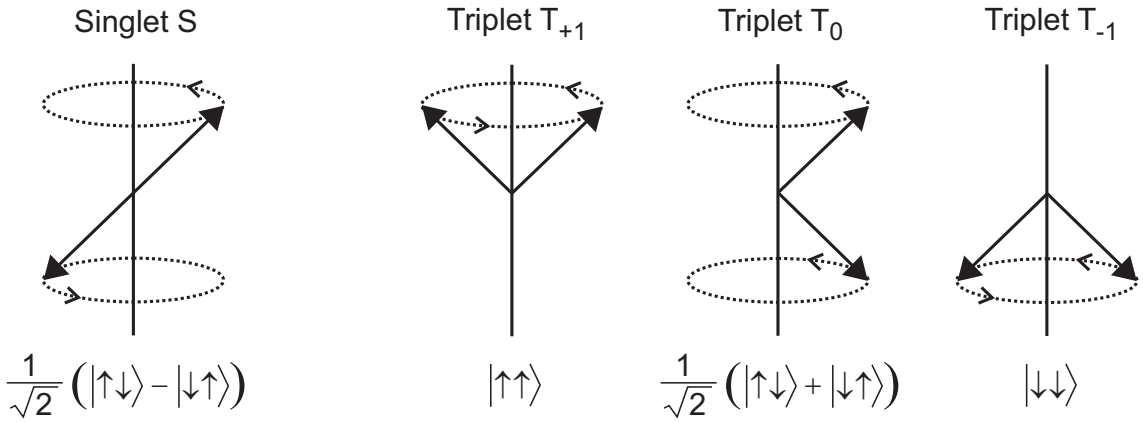

Figure 2.4: Schematic illustration of the possible spin states of an e-h pair. The corresponding wavefunctions of the different spin states are indicated.

According to this simplified vector diagram the spins of the participating electron and hole precess around a common quantization axis and point either upwards (indicating a spin-up state) or downwards (indicating a spin-down state). If the total spin of an e-h pair is 0 the e-h pair is in the singlet (S) state. If the total spin is 1 and is oriented either parallel (T_{+1}), perpendicular (T_0) or antiparallel (T_{-1}) to the quantization axis the e-h pair is in a triplet (T) state. When charge carriers with random spin configuration form e-h pairs it follows from spin statistics that 25 % of the formed e-h pairs are in the singlet state and 75 % of the e-h pairs are in a triplet state [Rot96]. However, it has been suggested in literature that the singlet e-h pair formation ratio may differ from 25 % in organic compounds with an extended conjugated system [Wil01, Woh01].

As the separation distance between electron and hole within an e-h pair becomes small enough for their wavefunctions to significantly overlap, the e-h pair evolves into an exci-

ton. Usually, excitons in organic materials are Frenkel excitons which are rather localized and have a binding energy of several 100 meV [Ker94, Roh99]. The spins of electron and hole in an exciton interact with each other via a spin-spin interaction with a Hamiltonian of the form [Fra92a]

$$H_{\text{Spin-Spin}} = -\hbar J(r)(1/2 - 2\mathbf{S}_\text{e}\mathbf{S}_\text{h}), \tag{2.1}$$

where $J(r) \sim \exp(-r)$ is a separation distance dependent exchange parameter and where $\mathbf{S}_\text{e}$ and $\mathbf{S}_\text{h}$ are the spins of electron and hole, respectively. Due to the small intercharge distance in excitons the spin-spin interaction is quite significant and leads to a splitting of several 100 meV between the energy levels of singlet and triplet excitons [Köh02].
The electroluminescence signal emitted from OLED devices is generated by the radiative decay of excitons. In this context it should be emphasized that the term "decay" refers to the annihilation process of excitons whereas the term "recombination" refers to the capture of electron and hole in the course of the exciton formation process [Fri99]. This is to be distinguished from the commonly used nomenclature in inorganic semiconductor physics, where "recombination" denotes the annihilation process of excitonic states.

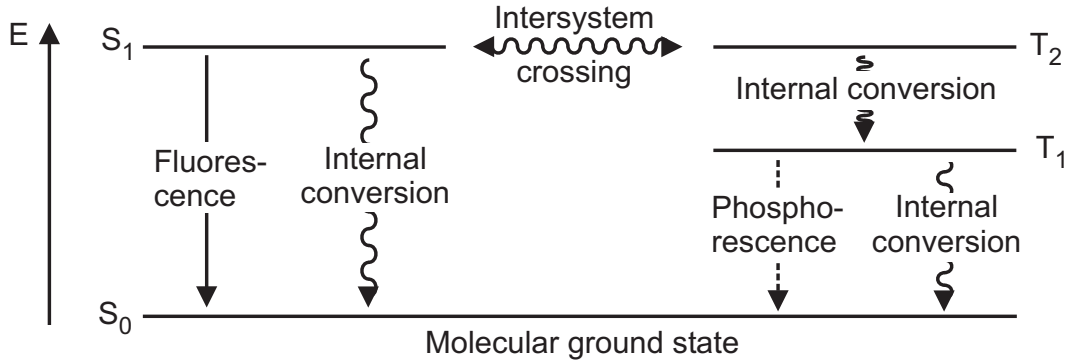

Figure 2.5: Simplified illustration of energy levels of excitonic states and transitions between them.

Figure 2.5 schematically illustrates possible transitions between excited states and the molecular ground state of an organic material. The decay of singlet excitons ($S_1 \rightarrow S_0$) can either be radiative in a process called fluorescence or it can occur nonradiatively via internal conversion processes. In the case of a radiative decay the energy of the emitted photons is smaller than the energetic difference between the LUMO and the HOMO level of the molecule. A radiative decay of triplet excitons is forbidden in fluorescent materials due to spin selection rules, which results in a theoretical limit of 25 % for the internal quantum efficiency of OLED devices based on this class of materials. To return to the molecular ground state, triplet excitons in fluorescent materials nonradiatively decay via internal conversion processes or they are quenched at an interface between the organic

material and a metal electrode. It should be noted that both e-h pairs and excitons can also dissociate back into free charge carriers under the influence of the applied electric field.
In order to also obtain light output from triplet excitons and to enhance the quantum efficiency of OLED devices, phosphorescent materials can be introduced into the device stack [Bal99]. These materials incorporate heavy metal atoms like Ir or Pt which give rise to a strong spin-orbit coupling. This spin-orbit coupling allows an intersystem crossing (ISC) and induces a mixing of singlet and triplet states, therefore providing a radiative decay channel for triplet excitons through a process called phosphorescence.
Before excitons decay they can diffuse through the organic material and transfer the excitation from a molecule to neighboring molecules by passing on the excitation energy. In a Förster transfer process the excitation is passed on via dipole-dipole interactions [För48], in a Dexter transfer process a simultaneous exchange of electrons takes place [Dex53].
A review of these transfer mechanisms is given in references [Hun03, Bra08].

2.3 Magnetic field effects in organic materials

In the past, different types of magnetic field effects have been observed in organic materials. The following sections are intended to give an overview of important experimental findings that were obtained in previous works. Early studies demonstrated that magnetic fields can influence the triplet-triplet annihilation process in organic materials and can change the intensity of the resulting delayed fluorescence signal. Following these initial investigations it was discovered that magnetic fields also have an effect on the photoconductivity of organic films. Finally, a broad interest in magnetic phenomena in organics started to arise when the magnetic field effect on device current and electroluminescent properties of OLED devices was discovered. Comprehensive reviews on experimental investigations of magnetic field effects in organic materials and in non-magnetic devices comprising organic materials can be found in references [Sok74, Zel88, Hu09].
It should be mentioned that the magnetoresistance of organic spin-valve devices (consisting of an organic layer sandwiched between two ferromagnetic electrodes) has also become a topic of great interest in recent years [Xio04, Nab07, Ded09]. In studies devoted to this topic the observed phenomena have been interpreted on the basis of the giant magnetoresistance effect [Bai88, Bin89] and the tunneling magnetoresistance effect [Jul75], both of which are known from inorganic semiconductor physics. However, since the investigations in this thesis were performed on non-magnetic devices the discussions in the following sections will be restricted to systems without ferromagnetic compounds.

2.3.1 Magnetic field effect on delayed fluorescence

In initial studies of magnetic field effects in organics the importance of triplet excitons for magnetic phenomena was investigated in organic crystals by analyzing the delayed fluorescence (DF) that originated from triplet-triplet annihilation events. When two triplet excitons collide they can form an intermediate state (T...T) and react to a singlet exciton in the excited state S_1 and a singlet exciton in the ground state S_0 according to the following reaction scheme:

$$T + T \longleftrightarrow (T...T) \longleftrightarrow S_1 + S_0.$$

Subsequently, the excited singlet exciton radiatively decays and emits the delayed fluorescence signal. The intensity I_{DF} of the delayed fluorescence is proportional to the square of the concentration of triplet excitons [Pop82]:

$$I_{DF} \sim \gamma n_T^2, \tag{2.2}$$

where γ is the triplet-triplet annihilation rate constant and n_T is the concentration of triplet excitons. In anthracene the DF intensity was found to increase under the influence of weak magnetic fields ($< 35\,mT$) and to decrease at larger magnetic fields [Joh70]. In a recent study Gärditz *et al.* also observed a non-monotonic dependence of the DF intensity on the magnetic field in OLED devices using Alq_3 as active material [Gär05]. These results were explained on the basis of a theory developed by Merrifield who proposed that an external magnetic field can affect the annihilation rate constant and can change the intensity of the DF signal [Mer68]. According to quantum mechanical considerations in this theory an increase of γ and an increase of the DF intensity can be expected with increasing magnetic field up to a maximum where the energy of the magnetic field reaches the energy of the zero-field splitting of the triplet excitons. At higher magnetic fields both γ and the DF intensity are expected to decrease.

Ern and Merrifield furthermore used DF measurements to investigate the magnetic field effect on the interaction between free charge carriers and triplet excitons in irradiated anthracene crystals [Ern68]. In this study the authors reported that the triplet exciton lifetime and the DF intensity are increased when an external magnetic field is applied. It was proposed that upon collision of a triplet exciton with a free charge carrier the exciton can either undergo a spin independent scattering process or it can be quenched. The important suggestion made in the study is that a magnetic field dependent reduction of the rate constant for the quenching process is responsible for the increased triplet lifetime that was experimentally observed.

2.3.2 Magnetic field effect on photocurrent

Starting in the year 1992 Frankevich *et al.* demonstrated that the photoconductivity of organic crystals and thin polymer films can be increased by up to 3 % under the application of a magnetic field on the order of 100 mT [Fra92a, Fra92b, Dya98]. At similar magnetic fields Kalinowski *et al.* obtained an increase in photocurrent by 6 % in a thin film of Alq_3 [Kal03b]. In both studies the results were explained in terms of a magnetic field dependent mixing of singlet and triplet e-h pairs which will be introduced in detail in section 2.4. It is known that after photoexcitation singlet excitons are generated in the system and form e-h pairs in an intermediate stage of the dissociation process due to the electric field. Frankevich *et al.* proposed that the magnetic field affects the relative amount of e-h pairs in the singlet and the triplet state. Moreover, singlet and triplet e-h pairs are considered to have different rates of geminate recombination. As a consequence, the change in the e-h pair population due to the magnetic field is assumed to alter the probability of dissociation and thus the probability of producing free charge carriers which contribute to the photocurrent.
Kalinowski *et al.* stated that a magnetic field reduces the probability of spin mixing in the e-h pair stage and leads to an increased concentration of singlet e-h pairs. This, in turn, is supposed to lead to a larger photocurrent response because it was previously suggested on the basis of theoretical considerations that singlet e-h pairs dissociate more easily than triplet e-h pairs and therefore dominate the photocurrent [Woh03, Hu07].
Finally, it should be mentioned that recent investigations demonstrated that even in modern organic solar cells based on a P3HT:PCBM blend moderate magnetic fields can increase the device efficiency by enhancing the photocurrent [Sha08].

2.3.3 Magnetic field effect on device resistance and electroluminescence

In 2003 Kalinowski *et al.* discovered that in Alq_3 based devices with non-magnetic electrode materials the application of a magnetic field of 500 mT increases the current flow through the devices as well as their light output by up to 3 % [Kal03a]. This novel phenomenon started to receive increasing attention one year later when Francis *et al.* demonstrated that a large change in resistance of more than 10 % can be achieved in polyfluorene (PFO) devices at room temperature and weak magnetic fields on the order of 10 mT (see figure 2.6) [Fra04]. This publication introduced the term “organic magnetoresistance effect” (OMR effect) and triggered several studies in the following years. Mermer *et al.* showed that the OMR effect is a general phenomenon and can be observed in both polymer and small molecule materials [Mer05a, Mer05b]. Furthermore, it was found that the

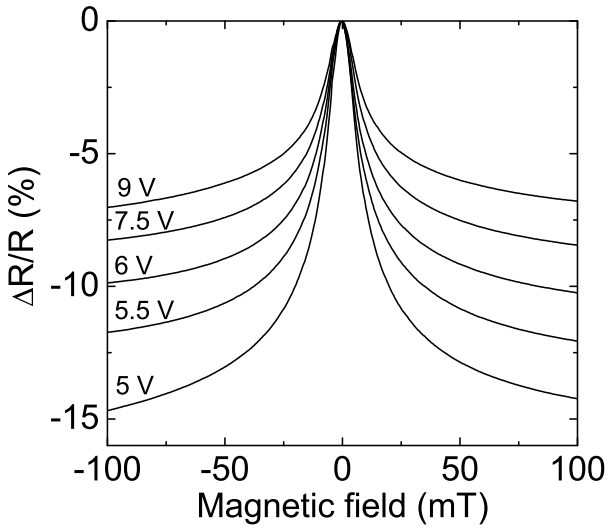

Figure 2.6:
Percentage change of resistance as a function of magnetic field for an ITO/PEDOT/PFO/Ca device at different voltages at room temperature according to reference [Fra04].

OMR effect is independent of the relative orientation of the magnetic field with respect to the device [Fra04, Mer05a].
Two universal line shapes were reported to be characteristic for the magnetic field dependence of the magnetoresistance $\Delta R/R = [R(B) - R(0)]/R(0)$. Depending on material and driving conditions the obtained curves for $\Delta R/R(B)$ could be fitted with either a Lorentzian line shape $\Delta R/R(B) \sim B^2/(B^2+B_0^2)$ or a non-Lorentzian line shape $\Delta R/R(B) \sim B^2/(|B|+B_0)^2$ [Mer05b]. The fitting parameter B_0 was shown to be on the order of 3–5 mT for most of the investigated materials [She06, Blo08b]. The relations were initially found as empirical fitting functions, later on it was suggested that they can be related to processes involving spin flips due to the hyperfine interaction [She06, Bob07].
The importance of spin dynamics for the OMR effect was also stressed in studies where a material with strong spin-orbit coupling strength was investigated. In these studies it was shown that at moderate magnetic fields below 100 mT no OMR effect [Wu07] or only very small magnetoconductance values [She07] can be observed in the phosphorescent material $Ir(ppy)_3$.
Regarding the sign of the magnetoresistance it is noticeable that mostly negative values have been reported for $\Delta R/R$ in literature [Fra04, She06, Des07b]. In addition, it was shown that sign changes of the magnetoresistance can occur depending on device architecture [Des07b, Hu07], operating voltage [Mer05b, Blo08b, Xin09] and temperature [Blo08a].

Apart from these commonly accepted features of the OMR effect a comparison of different literature reports in this context reveals several discrepancies regarding the experimental results. The most discussed issue in publications on the OMR effect is related to the question whether the organic magnetoresistance is a single-carrier effect or a double-carrier effect. Some authors are convinced that the injection of one type of charge carriers is

sufficient for the occurrence of the OMR effect and claim that a magnetoresistance can be measured in unipolar devices [Mer05b, Ngu08, Wan08]. In contrast, several other studies support the view that the injection of both electrons and holes is a prerequisite for the observation of the OMR effect [Kal03a, Hu07, Maj09]. Strong support for this point of view was for instance provided by Desai *et al.* who showed that in bipolar OLEDs the OMR effect can only be detected at applied voltages where light emission from the devices is detected [Des07a]. Theoretical models on the basis of a single-carrier mechanism [Bob07] as well as on the basis of double-carrier mechanisms [Kal03a, Pri06, Des07a] have been proposed to explain the OMR effect. Hence, it is necessary to perform more specific measurements which allow to finally decide between the two fundamental ways of explaining the OMR effect.

Another feature which has not been investigated carefully enough is the temperature dependence of the OMR effect. Only few publications show temperature dependent OMR measurements at all. In these studies, however, the magnetoresistance curves are presented only for selected voltages at each temperature, which leads to partially contradicting conclusions regarding the overall temperature dependence. In some studies it was stated that the OMR effect is relatively insensitive to temperature [Fra04, Mer05a] while other studies demonstrated that the OMR values decrease [Pri06] and can even change sign [Blo08a] as temperature is decreased. Hence, a conclusive discussion of the temperature dependence of the OMR effect on the background of a theoretical model is still missing.

Finally, it is very striking that for similar device structures the maximum OMR values reported in literature show quite remarkable variations even at room temperature. For devices based on Alq_3 published values for the current change at magnetic fields on the order of 100 mT cover the range from below 1 % [Nie08b] over several percent [Blo07, Des07a] up to values above 10 % [Pri06] or even above 20 % [Ngu08]. For polymer-based devices similar variations of the OMR values can be found in literature. Changes in current below 1 % [Hu07] and around 2 % [Blo08b] at 100 mT were reported for devices comprising PPV derivatives, whereas a magnetoconductance of 15 % was detected at similar fields in devices using PFO as active material [Fra04]. No explanation has been provided so far for these variations in OMR values.

In summary, this literature review shows that even though the OMR effect is readily observable in a variety of organic materials a number of issues need to be clarified in further investigations. It is the goal of this thesis to perform specific measurements which help to draw a conclusive picture of the OMR effect and the mechanism behind it.

2.4 Spin dynamics in organic materials

Spin dynamics of individual charge carriers and of charge carrier pairs are assumed to play a major role in the context of magnetic field effects in OLED devices. In this section the hyperfine interaction will be introduced and a possible influence of this interaction on the spin state of charge carriers during the hopping transport will be discussed. Furthermore, it will be explained how an intersystem crossing between e-h pairs with different spin states might be achieved in the presence of the hyperfine interaction. Finally, a possible influence of an external magnetic field on the presented processes will be pointed out.

Hyperfine interaction

The hyperfine interaction in general describes the interaction between the spin **S** of a charge carrier and the nuclear spin **I** of an atomic nucleus. The Hamiltonian for the hyperfine interaction is given by

$$H_{\text{Hyperfine}} = \hbar\, a\, \mathbf{S}\,\mathbf{I}, \tag{2.3}$$

where a is the hyperfine coupling constant which indicates the coupling strength between **S** and **I**. It is generally believed that the hyperfine interaction is of special importance for the spin dynamics in organic semiconductors [Sok74, Sch78, Zel88, Dya98]. According to this common opinion the spin of a charge carrier considerably interacts with the nuclear spins of neighboring hydrogen atoms during the hopping transport in organic materials. In a theoretical work Schulten *et al.* showed that this situation is equivalent to an exposure of the charge carrier spin to a local hyperfine field $\mathbf{B}_{\text{HF}}$ which is caused by the nuclear spins of the surrounding hydrogen atoms at each hopping site [Sch78]. In the absence of an external magnetic field the charge carrier spin is assumed to precess around these hyperfine fields $\mathbf{B}_{\text{HF}}$ at each hopping site with the Larmor frequency $\omega_0 = g\mu_{\text{B}}B_{\text{HF}}/\hbar$, where g is the g-factor of the charge carrier and μ_{B} is the Bohr magneton.
An important hypothesis made in this context is that both the nuclear spins and the resulting hyperfine fields are randomly oriented [Sch78]. As a consequence, the quantization axes for the charge carrier spin precession during the hopping transport are also supposed to have a random orientation. According to Schulten *et al.* hopping processes of a charge carrier are therefore accompanied by random changes in the direction and in the precession frequency of the charge carrier spin so that spin-flips from the spin-up state to the spin-down state or viceversa can occur [Sch78].
Figure 2.7 schematically illustrates this proposed spin evolution during hopping transport in the presence of random hyperfine fields. It should be noted that figure 2.7 only

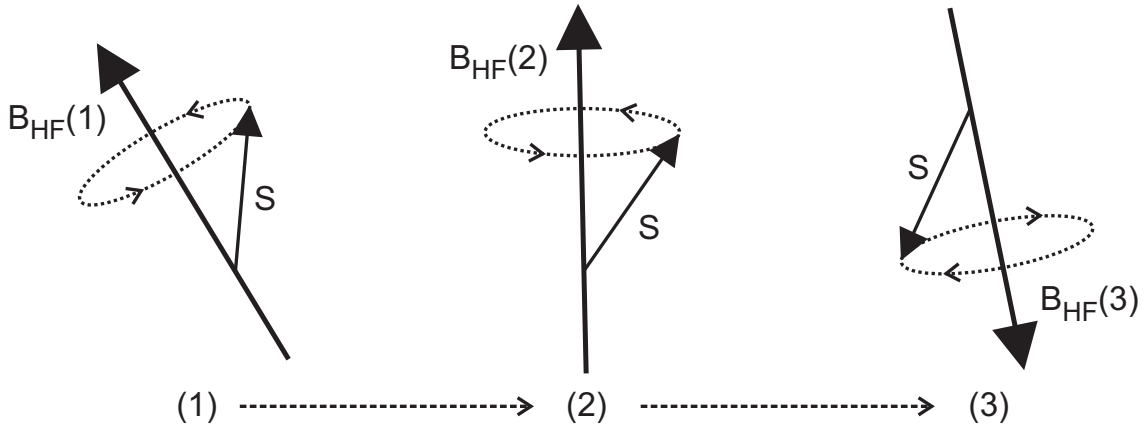

Figure 2.7: Schematic illustration of the precession of a charge carrier spin S in the presence of randomly oriented hyperfine fields B_{HF} at different hopping sites according to reference [Sch78]. In the process of hopping from site (2) to site (3) the charge carrier spin is flipped.

represents a simplified semiclassical approach to describe the quantum mechanical charge carrier spin motion. In order to conserve the total spin of the considered system, the transitions between different spin states of a charge carrier are assumed to be compensated by appropriate changes in the angular momentum of the nuclear spin system [Zel88]. According to studies from literature the characteristic spin evolution time for such transitions is related to the hyperfine coupling constant via $\tau_{\text{evo}} \sim 1/a$ and is on the order of $10^{-10} - 10^{-7}$ s [Zel88, She06].
In the presence of an external magnetic field **B** with $B \gg B_{\text{HF}}$ it is likely that the quantization axis for the spin precession is determined by the direction of the external field and that the probability for spin-flip events is reduced.

Even though no direct experimental evidence of a hyperfine interaction induced spin mixing in organic materials used in OLED devices has been provided so far, this mechanism is accepted in many publications regarding the OMR effect and serves as a starting point for theoretical modeling as well as for the interpretation of experimental results in the context of the OMR effect [Kal03a, Pri06, She06, Bob07, Ngu07b, Wag08]. Especially the small values of magnetic fields that are sufficient to cause the OMR effect are seen as an indication that the hyperfine interaction (with $B_{\text{HF}} \approx 1$ mT [Bob07]) plays a major role in the OMR mechanism. In fact, the bipolaron model which will be presented in section 2.5.1 heavily relies on the influence of the hyperfine interaction on the spin state of individual charge carriers.

Having considered the spin dynamics of single charge carriers the next step is to discuss the spin dynamics of pairs of charge carriers as suggested in references [Ste89, Fra92a]. It should be noted that according to reference [Zel88] magnetic fields are assumed to influence the spin dynamics of any processes involving two paramagnetic particles with non-zero spin. However, the following considerations will be restricted to e-h pairs which are formed in OLEDs during device operation. The Hamiltonian H which determines the spin state of an e-h pair in an organic material in the presence of an external magnetic field contains the following contributions [Fra92a]:

$$H = H_{\text{Zeeman}} + H_{\text{Hyperfine}} + H_{\text{Spin-Spin}}. \tag{2.4}$$

The first contribution accounts for the Zeeman effect and is described by

$$H_{\text{Zeeman}} = \mu_{\text{B}}\mathbf{B}(g_{\text{e}}\mathbf{S}_{\text{e}} + g_{\text{h}}\mathbf{S}_{\text{h}}). \tag{2.5}$$

Here, μ_{B} denotes the Bohr magneton, $\mathbf{B}$ the external magnetic field, g_{e} and g_{h} the g-factors of electron and hole, $\mathbf{S}_{\text{e}}$ and $\mathbf{S}_{\text{h}}$ the spins of electron and hole, respectively.
The second contribution represents the hyperfine interaction between the individual charge carriers and the nuclear spins $\mathbf{I}_m$ of m neighboring nuclei and can be written as

$$H_{\text{Hyperfine}} = \sum_m \hbar a \mathbf{S}_{\text{e}}\mathbf{I}_m + \sum_m \hbar a \mathbf{S}_{\text{h}}\mathbf{I}_m. \tag{2.6}$$

Finally, $H_{\text{Spin-Spin}}$ indicates the spin-spin interaction between electron and hole which was previously mentioned in section 2.2.2. Since only the case of large separation distances between electron and hole in an e-h pair will be considered in the following the spin-spin interaction is assumed to be negligibly small compared to the hyperfine interaction.
The resulting energy levels for pure singlet and triplet states of e-h pairs are illustrated in figure 2.8. A small broadening of the energy levels due to the hyperfine interaction is ignored in the figure.

In the absence of an external magnetic field the singlet e-h pairs have the same energy as the energetically degenerated triplet e-h pairs. Electrons and holes in the e-h pairs are assumed to be independently affected by the randomly oriented hyperfine fields so that transitions between the singlet state and the entire set of triplet states are considered to be possible for the e-h pairs (see figure 2.8a). Hence, an e-h pair is supposed to have an equal

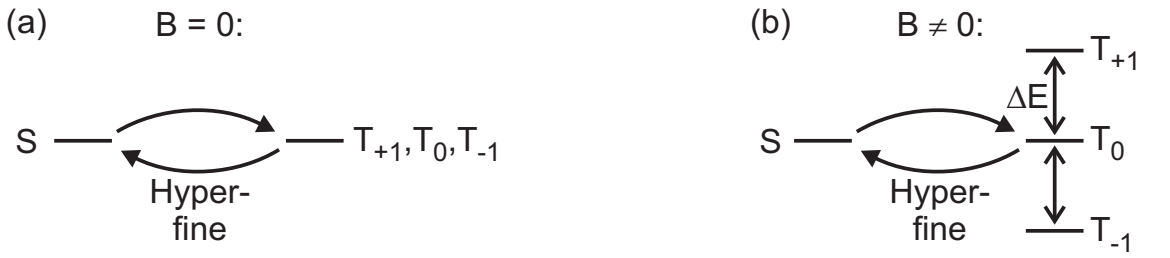

Figure 2.8: Schematic illustration of the singlet and triplet energy levels of e-h pair states and possible transitions between them according to reference [Fra92a].
(a) Without magnetic field the singlet e-h pairs mix with all triplet e-h pairs due to the hyperfine interaction. (b) In the presence of an external magnetic field the spin mixing only remains between the singlet e-h pairs and the triplet e-h pairs in the T_0 state.

probability of being in the singlet configuration or in one of the three triplet configurations. When an external magnetic field **B** is applied the e-h pair is exposed to a total magnetic field $\mathbf{B}_{\text{total}} = \mathbf{B} + \mathbf{B}_{\text{HF}}$ according to reference [Sch78]. This total magnetic field lifts the degeneracy of the triplet states and causes a Zeeman splitting of the triplet manifold into three distinct levels T_{+1}, T_0 and T_{-1} which are separated by an energy $\Delta E = \mu_{\text{B}} B_{\text{total}}$ (see figure 2.8b).

For strong external magnetic fields $B \gg B_{\text{HF}}$ the precession axes of electron and hole spins are supposed to coincide with the direction of **B**. However, the corresponding precession frequencies are expected to slightly differ due to the different hyperfine field components along **B**. This incoherence of electron and hole spins is assumed to induce transitions between the singlet and triplet e-h pairs. It is important to note that from an energetic point of view potential transitions between singlet and triplet states can only occur if the corresponding energy levels differ by less than the hyperfine interaction energy [Fra92a]. Hence, only transitions between the singlet state and the T_0 triplet state are considered to be possible, whereas the outer Zeeman components T_{+1} and T_{-1} are cut off from the interconversion process in strong magnetic fields. A saturation of the magnetic field effect is expected to occur at external fields for which the energetic splitting of the triplet sublevels exceeds the energy of the hyperfine interaction.
It was noted in reference [Ste89] that a difference in precession frequencies might not only be caused by the hyperfine interaction but could also be induced by the difference in g-factors for electrons (g_{e}) and holes (g_{h}). The probability of a transition due to this "Δg-mechanism" was shown to linearly increase with the magnetic field. However, for small magnetic fields below 100 mT the contribution of the Δg-mechanism to a potential spin mixing is negligible since $\Delta g = g_{\text{e}} - g_{\text{h}}$ usually is a very small quantity [De99].

The principle of magnetic field dependent spin conversion in e-h pairs is an essential part of some of the most promising theoretical models which are currently discussed as potential explanations for the OMR effect and which will be analyzed later in this thesis.
Here, a general issue concerning the energetics of the spin conversion processes in e-h pairs should be clarified. For a magnetic field of 100 mT the Zeeman splitting $\mu_B B_{\text{total}}$ of the triplet sublevels is on the order of several μeV, which is about three orders of magnitude smaller than the thermal energy ($\approx$ 25 meV) at room temperature. Therefore, at first glance one would not expect that a magnetic field significantly influences the population of the triplet sublevels since in thermal equilibrium the population will simply be determined by Boltzmann statistics. However, it was previously suggested that magnetic fields can indeed influence the spin conversion if the system has not yet reached thermal equilibrium [Sok74, Zel88]. According to this suggestion it is necessary that all processes involved in a magnetic field effect occur on timescales which are shorter than the spin-lattice relaxation time τ_{rel} which indicates how long it takes to reach the equilibrium population of all e-h pair sublevels as a result of spin-lattice interaction. In organic materials τ_{rel} usually is on the order of 10^{-7} s [Zel88, Dya98].
Furthermore, it was proposed that a potential spin conversion of e-h pairs can only take place if the lifetime τ of the e-h pairs is longer than the time of spin evolution τ_{evo} during which spins in the e-h pairs can possibly be perturbed by the hyperfine field [Zel88, Fra92a, Kal03a]. As already mentioned earlier in this section the spin evolution time is on the order of $10^{-10}-10^{-7}$ s. The lifetime of an e-h pair is determined by the interplay of recombination to an exciton (with a rate constant k_r) and dissociation into free charge carriers (with a rate constant k_d) and can be expressed as $\tau = (k_r + k_d)^{-1}$.

In summary, according to literature reports the following condition is expected to be essential for the observation of a magnetic field effect on the spin conversion in e-h pairs:

$$\tau_{\text{evo}} < \tau < \tau_{\text{rel}}. \tag{2.7}$$

On the one hand, an e-h pair must live long enough so that spin evolution can occur. On the other hand, the lifetime of the e-h pair must be short enough so that thermal equilibrium is not reached.

2.5 Most discussed models to explain the organic magnetoresistance

Since the discovery of the OMR effect large efforts have been made to reveal the microscopic mechanism that is responsible for the phenomenon. Even though several theoretical models are known from classical magnetoresistance effects in inorganic materials, none of these concepts can explain the OMR effect.
In non-magnetic metals the application of an external magnetic field causes a deflection of charge carriers due to the Lorentz force and results in a small positive magnetoresistance. However, due to the low mobility of organic semiconductors Lorentz force deflection of charge carriers would only lead to negligibly small magnetoconductance values below 10^{-4} % at magnetic fields of 10 mT [Pri06]. Theories that apply to magnetic field effects in spin-valve devices [Jul75, Bai88, Bin89], i.e., devices with ferromagnetic electrodes, can also be ruled out since the OMR effect is detected in devices without any magnetic layers. Moreover, the size of classical magnetoresistance effects depends on the relative orientation of the magnetic field direction and the direction of the current flow, whereas the OMR effect is isotropic with respect to the magnetic field orientation.

Several models that might explain the OMR effect have been developed in recent years and since then have been controversely discussed in literature. All models have in common that spin dynamics is considered to be of particular importance for the OMR effect. Each of the models considers a different stage of the OLED device operation process and attributes the OMR effect to magnetic field dependent changes in this stage. Figure 2.9 gives an overview by schematically illustrating the relevant processes that are analyzed in the corresponding models.

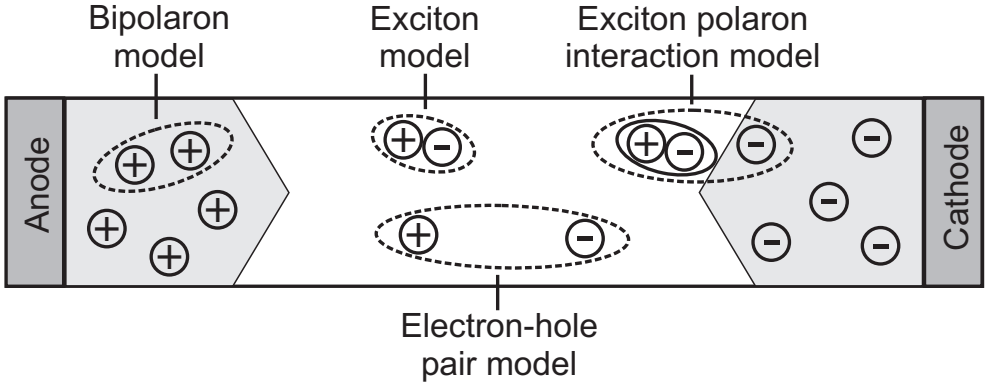

Figure 2.9: Schematic illustration of different processes in an OLED device which might be influenced by a magnetic field according to different models.

In the “bipolaron model” a single-carrier mechanism for the OMR effect is assumed and a magnetic field dependence of the hopping transport of individual charge carriers is proposed. The “exciton model” is based on a double-carrier mechanism and analyzes the

influence of a magnetic field on the formation rate of excitons. Finally, an “exciton polaron interaction model” has been proposed which assigns the OMR effect to a scattering of free charges by excitons.
The following sections are devoted to a detailed introduction of these three models which are considered to be most promising for a potential explanation of the OMR effect according to recent reports from literature. In addition, it is indicated in figure 2.9 that the OMR effect might also be caused by the influence of a magnetic field on charge carriers in the electron-hole pair state. The concept of this “electron-hole pair model” will be discussed in detail in section 3.6.

2.5.1 Bipolaron model

In 2007 Bobbert *et al.* proposed the bipolaron model which suggests that a magnetic field influences the mobility of free charge carriers and thus changes the current flow through a device [Bob07]. It was shown in section 2.2.2 that charge carrier transport in organic materials is accomplished by hopping processes of charges between localized states. In the bipolaron model it is assumed that in the course of these hopping processes it is possible that two charges of the same species (electron-electron or hole-hole) reside on the same hopping site and form a complex called a “bipolaron”. It should be emphasized that bipolarons are to be distinguished from e-h pairs or excitons which consist of two charge carriers with opposite charge. Due to the Coulomb repulsion the formation of bipolarons can only occur at hopping sites with particularly low energy, which are available due to the energetic disorder in site energies. In accordance with the Pauli exclusion principle the formation of a bipolaron is only possible if the two charge carriers that are involved have an antiparallel spin configuration.

Figure 2.10 illustrates the hopping process with and without magnetic field according to the bipolaron model. In the absence of an external magnetic field it is assumed that the spins of free charge carriers are subjected to the random hyperfine fields inside the material and can easily be flipped. It is argued that as a consequence hops to all unoccupied and singly occupied sites are allowed since a moving charge carrier is expected to adjust its spin accordingly in order to have an antiparallel spin configuration in the case of a double occupancy. The application of an external magnetic field is supposed to drastically reduce the probability of bipolaron formation and to force charge carriers to hop onto unoccupied states on their way through the device.

A crucial point in the bipolaron model is the hypothesis that charge carrier mobility and current density in a device are directly affected by magnetic field induced changes in the probability of bipolaron formation. It is claimed that due to an enhanced polaronic stabi-

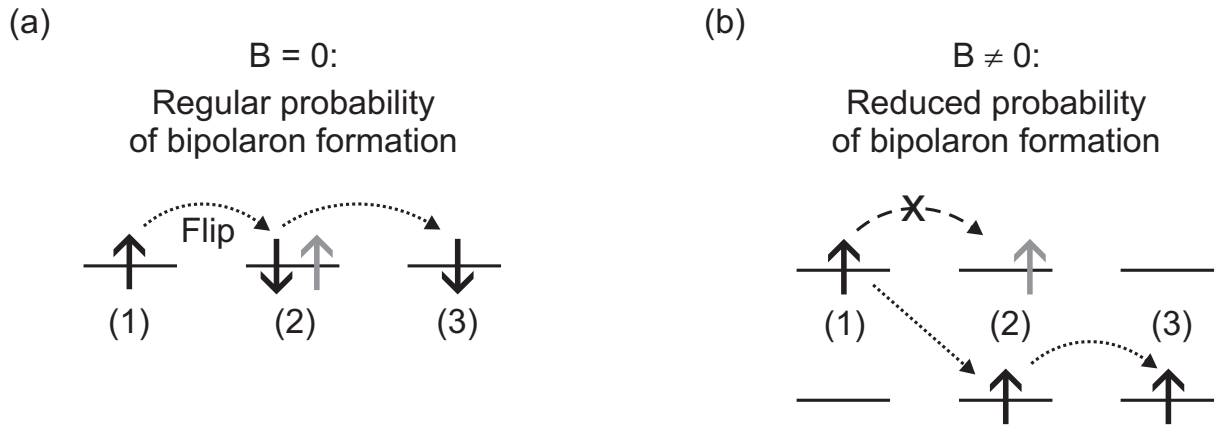

Figure 2.10: Schematic illustration of the hopping transport according to the bipolaron model (a) without applied magnetic field and (b) with applied magnetic field.

lization charge carriers have a lower mobility when they form bipolarons during hopping transport compared to the situation when no bipolarons are formed [Woh06, Bob07]. Since bipolaron formation is supposed to be reduced upon magnetic field application free charge carriers are expected to have a higher mobility in this case. At fixed voltage this is believed to cause an increase in current and to result in a positive magnetoconductance. On the other hand, a competing process is mentioned in the framework of the bipolaron model which might influence the magnetoconductance in the opposite way. According to the model the presence of a magnetic field reduces the number of available hopping sites for charge carrier transport since hops on singly occupied sites are not allowed any more. This "spin blocking" mechanism is claimed to reduce the current density in the device and to cause a negative magnetoconductance. In total, the magnetoconductance is assumed to be either positive or negative depending on the relative contributions of the competing effects. Bobbert *et al.* numerically evaluated the probability of bipolaron formation in a simplified two-site model and furthermore showed that by using Monte Carlo simulations it is possible to reproduce the two fundamental lineshapes that have been observed for the OMR effect in experiment [Bob07, Wag08].

A distinguishable property of the bipolaron model is the fact that none of the relevant processes involves e-h pairs or excitons. Hence, the model also predicts an OMR effect in unipolar devices where only one type of charge carrier is injected into the device, which clearly separates the bipolaron model from all other models that have been proposed for the OMR effect so far.

2.5.2 Exciton model

In 2006 Prigodin *et al.* presented a model for the OMR effect which is referred to as "exciton model" in literature and which is based on the idea that a magnetic field affects the current flow through a device by changing the exciton formation rate [Pri06]. According to the authors this exciton formation rate is generally the limiting factor for the current flow in bipolar OLED devices. It has previously been shown that in the case of a limitation by recombination the current flow I through a bipolar device can be expressed in the following way [Par59, Mar01]:

$$I \sim \frac{1}{\sqrt{\beta}} \left(\frac{U^2}{d^3} \right), \tag{2.8}$$

where β is the exciton formation rate, U is the applied voltage, and d is the thickness of the organic layer in the device. According to the exciton model the exciton formation rate β is sensitive to magnetic fields as a consequence of the magnetic field dependent spin mixing between singlet and triplet e-h pairs that was introduced in section 2.4. Referring to relation (2.8) the authors of the exciton model argue that a magnetic field dependence of the exciton formation rate directly causes a magnetic field dependence of the current, which is schematically depicted in figure 2.11. However, the physical mechanism through which the exciton formation rate and the current flow are related to each other is not specified by the authors of the model.

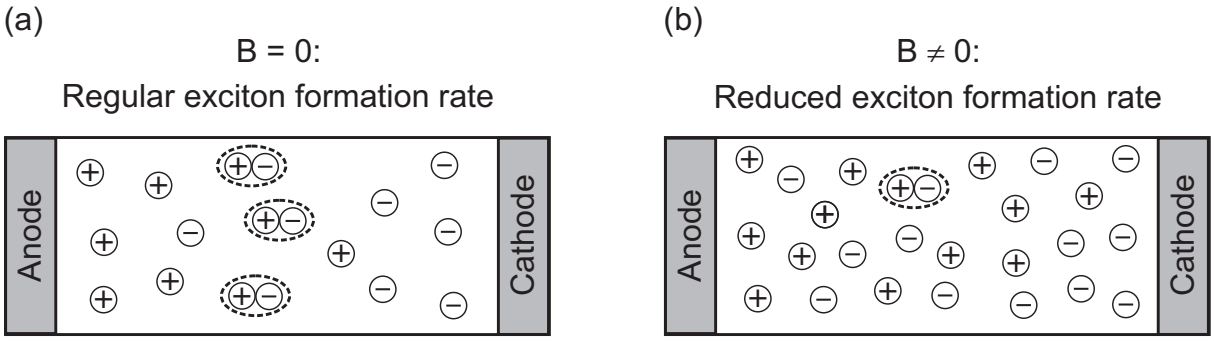

Figure 2.11: Schematic illustration of free charge carriers and excitons in a bipolar OLED device according to the exciton model (a) without applied magnetic field and (b) with applied magnetic field.

In the framework of the exciton model simple calculations on the basis of rate equations are presented in order to give an estimation of possible magnetoresistance values. It is assumed in the model that created e-h pairs can either dissociate into free charge carriers or can recombine and form excitons. The process of dissociation is thermally activated and occurs with dissociation rate constants $k_{\mathrm{d}}^{\mathrm{S}}$ and $k_{\mathrm{d}}^{\mathrm{T}}$ for singlet and triplet e-h pairs,

respectively. The process of recombination to an excitonic state occurs with recombination rate constants k_r^S and k_r^T for singlet and triplet e-h pairs, respectively.

Using expressions for the exciton formation rate with and without externally applied magnetic field Prigodin *et al.* derive an expression for the saturation value MR_{sat} of the magnetoresistance $\Delta R/R$ at large magnetic fields. In particular, the authors consider the case that the dissociation rate constants do not show a strong spin dependence ($k_d^S = k_d^T$) and that singlet e-h pairs recombine much faster than triplet e-h pairs ($k_r^S \gg k_r^T$). Under these conditions the saturation value MR_{sat} can be written as [Pri06]:

$$MR_{sat} = -\frac{1}{2}\frac{k_d^T}{\left(k_r^T + k_d^T\right)}. \tag{2.9}$$

Based on equation (2.9) different conclusions are drawn from the exciton model. The authors of the model state that the dependencies of the OMR effect on voltage and temperature are a consequence of the corresponding dependencies of the triplet dissociation rate constant k_d^T on these parameters. Moreover, the authors predict that according to the exciton model the absolute value of the magnetoresistance decreases with decreasing temperature and increases with increasing voltage.

2.5.3 Exciton polaron interaction model

In 2007 Desai *et al.* proposed the exciton polaron interaction model (EPI model) which suggests that triplet excitons play the key role in the OMR mechanism [Des07a, Des07b]. Due to the long lifetime of triplet excitons a large number of triplets are present in an OLED during device operation and diffuse through the active material until they decay or dissociate. In the EPI model it is argued that the mobility of free charge carriers is affected by scattering events involving triplet excitons. The application of a magnetic field is assumed to change the concentration of triplet excitons and to alter the current through the device.
According to the model the interaction between free charge carriers and triplet excitons can be described in the following way:

$$\mathrm{P} + \mathrm{T} \rightarrow (\mathrm{P}\ldots\mathrm{T}) \begin{cases} \xrightarrow{k_1} \mathrm{P} + \mathrm{T} & (1) \\ \xrightarrow{k_2} \mathrm{P} + \mathrm{S}_0^* & (2), \end{cases}$$

where P is a free charge carrier, T is a triplet exciton, (P ... T) is a pair state of charge carrier and triplet exciton, and S_0^* is an excited vibrational level of the molecular ground state.

Process (1) is governed by a rate constant k_1 and describes the event that a free charge carrier is scattered by a triplet exciton, which is assumed to result in a decrease of the charge carrier mobility. Process (2) occurs with a rate constant k_2 and is known as triplet-polaron quenching [Her07]. It describes the event that a triplet exciton nonradiatively decays after interacting with a free charge carrier. In an early study on magnetic field effects in organic crystals it was shown that process (2) is magnetic field dependent and that triplet-polaron quenching is reduced with increasing magnetic field strength [Ern68].

A crucial hypothesis in the EPI model is that the magnetic field increases the intersystem crossing rate from triplet excitons to singlet excitons, thus resulting in a higher singlet concentration and a reduced triplet concentration. As a motivation for this assumption the authors mention the observation that the device efficiency is increased in the presence of a magnetic field [Des07a]. However, the exact mechanism causing this magnetic field dependence is not specified in the model. Provided that a magnetic field reduces the concentration of triplet excitons the model predicts a reduction in the number of scattering events for charge carriers, which is believed to increase the charge carrier mobility and to enhance the current through the device (see figure 2.12). As a consequence, a positive magnetoconductance $\Delta I/I$ is expected to occur. The increase in the concentration of singlet excitons is supposed to enhance the luminescence output from the device and to cause a positive magnetoelectroluminescence $\Delta EL/EL$.

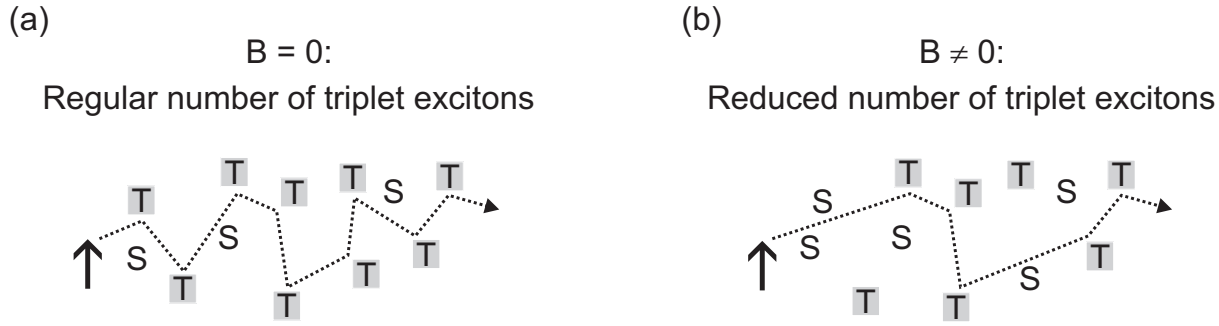

Figure 2.12: Schematic illustration of the charge carrier transport with scattering events at triplet excitons according to the exciton polaron interaction model (a) without applied magnetic field and (b) with applied magnetic field.

Desai *et al.* furthermore provided an explanation involving the dissociation of triplet excitons as the potential cause of negative values for the magnetoconductance [Des07b]. It is argued that triplet excitons can produce a secondary current after dissociation and provide a positive contribution to the overall current through the device. If the concentration of triplet excitons is reduced due to the application of a magnetic field the secondary current from dissociation is also decreased and according to the model a negative magnetoconductance $\Delta I/I$ is obtained.

Using a similar argumentation Hu *et al.* mentioned that triplet excitons can furthermore produce a secondary current by releasing trapped charge carriers from their traps [Hu07, Hu09]. The authors suggested that also in this case a negative magnetoconductance is expected if the triplet concentration in a device is reduced by applying a magnetic field.
In total, according to the EPI model the magnetoconductance is a superposition of positive and negative contributions which all originate from a magnetic field induced enhancement of the intersystem crossing rate from triplet excitons to singlet excitons.

2.6 Experimental and measurement techniques

This section introduces the experimental methods that were used in the course of this thesis. After a presentation of the fabrication process of OLED devices the experimental setups for the electro-optical device characterization and for the measurement of magnetic field effects will be presented. Finally, two measurement techniques will be discussed which were used to obtain information about the charge carrier mobility and the distribution of trap states inside the active material of OLED devices.

2.6.1 OLED processing

The entire OLED fabrication process was performed in a class 100 clean room. All OLED devices were fabricated on 0.7 mm thick float glass substrates covered with a patterned layer of indium tin oxide (ITO). Before device preparation the substrates were subjected to a multistep cleaning process in ultrasonic baths and were subsequently exposed to an oxygen plasma. The latter process is called reactive ion etching and is known to decrease the work function of ITO from -4.4 eV to about -4.8 eV [Din00], which improves the hole injection into the organic layers. On top of the ITO a layer of poly(3,4-ethylenedioxythiophene):poly(styrenesulfonate) (PEDOT:PSS) was spin-coated. The PEDOT:PSS has a HOMO of about -5.2 eV [Din00, Ma05] and was supplied by H. C. Starck as CLEVIOS P VP CH8000. In addition to an improvement of the hole injection PEDOT:PSS is used to planarize the rough surface of ITO, thus avoiding short circuits due to high local electric fields [Kug99]. As light emitting polymer a poly(paraphenylene vinylene) (PPV) derivative known as “Super-Yellow PPV” (SY-PPV) was used. The SY-PPV with a HOMO of -5.2 eV [Bol08] and a LUMO of -2.7 eV [Bol08] was supplied in toluene solution by Merck OLED materials GmbH. The SY-PPV was spin-coated under an inert N_2 atmosphere where the oxygen and water levels were kept below 10 ppm in order to prevent a contamination of the organic layer. The cathode consisting of a Ba layer and an Al cap-

ping layer was deposited by thermal evaporation inside a vacuum system with a pressure of typically 10^{-6} mbar. Finally, the device was encapsulated under inert atmosphere with a glass lid to protect the reactive Ba and the organic layers from oxygen and moisture. The final OLED chip consisted of 15 independent devices with an active area of 4 mm^2. Unless otherwise noted, the typical layer structure of the SY-PPV devices that were investigated in this thesis consisted of 120 nm ITO / 120 nm PEDOT:PSS / 100 nm SY-PPV / 3 nm Ba / 150 nm Al.

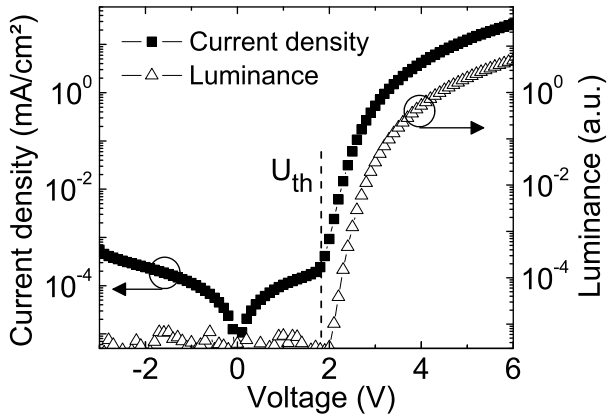

Figure 2.13:
Current-voltage and luminance-voltage characteristics of a SY-PPV device.

Figure 2.13 shows typical current-voltage (IV) and luminance-voltage (LV) characteristics of a pristine bipolar SY-PPV device. For low applied voltages the device is in an ohmic regime where possible leakage currents are superimposed on the injection current. At a certain voltage which will further on be referred to as "threshold voltage" U_{th} the charge carrier injection becomes efficient enough so that a substantial current through the diode exceeds the leakage currents and light emission from the device can be detected. It should be noted in this context that depending on the sensitivity of the light detection system an analysis of LV curves alone might only provide an upper limit for the value of U_{th}.

Apart from investigations in polymer-based devices the OMR effect was also measured in small molecule OLEDs during this thesis. Devices on the basis of tris-(8-hydroxyquinoline) aluminum (Alq_3) as emitter material were fabricated by thermal evaporation in a vacuum chamber with a base pressure of typically 10^{-6} mbar. The device structure comprised 120 nm ITO as anode, 40 nm N,N'-bis(naphthalen-1-yl)-N,N'-bis(phenyl)-benzidine (NPB) as hole-injection layer, followed by 100 nm Alq_3 as emitting layer and completed by 0.7 nm LiF and 150 nm Al as cathode.

2.6.2 Measurement setups

LIV and OMR measurement setup

The electro-optical device characterization and the measurement of magnetic field effects on current and luminance at room temperature were performed in a computer-controlled setup which is shown in figure 2.14. Setting up the entire measurement equipment and writing a LabVIEW program to automatically control the measurements was a substantial part of the work at the beginning of this thesis. In the setup an OLED chip with several individual devices was placed in a sample holder between the poles of an electromagnet in the dark. In the standard configuration the magnetic field was chosen to be perpendicular to the OLED chip. Up to eight devices could be sequentially addressed via a Keithley

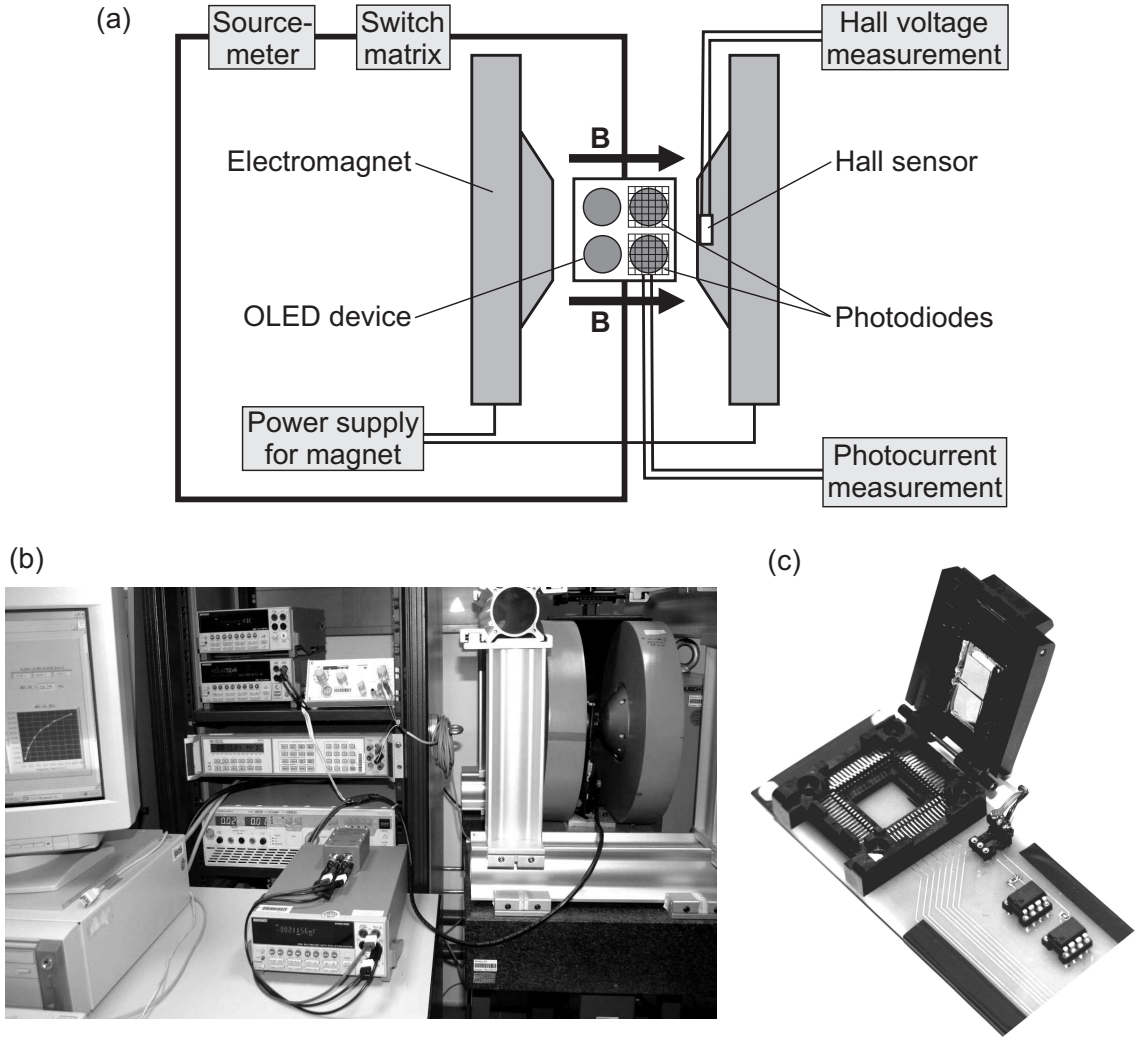

Figure 2.14: (a) Schematic illustration of the experimental setup for LIV and OMR measurements. (b) Picture of the entire experimental setup. (c) Picture of the sample holder for the OLED devices.

switching unit without removing the OLED chip from the setup. All electrical characterizations of the OLEDs were performed using a Keithley 2400 sourcemeter. Luminescence from the devices was measured with two Si-photodiodes that were placed in close proximity to the OLED. The photodiode signal was amplified and recorded with a Keithley 2000 digital multimeter. The area of each photodiode (1 cm^2) was large enough to cover four pixels on a chip. A disadvantage of this configuration, however, was the fact that the sensitivity of the photodiode was reduced due to the mismatch of pixel area and photodiode area. Spectral measurements of the electroluminescence were performed using a spectral camera PR 650 from Photo Research. The current through the electromagnet was driven by a Heiden Electronics 1150 power supply, the magnetic field strength was measured with a Hall sensor Siemens SBV 605. It was carefully checked that the photodiode signal and the electrical connections in the setup are not influenced by the magnetic field.
In typical OMR measurements the change in current flow I due to a magnetic field B was determined under constant voltage conditions. Especially in pristine devices the zero-field current showed a drift during the time of the measurement. In order to minimize the effects of this current drift, a procedure was used in which the zero-field current was determined before and after each field dependent measurement at fixed voltage [Des07a]. After averaging the two zero-field values of the current ($I(0) = [I_1(0) + I_2(0)]/2$) the magnetoconductance was calculated as $\Delta I/I = [I(B) - I(0)]/I(0)$. This measurement principle is illustrated in Figure 2.15. In a similar way the magnetoelectroluminescence was determined as $\Delta EL/EL = [EL(B) - EL(0)]/EL(0)$.

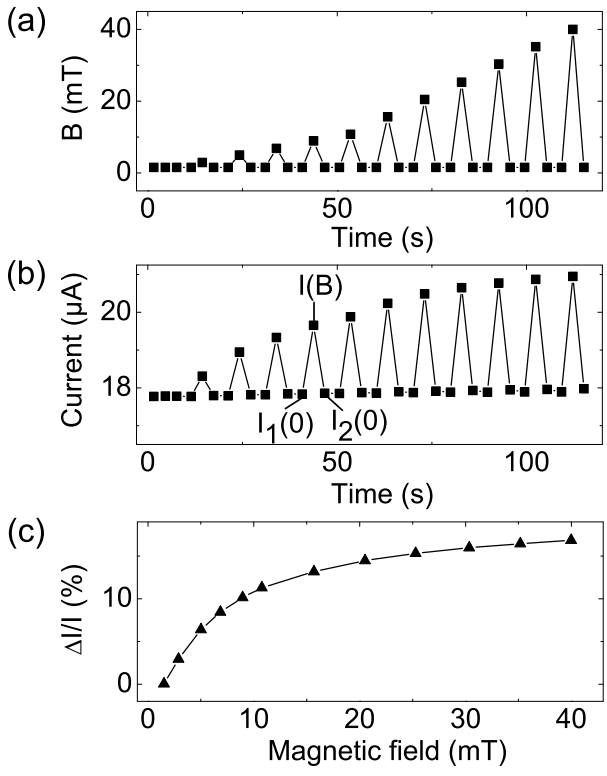

Figure 2.15:
Typical OMR measurement of a SY-PPV device: (a) Magnetic field as a function of time. (b) Current through the device as a function of time. (c) Calculated magnetoconductance as a function of magnetic field.

Even though in most graphs throughout this thesis results for $\Delta I/I$ and $\Delta EL/EL$ rather than for the magnetoresistance $\Delta R/R$ will be shown, the widely used nomenclature "OMR effect" will be kept as general denotation of magnetic field induced changes in current and luminance. It should be mentioned that due to the remanence of the electromagnet it was difficult to exactly obtain $B = 0\,\mathrm{mT}$ in the magnetic field dependent measurements. Even without current flow through the electromagnet remanent fields of up to 1 mT were present. Hence, the obtained values for $\Delta I/I$ and $\Delta EL/EL$ can be seen as lower limits for the actual values.
The standard measurement process started with the measurement of current-voltage and luminance-voltage characteristics at zero magnetic field. Subsequently, the OMR effect could be measured as a function of voltage, current and magnetic field. As an optional feature it was possible to electrically stress the OLED devices at constant current densities over an extended period of time. In intermediate intervals the stressing procedure was interrupted to perform OMR measurements at constant voltage.

For low-temperature measurements a different setup was used where the OLED was placed inside a closed-cycle helium cryostat from Helix Technology Corporation. An electromagnet driven by a Kepco BOP 50-8M power supply was used as magnetic field source. The measurement of IV characteristics and magnetoconductance curves was performed using a Hewlett Packard Semiconductor Parameter Analyzer 4155 A.

Photo-CELIV measurement setup

For an estimation of the charge carrier mobility in bipolar OLED devices the photo-CELIV (photogenerated charge carrier extraction by linearly increasing voltage) technique was applied [Jus00a]. In this method charge carriers are photogenerated in the device and subsequently extracted from the device under the influence of an electric field. Even though the principle of photo-CELIV is only slightly different from the widely applied time-of-flight (TOF) technique, it has advantages compared to TOF. In fact, photo-CELIV can be applied to bipolar devices with layer thicknesses on the order of 100 nm whereas TOF measurements require unipolar devices with large film thicknesses on the order of 1 μm. Hence, it is possible to perform photo-CELIV measurements and OMR measurements using the same OLED device. A disadvantage of the photo-CELIV method, however, is the fact that the technique only provides information about properties of the type of charge carriers which dominate the charge transport in the investigated material.

The measurement principle of photo-CELIV is schematically illustrated in figure 2.16a. A short laser pulse is absorbed by the organic layer in the device and is assumed to homogeneously photogenerate charge carriers within the layer. An offset forward bias U_{off} is

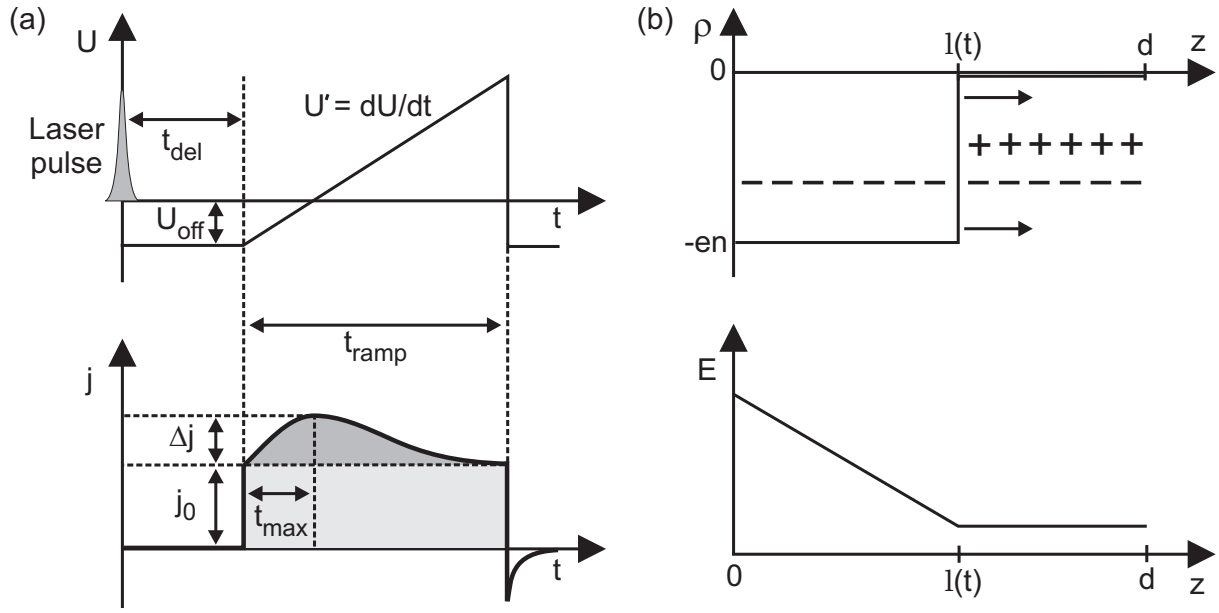

Figure 2.16: (a) Schematic illustration of a pulse sequence and a typical current transient of a photo-CELIV measurement according to reference [Moz05b]. See text for details. (b) Schematic illustration of the charge carrier density ρ and the resulting electric field E as a function of position z in an OLED device during extraction of holes after photoexcitation (adapted from reference [Ban09]).

applied to compensate the built-in potential and to establish flat band conditions within the device during and immediately after the laser excitation. This is done to ensure that the photogenerated charge carriers experience an electric field as small as possible. Hence, most of the charge carriers stay in the device and can recombine. After an adjustable delay time t_{del} the remaining charge carriers which have not recombined are extracted by the application of a linearly increasing reverse bias ramp with a duration t_{ramp} and a defined voltage rise speed $U' = \mathrm{d}U/\mathrm{d}t$. Since the device is reverse biased the contacts are blocking and no additional charges are electrically injected via the contacts.

The photo-CELIV current transient consists of two parts: Even without previous laser illumination the application of a triangular-shaped reverse bias ramp to the device leads to a rectangular-shaped current transient with a plateau value that corresponds to the displacement current density

$$j_0 = \frac{1}{A}\frac{\mathrm{d}Q}{\mathrm{d}t} = \frac{C}{A}\frac{\mathrm{d}U}{\mathrm{d}t} = \frac{\epsilon\epsilon_0 U'}{d}, \tag{2.10}$$

which describes the charging of the capacitance which is constituted by the device [Jus00a]. Here, A is the area of the electrodes, Q the electric charge on the electrodes, C the capacitance of the OLED, U the applied voltage, U' the voltage rise speed, d the

organic layer thickness, and ϵ and ϵ_0 are the dielectric constants of the organic material and of vacuum, respectively. After pre-illumination the extraction current transient additionally comprises a photocurrent on top of j_0. This photocurrent with a maximum current density Δj is caused by the extraction of the photogenerated charges which have not recombined during the delay time.

A derivation of the functional dependence $j(t)$ for photo-CELIV current transients was introduced by Juska *et al.* [Jus00a]. In this work the authors assume that at the beginning of the voltage ramp the densities of photogenerated holes (n_h) and electrons (n_e) are equal ($n_h = n_e = n$) and independent of the position z in the organic layer. Without loss of generality it can furthermore be assumed that holes dominate the charge carrier transport in the organic layer between the anode at $z = 0$ and the cathode at $z = d$, where d is the thickness of the organic layer. Figure 2.16b schematically illustrates the situation that after a certain time t holes have been extracted from the organic layer up to an extraction depth $0 < l(t) < d$ which moves with the velocity $\mathrm{d}l/\mathrm{d}t = \mu E(l(t), t)$. The electric field $E(z, t)$ is assumed to be position dependent in the region which has been depleted of holes and is considered to be constant in the rest of the layer.

After calculating the electric field from the Poisson equation and evaluating the potential drop across the organic layer the following expression can be obtained for the extraction current density [Jus00a]:

$$j(t) = \frac{\epsilon\epsilon_0 U'}{d} + \frac{en}{d}\left(1 - \frac{l(t)}{d}\right)\left(\mu U' t - \frac{en\mu}{2\epsilon\epsilon_0} l^2(t)\right). \tag{2.11}$$

Based on a numerical calculation of the extraction depth $l(t)$ in expression (2.11) it was proposed in reference [Jus00b] that the drift mobility μ of the extracted charge carriers in a photo-CELIV measurement can be determined in the following way:

$$\mu = \frac{2d^2}{3U' t_{\mathrm{max}}^2 (1 + 0.36\Delta j / j_0)}. \tag{2.12}$$

Further information on the derivation and the validity of expression (2.12) can be found in reference [Ban09]. Additional details regarding the interpretation of photo-CELIV results are presented in references [Jus00a, Jus00b, Öst04].

All photo-CELIV measurements shown in this thesis were carried out at room temperature in a computer-controlled setup. The charge carriers were photoexcited by laser pulses from a Spektron Nd:YAG laser with a repetition frequency of 10 Hz and a wavelength of 355 nm, which is the third harmonic wavelength of the laser. The control of the delay time

and the application of the triangular-shaped reverse bias ramps were performed using an Agilent 33220A pulse generator, the extraction current transients were recorded with a Yokogawa DL9040 digital oscilloscope.

TSC measurement setup

A convenient method for the investigation of charge carrier traps in organic semiconductors is the thermally stimulated current (TSC) technique. In a TSC measurement the trap states of an organic material are filled at low temperatures either by electrical charge injection or by photogeneration of charge carriers. Following this loading procedure, the material is heated up in a controlled way and the extraction current consisting of thermally released charges is recorded as a function of temperature. The area under a TSC curve is related to the amount of detrapped charges during a TSC scan. For an exact determination of the activation energy of trap states it is necessary to perform a series of consecutive TSC scans. Details on this so-called $T_{\mathrm{start}} - T_{\mathrm{stop}}$ method can be found in reference [Mal03].

For the TSC measurements presented in this thesis an OLED chip was placed inside a nitrogen-cooled continuous flow cryostate from Oxford Instruments. The temperature inside the cryostat was controlled via two heating elements that were connected to Oxford Instruments temperature controlling units. Initially, the chip was cooled down to 81 K in the dark and the charge carrier traps were electrically loaded at this temperature by applying a current of 75 mA/cm^2 for 1 min to a device. After a thermalization period of 15 min the chip was heated up to room temperature with a constant heating rate of 10 K/min. Under the influence of the built-in potential (0 V external voltage applied) the thermally released charge carriers were extracted from the device and detected as a TSC signal using a Keithley 6517A electrometer. A more detailed description of the setup used for the TSC measurements is presented in reference [Mal03].

3 Characterization of the OMR effect in OLEDs

This chapter summarizes the results that were obtained in a fundamental characterization of the OMR effect in polymer-based devices. After demonstrating the general influence of a magnetic field on the current flow and the luminescence output of OLED devices it will be pointed out how changes in the device architecture affect the OMR performance. In addition, temperature dependent OMR measurements as well as OMR measurements under illumination will be presented. In a detailed analysis of previously proposed theoretical models for magnetic field effects in OLEDs it will be shown that most of them are in conflict with experimental findings that were obtained in SY-PPV devices in the course of this thesis. Only one concept which proposes magnetic field dependent changes in the spin state of electron-hole pairs will be shown to provide possible explanations for all obtained experimental results.

It should be noted here that the absolute value of the OMR effect in OLEDs can be increased by electrically stressing the devices. This phenomenon is referred to as electrical conditioning and will be discussed in detail in chapter 4. Some of the presented results on basic OMR characteristics in chapter 3 were performed on devices which previously had been exposed to electrical stressing in order to get a better signal-to-noise ratio. In these cases the basic functional dependencies which will be discussed in chapter 3 were not affected by the conditioning procedure.

3.1 Magnetic field effect on current and luminescence

Figure 3.1 shows the influence of an external magnetic field on the electronic properties of a SY-PPV device with the layer structure 120 nm ITO / 120 nm PEDOT:PSS / 100 nm SY-PPV / 3 nm Ba / 150 nm Al. In three consecutive measurements presented in figure 3.1a the IV characteristics were recorded at zero magnetic field, at a magnetic field of 40 mT, and once again at zero magnetic field, respectively. From the resulting curves it is apparent that the application of a magnetic field reduces the device resistance and causes a positive change $\Delta I = I(B) - I(0)$ in current at constant voltage. To further analyze this behavior a constant voltage was applied to the device and the current was measured over time while the magnetic field was sweeped between 0 mT and 40 mT. As illustrated in figure 3.1b a

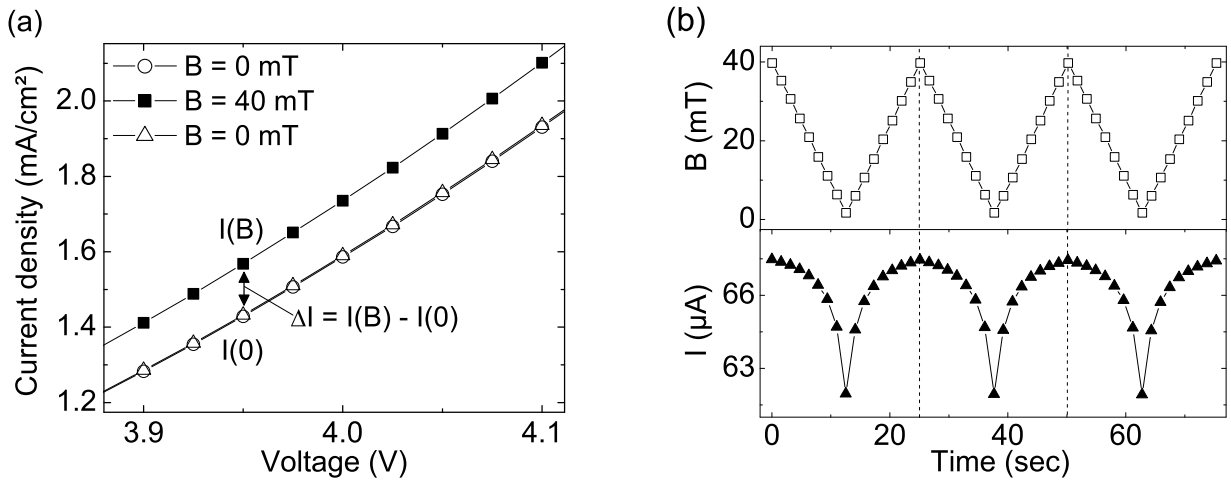

Figure 3.1: (a) Part of the IV characteristics of a conditioned SY-PPV device with and without applied magnetic field. The absolute change ΔI in current due to the magnetic field is indicated. (b) Current through a conditioned SY-PPV device at a voltage of 4 V under the influence of a varying magnetic field between 0 mT and 40 mT.

nonlinear increase in current can be observed when the magnetic field is linearly increased. The change in current is most pronounced at small magnetic fields below 40 mT. Control measurements at larger fields showed only small additional changes in current. In order to focus on the significant region of the magnetic field effect, all magnetic field dependent measurements presented in this thesis were performed at magnetic fields between 0 mT and 40 mT.

Additional measurements involving magnetic field sweeps confirmed other features of the OMR effect which have already been known from reference [Fra04]: The OMR effect in SY-PPV devices was found to be independent of the magnetic field orientation with respect to the OLED chip and showed no hysteretic behavior when the magnetic field was sweeped.

Figure 3.2 shows measurements of the magnetoconductance $\Delta I/I = [I(B) - I(0)]/I(0)$ as a function of applied magnetic field and voltage for a conditioned SY-PPV device. In the magnetic field dependent measurement in figure 3.2a the sharp rise at low magnetic fields followed by a saturation is similar to what has been observed in figure 3.1b. The nonlinear dependence of $\Delta I/I$ on the magnetic field can be fitted with the expression

$$\frac{\Delta I}{I}(B) \sim \frac{B^2}{(|B| + B_0)^2} \tag{3.1}$$

which was introduced in an early publication on the OMR effect [Mer05b]. The obtained value of the fitting parameter $B_0 = 3$ mT for the magnetoconductance in SY-PPV is identical to the value of B_0 which was reported in the context of positive magnetoconductance

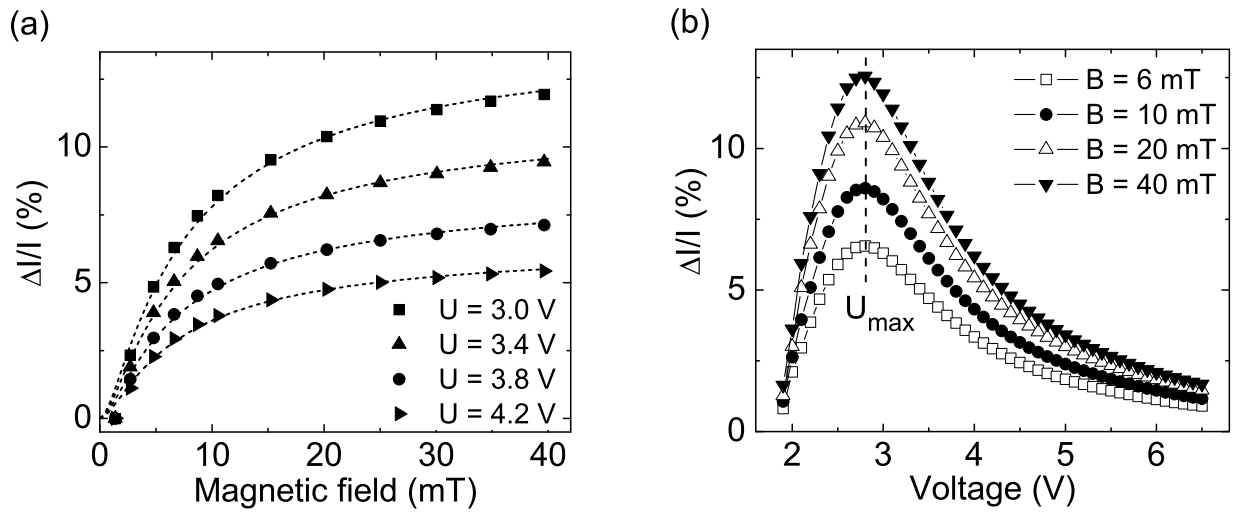

Figure 3.2: (a) Percentage change of current through a conditioned SY-PPV device as a function of magnetic field for different voltages. The dotted lines are fits according to equation (3.1) with $B_0 = 3\,\mathrm{mT}$. (b) Percentage change of current through a conditioned SY-PPV device as a function of voltage for different magnetic fields. The voltage $U_{\max}$ with the maximum value of the magnetoconductance is indicated.

in MDMO-PPV in reference [Blo08b]. A remarkable feature to note is the fact that the lineshape of $\Delta I/I(\mathrm{B})$ is independent of the driving voltage. The magnetoconductance at fixed magnetic field in figure 3.2b demonstrates a non-monotonic dependence on the applied voltage with a maximum of $\Delta I/I$ at a voltage $U_{\max}$. The values of $\Delta I/I$ are positive and do not show a sign change at voltages below the threshold voltage of light emission [Blo08b, Xin09] or in the higher voltage regime [Mer05b] as it was reported for different materials in literature. In fact, reliable OMR signals could only be measured for voltages above 2 V where a substantial charge carrier injection into the device occurred.

Since electroluminescence (EL) is directly linked to charge carrier recombination in OLEDs it is obvious that a change in current also produces a change in the light output (see figure 3.3). The application of a magnetic field influences the LV characteristics similar to figure 3.1a, and the magnetic field dependent change in the electroluminescence signal $\Delta EL(B) = EL(B) - EL(0)$ at fixed voltage is calculated in an analogous way. The increased light output implies that the concentration of singlet excitons which decay radiatively in the device increases when a magnetic field is applied. The magnetic field dependence

$$\frac{\Delta EL}{EL}(B) \sim \frac{B^2}{(|B| + B_0)^2} \tag{3.2}$$

of the relative change in electroluminescence is identical to what has been observed for the magnetoconductance signals [Mer05b]. Moreover, the same fitting parameter $B_0 = 3\,\mathrm{mT}$

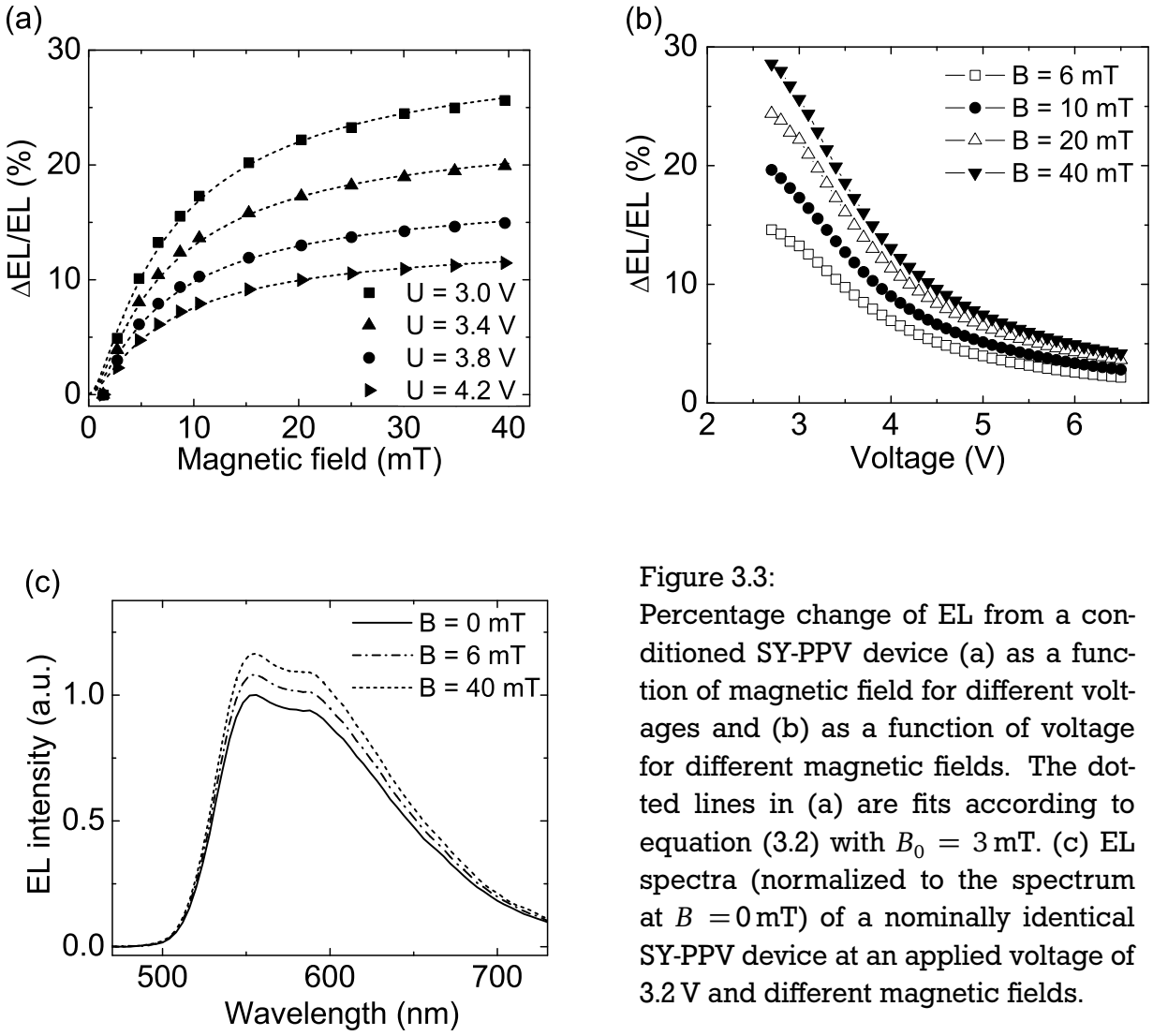

Figure 3.3:
Percentage change of EL from a conditioned SY-PPV device (a) as a function of magnetic field for different voltages and (b) as a function of voltage for different magnetic fields. The dotted lines in (a) are fits according to equation (3.2) with $B_0 = 3\,\mathrm{mT}$. (c) EL spectra (normalized to the spectrum at $B = 0\,\mathrm{mT}$) of a nominally identical SY-PPV device at an applied voltage of 3.2 V and different magnetic fields.

can be used to describe the line shape of the magnetic field dependent curves in figure 3.3a, which also suggests that magnetoconductance and magnetoelectroluminescence share a common origin. The absolute values of $\Delta EL/EL$ in figure 3.3a are larger by a factor of about 2 compared to the corresponding values of $\Delta I/I$.

The voltage dependence of $\Delta EL/EL$ is plotted in figure 3.3b. In pristine devices the magnetoelectroluminescence starts to appear at the threshold voltage of light emission and monotonically decreases as the voltage is increased. After considerable electrical stressing (especially in devices with an emission layer thicker than 100 nm) a non-monotonic behavior of $\Delta EL/EL(U)$ can sometimes be observed.

It is interesting to note that the spectral position of the EL signal remains unchanged when a magnetic field is applied. This result is illustrated in figure 3.3c and indicates that no shift of the singlet energy level is induced by the magnetic field.

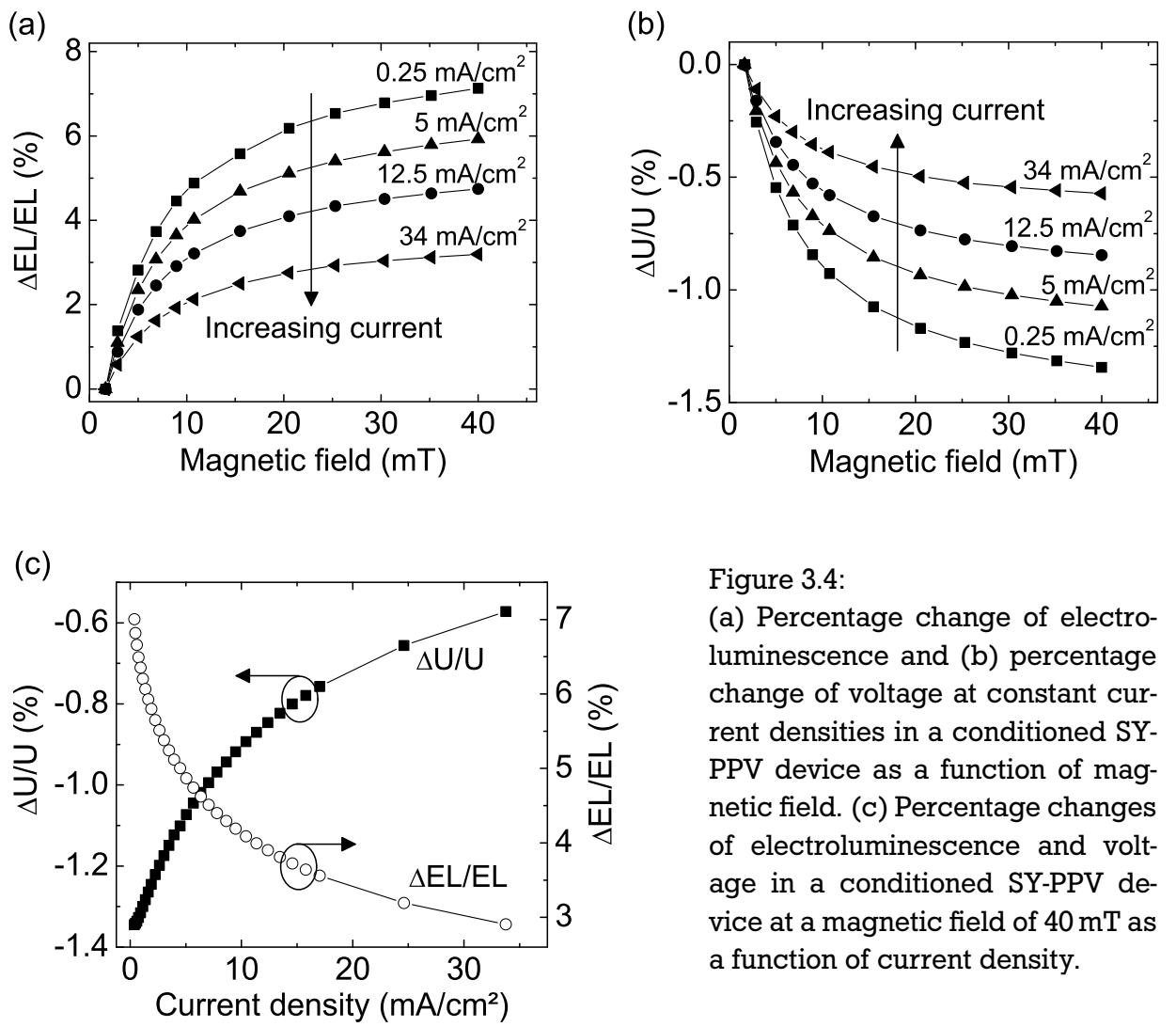

Figure 3.4:
(a) Percentage change of electroluminescence and (b) percentage change of voltage at constant current densities in a conditioned SY-PPV device as a function of magnetic field. (c) Percentage changes of electroluminescence and voltage in a conditioned SY-PPV device at a magnetic field of 40 mT as a function of current density.

A further investigation revealed that the increase in electroluminescence in the presence of a magnetic field is not exclusively caused by the increase in current. In addition, it was found that the application of a magnetic field also increases the device efficiency since it leads to a higher EL signal even in the case of a device operation at constant current (see figure 3.4a). In accordance with the previously observed reduction of device resistance in the presence of a magnetic field the data in figure 3.4b demonstrate that the voltage at constant current decreases when a magnetic field is applied. Additional measurements demonstrated that the absolute value of $\Delta U/U$ at a particular current density is smaller than $\Delta I/I$ at a corresponding constant voltage. This is a consequence of the general current-voltage dependence in OLED devices and has been discussed in reference [Mer05a].

Figure 3.4c shows $\Delta U/U$ and $\Delta EL/EL$ at fixed magnetic field as a function of current density. It is particularly important to notice that the absolute values of both magnetic field effects decrease with increasing current density.

It should be mentioned that in addition to the EL signal it was also tested whether or not the PL signal of SY-PPV devices is influenced by a magnetic field. The measurements showed no change of the PL signal upon application of a magnetic field, which is in agreement with reports from literature [Oda06, Hu09]. Since the PL signal is produced by the radiative decay of optically generated singlet excitons this indicates that singlet excitons are not affected by a magnetic field after their creation.

3.2 Influence of device architecture on OMR

3.2.1 Influence of emitter

It is known from literature that different emitter materials used in OLED devices lead to different values of the magnetoconductance [Mer05b]. However, no systematic relation between chemical structures and the values of the OMR effect has been found so far. In addition, the selection of a particular material with good OMR performance is difficult due to the fact that large variations of OMR values have been reported in literature even for similar materials and device structures. It has generally been accepted that appreciable OMR values can only be obtained in fluorescent materials [Wu07] and that the presence of hydrogen atoms is essential for the occurrence of the OMR effect [Ngu07a, Ngu07b]. OLED devices for OMR investigations need to show a stable device performance so that accurate and reproducible measurements of the device resistance are possible in a large voltage range. Moreover, large values of the OMR effect are desirable in order to achieve a good signal-to-noise ratio.

In the course of this thesis devices with different polymer materials (including different PPV derivatives, polyfluorene (PFO), poly (3-hexylthiophene) (P3HT), and a polyspiro copolymer [Spr03]) as active layers were fabricated. After initial tests the polymer SY-PPV was selected as the material of choice for extensive OMR investigations since it fulfills the requirements for reliable measurements. The material is commercially available in high quality and has been intensively investigated in literature [Edm04, Sha07, Bol08]. In addition, it will be shown in chapter 4 that in SY-PPV devices high magnetoconductance values even above 20 % at moderate magnetic fields can be achieved.

It should be mentioned that many literature reports on the OMR effect are based on devices comprising the small molecule material Alq_3 [Kal03a, Pri06, Blo07, Des07a, Ngu08]. During this thesis devices with inhouse-synthesized Alq_3 from the Siemens AG as well as devices with commercially available Alq_3 from H. W. Sands Corporation were investigated. However, in both kinds of devices only small magnetoconductance values below

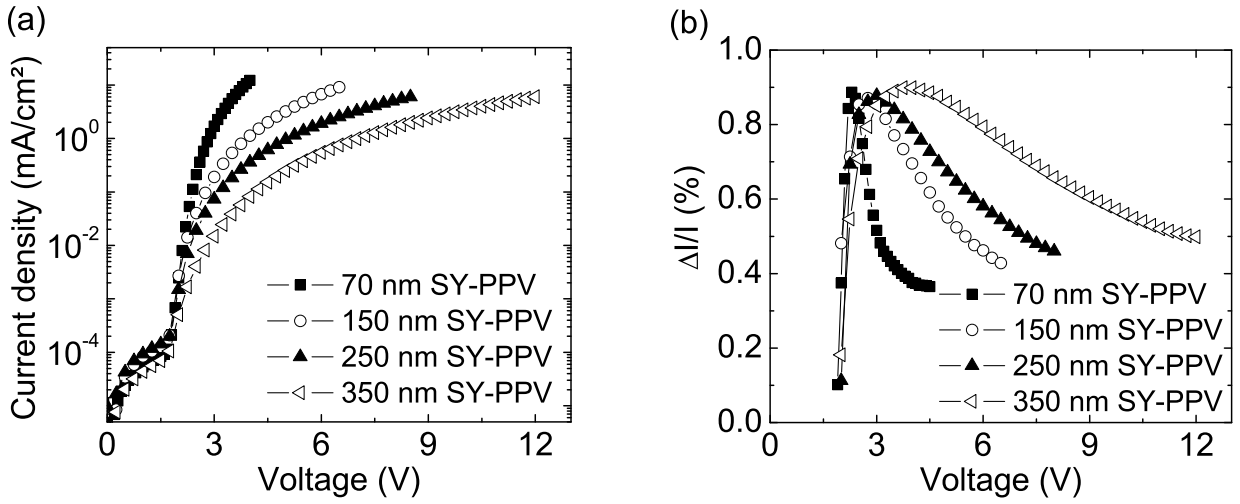

Figure 3.5: (a) IV characteristics at zero magnetic field and (b) magnetoconductance as a function of voltage at a magnetic field of 40 mT for pristine SY-PPV devices with different emitter thicknesses.

3 % at 40 mT could be obtained after electrical stressing. These values are significantly lower than the corresponding values achieved in SY-PPV devices.

Figure 3.5 shows an investigation of pristine SY-PPV devices with different thicknesses of the emission layer. A larger emitter thickness leads to a lower current density at fixed voltage. The reason for this observation is that at fixed voltage the average electric field which drives charge carrier injection and transport is lower in thicker devices. In the pristine state all investigated devices showed a comparable magnetoconductance of close to 1 % independent of the emitter thickness. After electrical stressing a clear dependence of the OMR effect on the emitter thickness was observed and larger magnetoconductance values were obtained in devices with a thicker emitter layer.

In addition to a variation of the emitter material itself it was also investigated whether or not changes in the charge carrier balance inside the emitter layer influence the OMR effect. For this purpose SY-PPV:PtOEP devices with 100 nm emitter thickness were fabricated in which small amounts of the phosphorescent material platinum octaethylporphyrin (PtOEP) were added to the SY-PPV. A comparison of the energy levels in figure 3.6a demonstrates that the LUMO in PtOEP is about 0.5 eV lower than in SY-PPV, which makes PtOEP molecules efficient charge carrier traps for electrons in SY-PPV and therefore shifts the charge carrier balance towards holes. The hole transport, in contrast, is not expected to be significantly affected since the HOMO of SY-PPV is located about 0.1 eV above the HOMO of PtOEP. Apart from influencing the charge carrier transport the admixture of PtOEP to SY-PPV furthermore opens an efficient channel for a conversion of singlet excitons into triplet excitons in the SY-PPV [Ran09]. This is schematically illustrated in figure

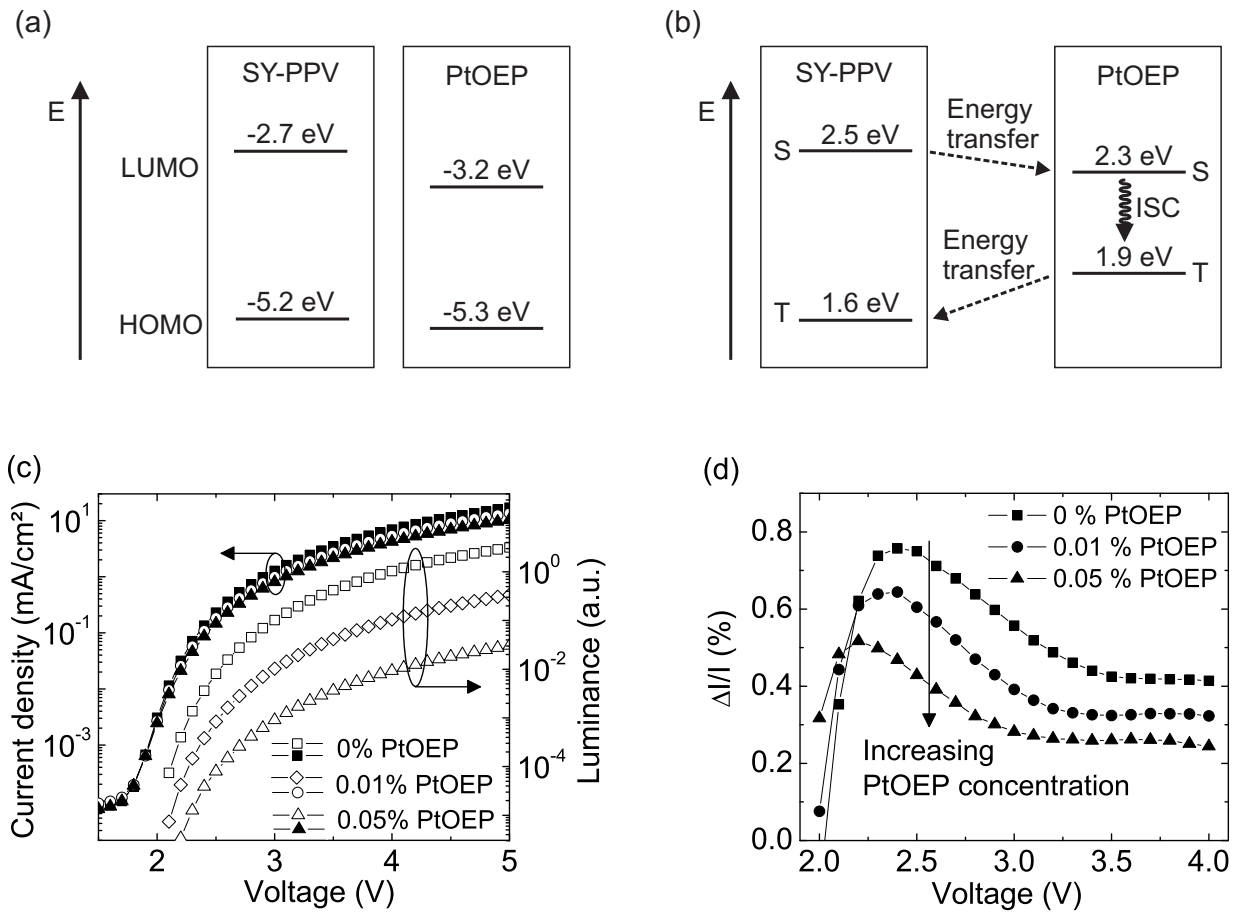

Figure 3.6: (a) Schematic illustration of the energetic position of HOMO and LUMO in SY-PPV and in PtOEP according to references [Mäk02, Bol08]. (b) Schematic energy diagram illustrating the energy transfer between excitonic states in SY-PPV and PtOEP according to references [Öst99, Bag03, Ran09]). (c) IV and LV characteristics of pristine SY-PPV:PtOEP devices with different PtOEP concentrations. (d) Magnetoconductance as a function of voltage at a magnetic field of 40 mT for the devices from part (c).

3.6b where the corresponding singlet and triplet energy levels for SY-PPV and PtOEP are shown. It can be seen that a Förster type energy transfer [För48] can occur from the singlet level in SY-PPV to the (energetically lower lying) singlet level in PtOEP. A very efficient intersystem crossing in the PtOEP allows for an internal transition from the singlet to the triplet state. Following this, the energy can be transferred back to the triplet state of SY-PPV via a Dexter type energy transfer [Dex53]. Evidence for these energy transfer routes was provided by the fact that the PL signal of the investigated SY-PPV:PtOEP devices was significantly smaller than the PL signal of pure SY-PPV devices. In addition, no direct phosphorescence from PtOEP could be detected in the PL spectrum of the SY-PPV:PtOEP devices. Similar results were also reported in reference [Ran09] where organic solar cells on the basis of SY-PPV:PtOEP were investigated.

Figure 3.6c shows IV and LV characteristics of ITO / PEDOT / (1-x) % SY-PPV: x % PtOEP / Ba / Al devices with different weight concentrations of PtOEP. The current at fixed voltage is slightly reduced when PtOEP is added to SY-PPV. It is important to note that in SY-PPV the hole mobility is significantly higher than the electron mobility [Blo01, Man07]. Hence, a trapping of electrons is expected to only have a moderate influence on the overall current, which is in line with the observed IV characteristics in figure 3.6c. Nevertheless, the overall current becomes even more hole-dominated when PtOEP is added to SY-PPV. At the same time, the luminance of a SY-PPV device at fixed voltage is reduced by two orders of magnitude without changing its spectral position when 0.05 % PtOEP are added to the SY-PPV. This pronounced reduction in luminance can be caused by several reasons: Due to the strongly reduced number of free electrons a smaller number of electron-hole pairs and radiatively decaying excitons is formed in the device. A second reason for the reduced luminance in the SY-PPV:PtOEP devices is the very efficient energy transfer from the singlet state in SY-PPV to the singlet state in PtOEP as indicated in figure 3.6b. Moreover, the recombination zone is shifted towards the cathode which additionally facilitates a quenching of the EL signal.
In figure 3.6d the corresponding magnetoconductance curves of pristine SY-PPV and SY-PPV:PtOEP devices are plotted as a function of voltage. It is clearly seen that a higher concentration of PtOEP leads to a smaller magnetoconductance.

3.2.2 Influence of cathode

A possible way of influencing the charge carrier balance inside the emitter material of a device without affecting the ratio between singlet and triplet excitons is the use of different cathode materials. Due to different work functions of individual cathode materials the injection barrier for electrons can be modified and the efficiency of the electron injection can be changed. In the following investigation two SY-PPV devices with different cathode materials will be compared. In order to provide identical conditions for hole injection, both devices contain ITO and PEDOT:PSS as anode material and hole injection layer, respectively. In one device the cathode consists of a 3 nm thin Ba layer protected by a 150 nm thick Al capping layer. Since the work function of Ba ($\Phi \approx -2.5$ eV [Lid99]) matches well with the LUMO level of PPV (≈ -2.7 eV [Bol08]) a good electron injection into the SY-PPV is permitted. Therefore, the device with the Ba/Al cathode will further on be referred to as bipolar device.
A second device was fabricated without the Ba layer and only with a 150 nm thick Al layer as cathode. Due to its large work function ($\Phi \approx -4.2$ eV [Lid99]) Al only allows for a weak electron injection so that the device with the Al cathode can be referred to as a hole-dominated device. Fewer electrons are injected into the device and fewer e-h pairs

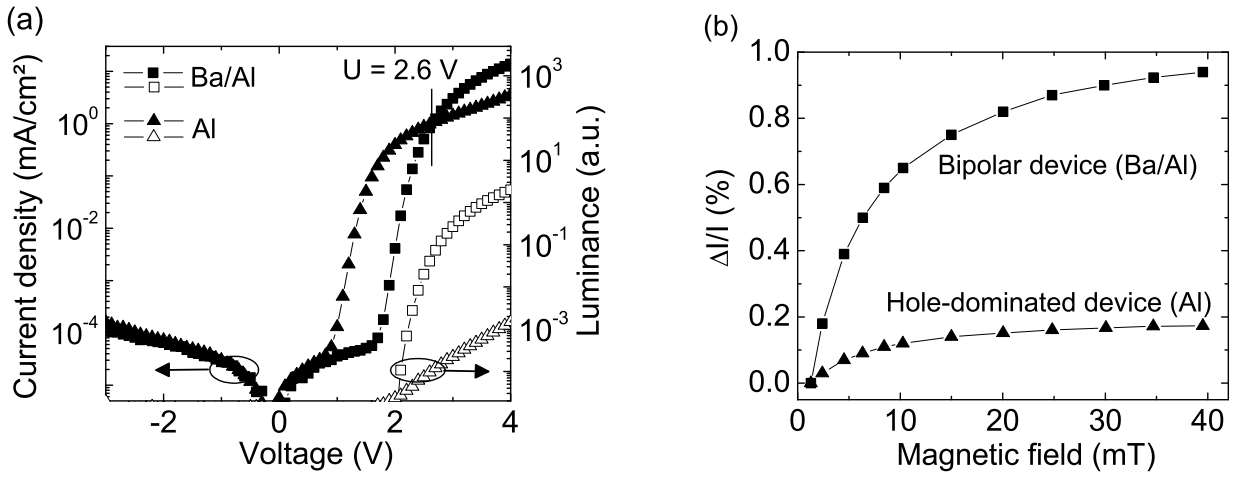

Figure 3.7: (a) IV and LV characteristics of SY-PPV devices with Ba/Al and Al cathode, respectively. (b) Magnetoconductance at a voltage of 2.6 V as a function of magnetic field for the devices from part (a).

are formed inside the device in the case of the hole-dominated Al device compared to the bipolar Ba/Al device.

Figure 3.7a shows IV and LV characteristics of the devices with different cathodes and demonstrates the consequence of varying the electron injection barrier height. Similar curves have also been reported by Blom *et al.* for devices with Ca/Al and Al cathodes, respectively [Blo00]. The smaller built-in potential in the hole-dominated device leads to a lower threshold voltage of efficient charge carrier injection and a higher current flow in the region between 1 V and 2.5 V compared to the bipolar device. For voltages around 2.6 V the current densities in the bipolar and hole-dominated devices are comparable. However, the electroluminescence output in this voltage region is more than two orders of magnitude lower in the hole-dominated device. As a consequence of the reduced electron injection efficiency in the hole-dominated device it can be assumed that only a small number of e-h pairs are formed which eventually evolve into excitons and can decay radiatively. In addition, it should be mentioned that similar to the case of the SY-PPV:PtOEP devices the recombination zone in the hole-dominated device might be shifted towards the cathode and the electroluminescence signal might partially be quenched.
In figure 3.7b the magnetoconductance is plotted as a function of magnetic field for pristine devices with Ba/Al and Al cathode, respectively. The bipolar device exhibits a magnetoconductance of around 1 % whereas in the hole-dominated device an effect of less than 0.2 % is detected at a magnetic field of 40 mT. It is important to note that the curves were recorded at a voltage of 2.6 V where a comparable current density of about 1 mA/cm^2 was measured in both devices. This directly shows that the value of the OMR effect can not simply be controlled by the value of the current density.

Different literature reports also suggest that a balanced injection of both electrons and holes is advantageous for the OMR effect. In an investigation of Alq_3 devices with different cathode materials Desai *et al.* found that the magnetoconductance values are large when a good charge carrier balance is achieved in the devices [Des07a]. In contrast, no magnetoconductance or only small values of $\Delta I/I$ were typically detected in unipolar devices [Gär05, Ngu08, Wan08].

3.2.3 Influence of hole injection layer

In all devices that were investigated in the course of this thesis a hole injection layer of PEDOT was spin-coated on top of the ITO anode. Apart from facilitating the injection of holes a PEDOT layer is known to increase the device stability by smoothening the ITO surface and therefore reducing the probability of shorts [Kug99]. Since PEDOT represents an additional organic compound in the device (apart from SY-PPV) it was investigated whether or not it also has an influence on the OMR effect.

In figure 3.8 a comparison of SY-PPV devices with and without PEDOT layer is shown. Apart from the fact that the leakage currents are smaller in the device without PEDOT the important observation to make is that both the IV characteristics and the magnetoconductance values only show minor variations when the PEDOT layer is omitted in the device. This demonstrates that the relevant processes which cause the OMR effect really take place inside the emitter layer and not in the PEDOT.

Finally, it should be mentioned that a variation of the hole injection efficiency by using alternative anode materials instead of ITO is known to affect the OMR effect in a similar way as a variation of the electron injection efficiency by using different cathode materials [Ngu08].

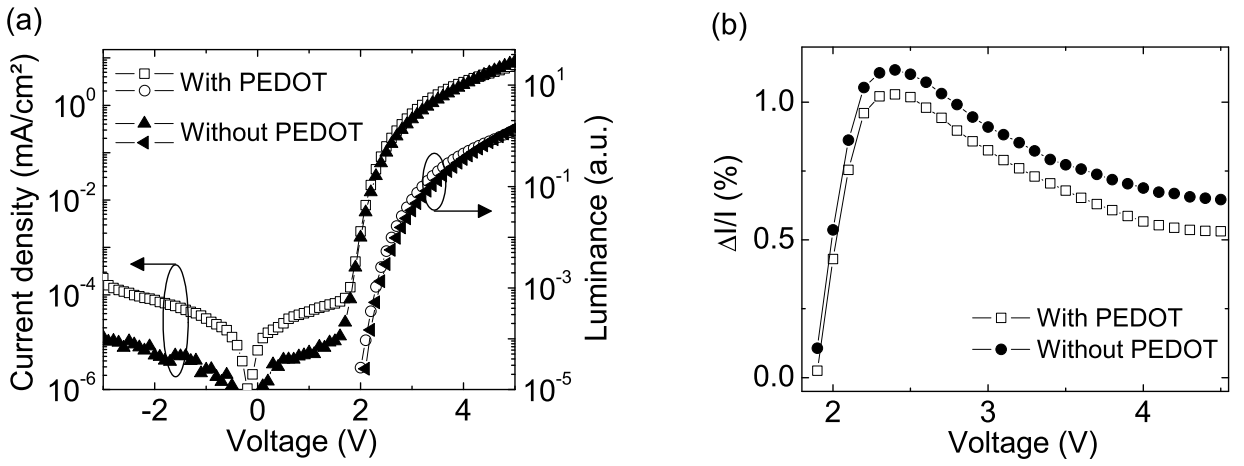

Figure 3.8: (a) IV and LV characteristics of pristine SY-PPV devices with and without PEDOT as hole injection layer, respectively. (b) Magnetoconductance at a magnetic field of 40 mT as a function of voltage for the devices from part (a).

3.3 Temperature dependence of OMR

The OMR effect in bipolar SY-PPV devices was also investigated as a function of temperature. Figure 3.9a shows IV characteristics recorded at different temperatures between room temperature and 90 K. Reducing the temperature monotonically decreases the current at fixed voltage by several orders of magnitude and increases the threshold voltage of substantial charge carrier injection. These results are a consequence of the fact that both charge carrier injection and charge carrier transport are temperature activated processes which become less efficient as temperature is decreased [Bäs93, Ark98].

As illustrated in figure 3.9b the maximum value of the magnetoconductance $\Delta I/I$ shows a non-monotonic dependence on temperature. Starting at room temperature the maximum $\Delta I/I$ first increases as temperature is reduced, then shows a maximum at 210 K and finally decreases as temperature is further reduced. It should be noted that previously a similar non-monotonic dependence on temperature has been reported for the magnetic field effect on photocurrents in different PPV derivatives [Fra92a]. In figure 3.9c

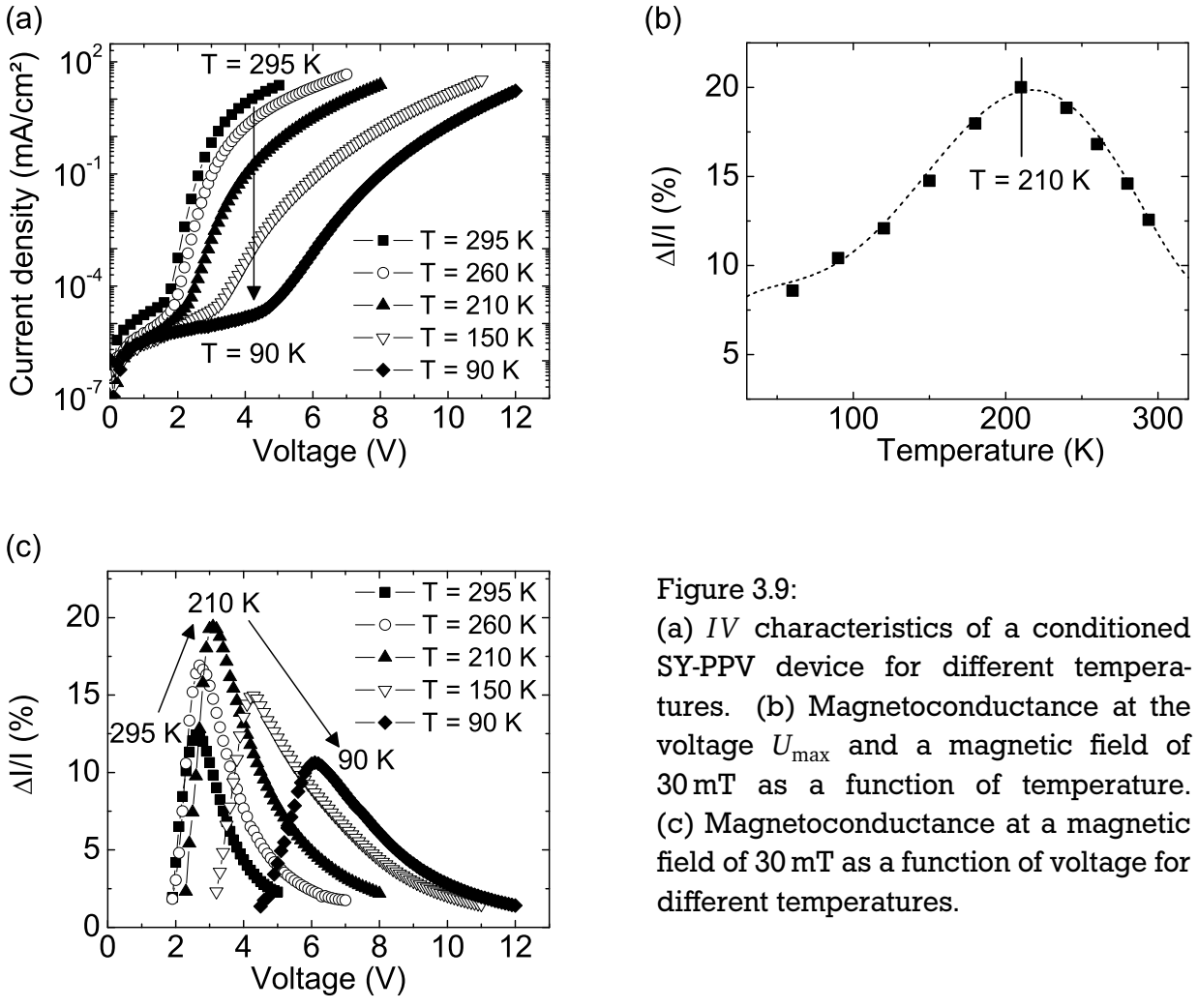

Figure 3.9:
(a) IV characteristics of a conditioned SY-PPV device for different temperatures. (b) Magnetoconductance at the voltage U_{max} and a magnetic field of 30 mT as a function of temperature. (c) Magnetoconductance at a magnetic field of 30 mT as a function of voltage for different temperatures.

magnetoconductance curves as a function of voltage at different temperatures are plotted. It is clearly seen that at lower temperatures a larger voltage is necessary to achieve the maximum $\Delta I/I$. A comparison of figures 3.9a and 3.9c furthermore demonstrates that the voltage at which the magnetoconductance starts to occur coincides with the threshold voltage of substantial charge carrier injection and is also shifted to higher voltages for lower temperatures.

3.4 Influence of illumination on OMR

In a further experiment it was investigated how the OMR effect is influenced by illumination with an external light source and by the resulting photogeneration of additional charge carriers in the OLED device.

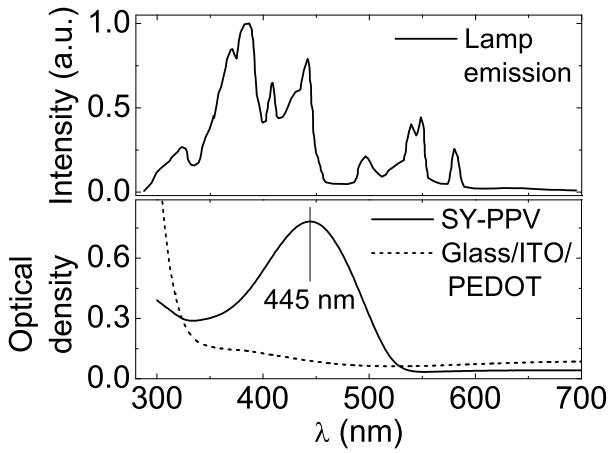

Figure 3.10:
Emission spectrum of the light source Bluepoint 2 and absorption spectra of a 100 nm SY-PPV film on quartz glass and of 120 nm ITO / 120 nm PEDOT on float glass.

Figure 3.10 shows the emission spectrum of the employed light source Bluepoint 2 from Dr. Hönle AG and absorption spectra for the OLED device (measured with a Perkin Elmer absorption spectrometer UV/Vis Lambda 35). The main part of the lamp emission spectrum covers the range from 300 nm to the maximum absorption wavelength of SY-PPV at 445 nm. Only light with wavelengths below 340 nm is considerably absorbed by the ITO-coated float glass and the PEDOT layer so that most of the light reaches the SY-PPV layer. The distance between the OLED device and the light source was chosen in such a way that the device was illuminated with a power density of about 10 mW/cm^2. For the experiment the current flow through a previously electrically stressed SY-PPV device as well as its magnetoconductance were permanently measured over a time period of 25 min with two intermediate illumination intervals of 5 min. This procedure was performed for an applied voltage of 2 V where no OMR was detected in the device in the dark and for a voltage of 4 V where a large magnetoconductance of 23 % at 40 mT was detected in the device without illumination.

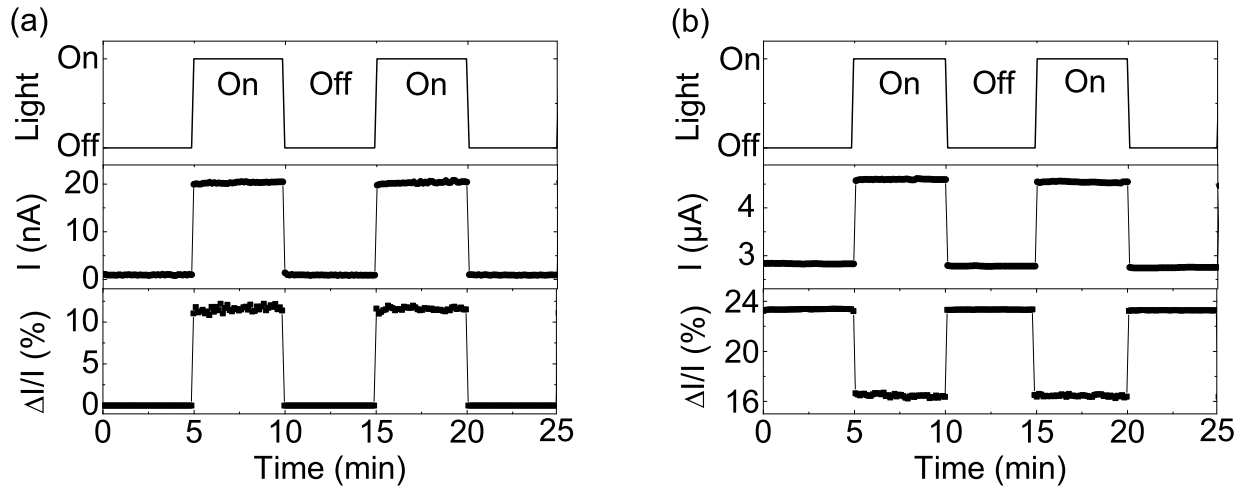

Figure 3.11: Temporal evolution of current at zero magnetic field and magnetoconductance at 40 mT in a conditioned SY-PPV device for an applied voltage of (a) $U = 2\,\mathrm{V}$ and (b) $U = 4\,\mathrm{V}$ during interval illumination with an external light source.

Figure 3.11 demonstrates that for both applied voltages the current through the device is higher during the illumination intervals since additional charge carriers are photogenerated. The stability of the current level during illumination and the sudden changes in current when the light source is switched on and off demonstrate that the device is not heated by the illumination procedure. An analysis of the reaction of $\Delta I/I$ to the illumination shows remarkable differences between the two applied voltages. At 2 V the illumination leads to the appearance of a magnetoconductance of 12 % which immediately vanishes when the light source is switched off. An opposite trend can be observed at 4 V where the magnetoconductance is reduced from 23 % to 17 % upon illumination and immediately returns to the original value of 23 % when the illumination stops.

3.5 Evaluation of most discussed OMR models from literature

In summary, several important features of the OMR effect have been observed in OLED devices based on SY-PPV and can be used to analyze the validity of theoretical models which might potentially explain the OMR effect.

1. Under constant voltage operation the application of a magnetic field increases the current density through a bipolar SY-PPV device and increases its light output.
2. Magnetic field effects on current and electroluminescence are only observed above the threshold voltage of substantial charge carrier injection and show a nonlinear dependence on the magnetic field.

3. The magnetoconductance shows a non-monotonic dependence on voltage, the magnetoelectroluminescence typically decreases monotonically with increasing voltage.
4. Under constant current operation the application of a magnetic field decreases the voltage and increases the electroluminescence intensity. The absolute values of $\Delta U/U$ and $\Delta EL/EL$ at fixed magnetic field decrease with increasing current density.
5. The magnetoconductance in hole-dominated SY-PPV devices is smaller than in comparable bipolar devices.
6. The maximum value of the magnetoconductance shows a non-monotonic dependence on temperature.
7. Illumination with an external light source can increase or decrease the magnetoconductance values in a SY-PPV device depending on the voltage range of device operation.

In the following paragraphs a detailed analysis will be presented which allows to evaluate the three models which are most intensively discussed in literature on the OMR effect. Even though each of these models can account for some experimental results, it will be pointed out that none of the models is suited for a fully consistent interpretation of all data that have been obtained in magnetic field dependent measurements of SY-PPV devices.

3.5.1 Evaluation of the bipolaron model

In the bipolaron model it is claimed that the charge carrier mobility is influenced via a magnetic field dependent formation of doubly occupied hopping sites.
The bipolaron model is in contradiction to the experimental finding that the light output from a SY-PPV device at constant current density can be increased by the application of a magnetic field (see figure 3.4). In general, an increase in the device efficiency at constant current density can only be due to an increase in the number of formed singlet excitons or due to a reduction of exciton quenching, for instance by shifting the recombination zone in SY-PPV devices away from the cathode. Since the proposed mechanisms in the framework of the bipolaron model do not affect the ratio between singlet and triplet excitons the only possible explanation for a positive $\Delta EL/EL$ at constant current density in accordance with the bipolaron model is a shift of the recombination zone away from the cathode. This can only be achieved if the magnetic field reduces the hole mobility in SY-PPV, which would result in a higher voltage (i.e., a positive $\Delta U/U$) in order to keep the current density in the device constant. However, this is in contradiction to the strictly negative values of $\Delta U/U$ at constant current density which were observed in figure 3.4.
Since the bipolaron mechanism only involves one species of charge carriers the OMR ef-

fect is also predicted to be measurable in unipolar devices where no e-h pair and exciton formation takes place. Francis *et al.* claimed that they indeed succeeded in measuring a magnetoconductance of several percent in a hole-only device using an ITO/PFO/Au stack [Fra04]. However, a closer look at their results shows that the measurements were performed at very high operating voltages above 40 V where a weak EL signal from the device was detected. Hence, this demonstrates that both types of charge carriers were present in the device and that the charge transport was not unipolar as stated by the authors. In a different study Gärditz *et al.* showed that no magnetoconductance values above 0.03 % could be achieved in electron-only Alq_3 devices [Gär05]. Wang *et al.* recently reported a small magnetoconductance of about 1 % in electron-only MEH-PPV devices at $T = 6\,K$ [Wan08]. However, the authors did not mention whether this value of the OMR effect persists up to room temperature. In yet another study a magnetoconductance of several percent was detected in "almost hole-only" Alq_3 devices whereas no OMR effect was measured in "almost electron-only" Alq_3 devices [Ngu08]. In order to explain the latter results on the basis of the bipolaron model, it was proposed in reference [Ngu08] that bipolarons in general might only be formed by the type of charge carriers which have a lower mobility and do not dominate the charge transport in the investigated materials (i.e., holes in Alq_3). Following this assumption the reduced magnetoconductance in hole-dominated SY-PPV devices compared to bipolar SY-PPV devices at comparable current density (see figure 3.7b) could potentially be explained by the smaller concentration of injected electrons, which are known to have a lower mobility than holes in PPV [Blo01, Man07]. However, no direct physical evidence exists which could justify a restriction of the bipolaron model to the charge carriers with lower mobility in an organic material. In fact, even the authors of reference [Ngu08] themselves pointed out that their suggested limitation of the bipolaron model is only speculative at the moment.
Finally, it should be added that even though charge carrier mobilities in organic semiconductors have been extensively studied for a long time no direct proof of a magnetic field dependence of mobility has been reported in literature on charge carrier transport measurements so far.

3.5.2 Evaluation of the exciton model

In the exciton model it is proposed that magnetic field dependent changes of the exciton formation rate affect the current flow in a bipolar device.
However, it was shown in literature that the fundamental relation (2.8) in section 2.5.2 which connects current density and the exciton formation rate is only valid in the regime of recombination-limited currents where electrons and holes form an e-h plasma and have a weak recombination probability [Mar01]. Hence, all conclusions that are based on this

relation can only be true in the situation of recombination-limited currents and do not apply to the situation of space-charge-limited currents as it was stated by the authors in the context of the e-h pair model [Pri06]. Furthermore, it was demonstrated in literature that in order to reach this situation of recombination-limited currents large electric fields above 25 V/μm need to be present in devices based on OC_1C_{10}-PPV [Mar01]. Assuming that a similar value holds for SY-PPV it can be estimated that in the standard OLEDs used in this thesis (100 nm SY-PPV thickness) voltages above 5 V would have been necessary in order to form an e-h plasma with recombination-limitation. In contrast, it is evident from figure 3.2 that the OMR effect in these devices already starts to occur at much lower voltages.
In the exciton model the dependence of the OMR effect on the operating voltage is assumed to be caused by the electric field dependence of the dissociation rate of triplet e-h pairs and is predicted to result in an increase in the magnetoconductance with increasing voltage. However, this is in clear contradiction to the decrease of $\Delta I/I$ for voltages above U_{max}, which was shown in figure 3.2b and also reported in literature [Des07a].
It is furthermore argued in the framework of the exciton model that according to equation (2.9) the OMR values should monotonically decrease with decreasing temperature since the dissociation probability of triplet e-h pairs is reduced. This is not in line with the experimental results in figure 3.9c where it was demonstrated that a non-monotonic temperature dependence is observed for the magnetoconductance at fixed voltage.
In the exciton model no explicit statements are made concerning the change $\Delta EL/EL$ in electroluminescence under the influence of a magnetic field. It is only assumed that a decrease of the exciton formation rate due to a magnetic field leads to an increase in the current flow through the device. A reduced exciton formation rate, however, would lead to a reduced number of singlet excitons and a decrease of the EL intensity. Hence, $\Delta I/I$ and $\Delta EL/EL$ would be expected to have opposite signs according to the exciton model. This is in clear contradiction to the observation that both $\Delta I/I$ and $\Delta EL/EL$ can be positive, which was demonstrated in figures 3.2 and 3.3 and in references [Des07a, Wu07, Ngu08].

3.5.3 Evaluation of the exciton polaron interaction model

In the EPI model a magnetic field is assumed to influence the number of triplet excitons which potentially act as scattering centers for free charge carriers.
One key aspect of the EPI model is the idea that a magnetic field increases the intersystem crossing rate for transitions from the excitonic triplet state to the excitonic singlet state. Hence, the concentration of singlet excitons is assumed to be increased at the expense of the concentration of triplet excitons in the presence of a magnetic field. This is in contradiction to results from Reufer *et al.* who demonstrated that the concentrations of singlet excitons and triplet excitons in organic materials with efficient intersystem crossing are

both increased in a comparable way upon application of a magnetic field [Reu05].
Furthermore, own magnetic field dependent measurements of the PL signal from SY-PPV devices as well as literature data on PL measurements of Alq_3 devices [Gär05] showed no influence of a magnetic field on the (in fluorescent materials very small) intersystem crossing rate.
In addition, it seems unplausible from an energetic point of view to have a considerable amount of transition events from excitonic triplet states to excitonic singlet states in these materials. The energetic difference between singlet level and triplet level in organic materials is typically on the order of several 100 meV ($\approx$ 700 meV in Alq_3 [Cöl04] and in conjugated polymers [Köh02]). This energetic difference is significantly larger than the thermal energy at room temperature ($\approx$ 25 meV) and the Zeeman splitting (on the order of μeV) for the magnetic fields under consideration.
Finally, it is mentioned in the framework of the EPI model that the observation of the OMR effect is expected to occur only for voltages above the threshold voltage of light emission. However, it is questionable whether scattering events between charges and triplet excitons can already cause significant changes in current at low voltages where the concentrations of charge carriers and excitons inside the device are still low.

3.6 Discussion of the electron-hole pair model

It is remarkable that in recent literature the discussion regarding the mechanism behind the OMR effect is mainly focused on the three proposed theoretical models which were evaluated in the previous sections. Two out of these three models (i.e., the exciton model and the exciton polaron interaction model) are to a certain extent based on the concept of a magnetic field dependent mixing of different spin states in charge carrier complexes of electrons and holes. This concept which was discussed in section 2.4 was originally introduced by Frankevich *et al.* in order to explain magnetic field effects on photocurrents [Fra92a]. According to this study a magnetic field affects the lifetime of e-h pairs and changes their concentration in the steady state. Even though it is often overlooked in recent publications, Kalinowski *et al.* were first in suggesting the importance of a magnetic field influence on the spin conversion of e-h pairs for the OMR effect. Already in their original publication on the discovery of the OMR effect in Alq_3 devices Kalinowski *et al.* proposed that magnetic field dependent changes in the stage of e-h pairs lead to an increased ratio between singlet and triplet excitons in a device [Kal03a]. Furthermore, it was argued that the observed increase in current flow through Alq_3 devices can be attributed to an increased number of singlet excitons diffusing to the cathode and contributing to the charge carrier injection. However, the final step of the proposed argumentation can be challenged by the fact that singlet excitons typically have very short lifetimes so that

a considerable diffusion of singlet excitons to the cathode (in order to cause a significant change in current) seems unlikely.
In summary, it can be stated that even though the principle of magnetic field dependent spin-conversion of e-h pairs is a substantial part of previously suggested models a consistent link between this principle and the experimental results regarding the OMR effect has not been provided so far.

In the following section an e-h pair model for the OMR effect will be discussed which is largely based on ideas from Frankevich *et al.* [Fra92a] and Kalinowski *et al.* [Kal03a] but modified in a way to allow a plausible explanation of magnetic field induced changes in current and electroluminescence in OLED devices [Bag09b]. Even though it is not claimed here that the e-h pair model is the only correct way of describing the OMR effect, it will be shown in section 3.7 that the model allows a qualitative explanation of all functional dependencies of the OMR effect which were obtained in SY-PPV devices in the course of this thesis.

3.6.1 General description of the electron-hole pair model

The main idea of the e-h pair model is that a magnetic field affects the lifetime of e-h pairs and changes their overall concentration in a device in the steady state, which is eventually assumed to cause changes in the current flow and the light output from the device.

During the device operation of an OLED uncorrelated electrons and holes approach each other under the influence of an electric field and form correlated e-h pairs. A magnetic field is assumed to influence the spin state of e-h pairs when the intercharge separation distance is in a range where spin conversion due to the hyperfine interaction can possibly occur within the e-h pair. A prerequisite for this potential spin mixing is that electrons and holes are already coulombically bound but still separated from each other far enough so that the spin-spin interaction is negligibly small compared to the hyperfine interaction. Since an e-h pair either recombines and forms an exciton or dissociates back into free charge carriers the lifetime of an e-h pair is determined by the interplay of recombination and dissociation rate constants, respectively. It is important to note that these rate constants are assumed to depend on the spin state of the e-h pair, which makes the lifetime of e-h pairs a key parameter for the characterization of the magnetic field effect in the e-h pair model.

In section 2.4 it was shown that in the absence of a magnetic field a spin mixing due to the hyperfine interaction can possibly occur and the e-h pairs can be considered to have an equal probability of being in the singlet state or in one of the three triplet configurations. Hence, all e-h pairs are assumed to have a common lifetime in this case. The application of

an external magnetic field which is stronger than the hyperfine interaction strength causes a Zeeman splitting and lifts the degeneracy of the three triplet levels. It is argued that due to the Zeeman splitting and due to the fact that thermal equilibrium is not yet reached the spin mixing only remains between the singlet state and the T_0 triplet state, whereas the T_{+1} and the T_{-1} states are pure triplet states that can no longer mix with the singlet state. As a consequence, the external magnetic field is assumed to also change the average lifetime of the e-h pairs in the device. The lifetime, in turn, determines the concentration of e-h pairs which are present in an OLED device in the steady state during device operation. As it will be shown below, the application of a magnetic field is supposed to change the average e-h pair lifetime in such a way that the concentration of e-h pairs in the steady state is increased. As a consequence, the concentration of singlet excitons from e-h pair recombination and the concentration of free charges from e-h pair dissociation are also assumed to increase.

Based on these considerations the magnetic field effects on current and electroluminescence might be explained in the following way: The dissociation of e-h pairs in a device can produce secondary charge carriers (which is equivalent to an effectively reduced Langevin recombination rate constant in the device [Neu05]). An external magnetic field is assumed to influence the e-h pair lifetime and to directly affect the number of produced secondary charge carriers. According to reports from literature this production of secondary charge carriers can reduce space charge effects and improve both charge carrier injection and charge carrier transport in a device [Mar01, Neu05, Hu07]. The magnetoconductance $\Delta I/I$ at constant voltage is therefore considered to be a consequence of the enhanced current flow due to this space charge cancellation. In combination with the magnetic field dependent change in the concentration of formed singlet excitons the enhancement of the current flow is suggested to be responsible for the increase in the light output of the device, which can be measured as magnetoelectroluminescence $\Delta EL/EL$ in experiment.

According to the e-h pair model a prerequisite for the observation of large values for $\Delta I/I$ and $\Delta EL/EL$ is that a large number of e-h pairs participates in the magnetic field dependent spin mixing due to the hyperfine interaction. This situation can only be achieved if the e-h pairs have a lifetime which is longer than the time of spin evolution. In this context it is important to take into account a possible influence of the externally applied voltage on the magnetic field effects. The voltage causes an electric field inside the device which controls the speed at which injected electrons and holes approach each other. With increasing voltage (and increasing electric field) the speed of the charge carriers increases, which in turn causes a decrease of the e-h pair lifetime. As a consequence, it is expected that fewer e-h pairs can be affected by the magnetic field and that the obtained values for both $\Delta I/I$ and $\Delta EL/EL$ decrease with increasing voltage.

3.6.2 Mathematical description of the electron-hole pair model

In the following it will be analyzed under which conditions it is possible at all to obtain positive values for both $\Delta I/I$ and $\Delta EL/EL$ as it was experimentally observed in SY-PPV devices in this thesis. For this purpose, a more formal treatment of the e-h pair model will be presented which allows to draw general conclusions about the sign of the magnetic field effects on current and luminance. Similar considerations were already made by Frankevich *et al.* in the context of magnetic field dependent photocurrents [Fra92a]. Here, these ideas are transferred to the case of charge carrier recombination in OLED devices [Bag09b]. For a better understanding of the following argumentation the relevant energy levels of charge carrier pair states and transition rates between them are depicted in figure 3.12 similar to an illustration which was previously introduced in reference [Fra92a].

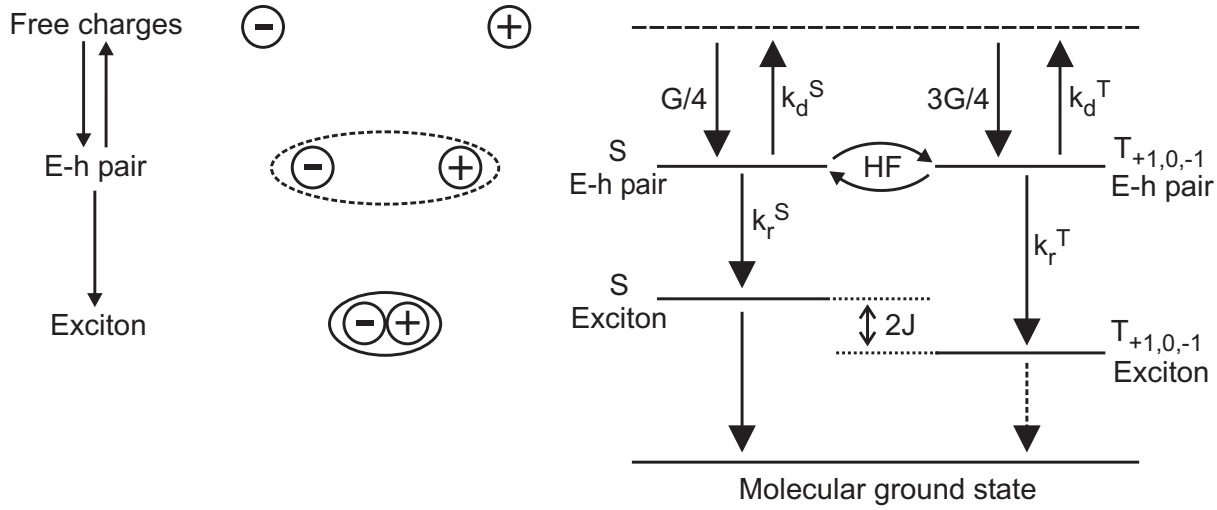

Figure 3.12: Schematic energy level diagram and relevant rate constants for transitions involving free charge carriers, electron-hole pairs and excitons at zero magnetic field. S and T indicate singlet and triplet states, respectively. G denotes the creation rate of e-h pairs. $k_{\mathrm{d}}^{\mathrm{S}}$ and $k_{\mathrm{d}}^{\mathrm{T}}$ are the dissociation rate constants, $k_{\mathrm{r}}^{\mathrm{S}}$ and $k_{\mathrm{r}}^{\mathrm{T}}$ are the recombination rate constants for singlet and triplet e-h pairs, respectively. See text for details.

Electrons and holes are injected into the device and form e-h pairs with a total generation rate G which depends on the current density in the device. Moreover, the ratio of the formation rates $\mathrm{d}N_{\mathrm{S}}/\mathrm{d}t$ of singlet e-h pairs and $\mathrm{d}N_{\mathrm{T}}/\mathrm{d}t$ of triplet e-h pairs is determined by the formation cross sections for e-h pair formation in the singlet state (σ_{S}) and in the triplet state (σ_{T}), respectively [Woh03]:

$$\frac{\mathrm{d}N_{\mathrm{S}}/\mathrm{d}t}{\mathrm{d}N_{\mathrm{T}}/\mathrm{d}t} = \frac{\sigma_{\mathrm{S}} G}{3\sigma_{\mathrm{T}} G} = \frac{\sigma_{\mathrm{S}}}{3\sigma_{\mathrm{T}}}. \tag{3.3}$$

For simplicity, only the case of spin independent e-h pair formation with $\sigma_S/\sigma_T = 1$ will be considered in the following. It is assumed that in zero magnetic field singlet and triplet e-h pairs are fully mixed and can be described by a common lifetime τ_0 which is given by the following expression:

$$\tau_0 = \frac{1}{(k_r^S + k_d^S) + 3(k_r^T + k_d^T)}, \tag{3.4}$$

where k_r^S and k_r^T denote the recombination rate constants, and k_d^S and k_d^T denote the dissociation rate constants of pure singlet and triplet e-h pair states, respectively. The concentration N_0 of e-h pairs at zero magnetic field in the steady state can be written as

$$N_0 = \left(\frac{G}{4} + \frac{3G}{4}\right)\tau_0 = G\tau_0. \tag{3.5}$$

In the presence of a strong magnetic field the spin mixing is supposed to be restricted to the singlet and the T_0 triplet state. As a consequence, the e-h pair population is assumed to be divided into a set of three independent subpopulations. For the S-T_0 subpopulation the lifetime τ_{ST} is given by

$$\tau_{ST} = \frac{1}{(k_r^S + k_d^S) + (k_r^T + k_d^T)}. \tag{3.6}$$

The T_{+1} and the T_{-1} states can be treated as two additional subpopulations with equal lifetime τ_T which can be written as

$$\tau_T = \frac{1}{k_r^T + k_d^T}. \tag{3.7}$$

Since the system is assumed not to be in thermal equilibrium the occupations of the T_{+1} and the T_{-1} subpopulations are considered to be equal. The concentration N_B of e-h pairs in the presence of a magnetic field can be written as a sum of the contributions from the individual subpopulations:

$$N_B = N_{ST} + 2N_T = \frac{G}{4}(2\tau_{ST} + 2\tau_T), \tag{3.8}$$

where N_{ST} and N_T are the concentrations of e-h pairs in the mixed state and in the triplet subpopulations, respectively. Using expressions (3.5) and (3.8) for the concentration of e-h pairs without and with applied magnetic field it is straight forward to calculate the magnetic field effect $\Delta N/N$ for the concentration of e-h pairs in the steady state.

Introducing the relation

$$\frac{\tau_S}{\tau_T} = \frac{k_r^T + k_d^T}{k_r^S + k_d^S} \tag{3.9}$$

for the ratio between the lifetimes of pure singlet and triplet e-h pair states, respectively, it is possible to express $\Delta N/N$ in the following way:

$$\frac{\Delta N}{N} = \frac{N_B - N_0}{N_0} = \frac{4\left(\tau_S/\tau_T\right)^2 + 3\tau_S/\tau_T + 1}{2\left(1+\tau_S/\tau_T\right)\tau_S/\tau_T}. \tag{3.10}$$

From equation (3.10) it is apparent that $\Delta N/N$ is always positive. Thus, one of the main statements within the e-h pair model is that a magnetic field increases the steady state concentration of e-h pairs by influencing the spin mixing between different e-h pair states.

In appendix A it is shown that in a similar way it is possible to derive expressions for the magnetic field effects on the concentration of singlet excitons ($\Delta S/S$), on the concentration of triplet excitons ($\Delta T/T$) and on the concentration of secondary charge carriers from e-h pair dissociation ($\Delta Q/Q$) in the limit of large magnetic fields:

$$\frac{\Delta S}{S} = \frac{\tau_S/\tau_T - 1}{2\left(1+\tau_S/\tau_T\right)}, \tag{3.11}$$

$$\frac{\Delta T}{T} = \frac{1 - \tau_S/\tau_T}{6\left(1+\tau_S/\tau_T\right)\tau_S/\tau_T}, \tag{3.12}$$

$$\frac{\Delta Q}{Q} = \frac{\left(\tau_S/\tau_T - 1\right)\left(\tau_S/\tau_T - k_d^T/k_d^S\right)}{2\left(1+\tau_S/\tau_T\right)\tau_S/\tau_T\left(1+3k_d^T/k_d^S\right)}. \tag{3.13}$$

The change $\Delta Q/Q$ of the concentration of secondary charge carriers is assumed to be responsible for the magnetoconductance $\Delta I/I$ while the change $\Delta S/S$ of the concentration of singlet excitons presumably causes the magnetoelectroluminescence $\Delta EL/EL$.

Figure 3.13a illustrates the magnetic field effects $\Delta N/N$, $\Delta S/S$ and $\Delta T/T$ as a function of the ratio τ_S/τ_T of the lifetimes of singlet and triplet e-h pairs. It is apparent that according to the e-h pair model a positive $\Delta S/S$ (and, hence, a positive $\Delta EL/EL$) can only be observed if the lifetime of singlet e-h pairs is longer than the lifetime of triplet e-h pairs ($\tau_S/\tau_T > 1$). In the case of spin independent e-h pair formation ($\sigma_S/\sigma_T = 1$) the maximum possible value of $\Delta S/S$ is 50 %. However, even larger values can be obtained when the assumption is made that the process of e-h pair formation is spin dependent and

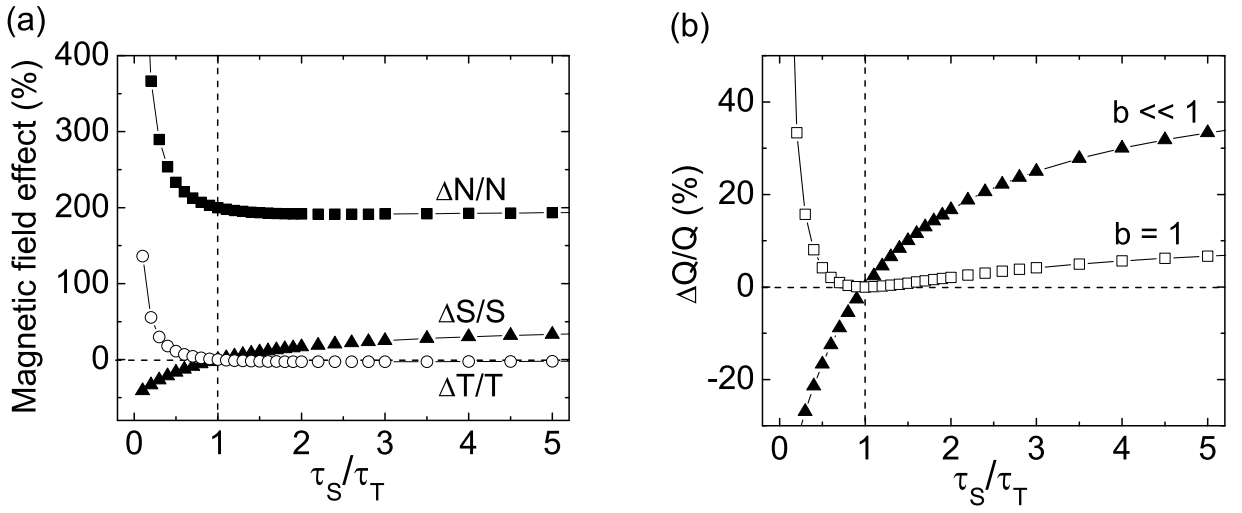

Figure 3.13: (a) Calculated magnetic field effects for the concentration of e-h pairs ($\Delta N/N$), for the concentration of singlet excitons ($\Delta S/S$) and for the concentration of triplet excitons ($\Delta T/T$) as a function of τ_S/τ_T in the limit of large magnetic fields. (b) Calculated magnetic effect for the concentration of secondary charge carriers from e-h pair dissociation ($\Delta Q/Q$) for different values of $b = k_d^T/k_d^S$ as a function of τ_S/τ_T in the limit of large magnetic fields. See text for details.

$\sigma_S/\sigma_T > 1$. In fact, it was recently shown experimentally that for a variety of polymer materials this is indeed the case [Woh01, Dho02, Woh02].

It is important to note that independent of the ratio of σ_S/σ_T the maximum (negative) value of the magnetic field effect $\Delta T/T$ for the concentration of triplet excitons is only about -3 %. At first glance, this might seem to be in contradiction with results from literature where it was shown that in certain polymer-based devices the intensities of both fluorescence and phosphorescence are increased when the devices are exposed to a magnetic field [Reu05]. However, the investigated devices contained a material with a considerable intersystem crossing rate between the excitonic singlet state and the excitonic triplet state. Hence, the results can be brought in line with the e-h pair model by considering the possibility that in materials with very efficient intersystem crossing the large increase $\Delta S/S$ in the concentration of singlet excitons upon magnetic field application can also cause $\Delta T/T$ to become positive.

Figure 3.13b shows the magnetic field effect on the concentration of secondary charge carriers which are assumed to be responsible for the magnetoconductance. The value and sign of $\Delta Q/Q$ (and, hence, $\Delta I/I$) depend on the ratio τ_S/τ_T between singlet and triplet e-h pair lifetimes as well as on the ratio $b = k_d^T/k_d^S$ between the dissociation rate constants of the corresponding e-h pairs.

In summary, an analysis of equations (3.11) and (3.13) shows that positive values for both $\Delta I/I$ and $\Delta EL/EL$ can only be obtained when the conditions $\tau_S/\tau_T > 1$ and $\tau_S/\tau_T > b$ are fulfilled. In fact, it was suggested in literature that singlet e-h pairs have a lower binding energy than triplet e-h pairs [Kal03a, Woh03], which makes it reasonable to assume $b < 1$. Hence, it is likely that the only condition to obtain positive values of both $\Delta I/I$ and $\Delta EL/EL$ is that the lifetime of pure singlet e-h pair states is longer than the lifetime of pure triplet e-h pair states, which results in $\tau_S/\tau_T > 1$.

These considerations demonstrate that in principle it is possible to explain positive values of $\Delta I/I$ and $\Delta EL/EL$ in the framework of the e-h pair model. However, a major drawback of the presented analysis is the fact that the ratio τ_S/τ_T is hard to determine because the relevant parameters τ_S and τ_T are quantities which are not directly accessible in experiment.

3.7 Experimental verification of the electron-hole pair model

On the basis of the e-h pair model it is now possible to interpret the results which have been obtained in SY-PPV devices and which were summarized on pages 50 and 51.

1. According to the e-h pair model the application of a magnetic field is assumed to increase the concentration of e-h pairs inside the organic material. The secondary current from the dissocation of e-h pairs is supposed to lead to an increased current flow and to the positive values of $\Delta I/I$ in figure 3.2. Moreover, the increased concentration of e-h pairs and the increased concentration of singlet excitons upon magnetic field application are a potential explanation for the larger EL intensity and the positive values of $\Delta EL/EL$ that are observed in figure 3.3.
   It should be noted that mostly positive values of $\Delta I/I$ and $\Delta EL/EL$ were reported in literature for a variety of materials [Fra04, Des07a, Wu07]. Only in a few cases small negative values of $\Delta I/I$ were observed for particular operating voltages or selected temperatures [Mer05b, Blo08a]. This is not in contradiction to the e-h pair model since figure 3.13b shows that the expression for the magnetic field induced change $\Delta Q/Q$ of the concentration of secondary charge carriers (which is related to the magnetoconductance $\Delta I/I$) can become negative in certain parameter ranges.

2. Since the formation of e-h pairs is fundamental for the e-h pair model the presence of both electrons and holes in a device is supposed to be a prerequisite for the occurrence of the OMR effect. This consideration is in line with the experimental finding that the OMR effect can only be observed above the threshold voltage of efficient charge carrier injection, which is shown in figure 3.2 and reported in references [Des07a, Des07b]). Additionally, the e-h pair model might explain why the appli-

cation of a magnetic field changes the EL intensity (see figure 3.3) whereas it does not influence the PL intensity. In order to obtain electroluminescence, both types of charge carriers have to be electrically injected and need to pass the e-h pair stage before they can form excitons that decay radiatively. In the process of photoluminescence singlet excitons are optically excited and immediately decay after excitation without ever being in the e-h pair stage where a magnetic field dependent spin conversion process could take place.

The characteristic line shape and the involved fitting parameter B_0 for the magnetic field dependent curves of $\Delta I/I$ and $\Delta EL/EL$ in figures 3.2 and 3.3 might be an indication that spin mixing due to the hyperfine interaction indeed is involved in the OMR mechanism. It was reported in literature that a similar line shape can be derived from the hyperfine interaction Hamiltonian and that the fitting parameter B_0 of the magnetic field dependent curves might be related to the strength of the hyperfine interaction [She06]. The observed value $B_0 = 3\,\mathrm{mT}$ in the measurements of SY-PPV devices is identical to a reported value of B_0 for MDMO-PPV in reference [Blo08b]. Furthermore, it should be mentioned that in other measurements of magnetoresistance [Mer05b, She06] and photocurrents [Fra92a] similar nonlinear magnetic field dependencies were observed and were also explained in terms of hyperfine interaction induced spin mixing.

3. Based on the e-h pair model it is also possible to suggest a mechanism which leads to the non-monotonic shape of the voltage dependent magnetoconductance curves that are shown in figure 3.2b. To explain this non-monotonic shape it is assumed that the value of $\Delta I/I$ is determined by two processes with opposite dependence on the voltage. With increasing voltage more charge carriers are injected into the device and a larger number of e-h pairs are formed which can potentially be influenced by the magnetic field. At low voltages around the built-in potential the internal electric field is still low and the influence of this field on the lifetime of e-h pairs is still negligible. Hence, it seems reasonable that a monotonic increase of the $\Delta I/I(U)$ curve can be observed in this range. However, with increasing voltage and increasing electric field the lifetime of the e-h pairs is assumed to be reduced so that fewer e-h pairs live long enough for spin evolution to take place. This is considered to be responsible for the monotonic decrease of the $\Delta I/I(U)$ curve which prevails at higher voltages. According to the e-h pair model the existence of a voltage U_{max} with maximum OMR effect is a direct consequence of this competition between an increase in e-h pair density and an electric-field induced reduction of the lifetime of e-h pairs.

   It should be mentioned that the non-monotonic shape of the $\Delta I/I(U)$ curve was also reported in reference [Des07a]. However, several other publications only show a monotonic decrease of the magnetoconductance with increasing voltage

[Fra04, Mer05b, Pri06]. In the latter studies rather high voltages were applied to the investigated devices. Hence, it is likely that the voltages exceeded the corresponding values of U_{max} so that the influence of the electric field on the e-h pair lifetime dominated the OMR effect.

4. The magnetic field dependent measurements at constant current in figure 3.4 can be interpreted as an additional support for the assumption that the lifetime of e-h pairs is of particular importance for the OMR effect. Operating a device at constant current density ensures that a constant number of e-h pairs are formed in the device. The observed increase in electroluminescence upon application of a magnetic field indicates an increased concentration of singlet excitons, which is in line with equation (3.11). Since the magnetic field dependent secondary current from e-h pair dissociation presumably reduces the amount of space charges a smaller voltage is necessary in the presence of a magnetic field to maintain the same current flow through the device as in the zero-field case. Altogether, the influence of the electric field on the lifetime of e-h pairs is supposed to be responsible for the decrease of both $|\Delta U/U|$ and $\Delta EL/EL$ at constant magnetic field with increasing current density in figure 3.4c.

5. The e-h pair model furthermore provides a possible explanation for the observation that the charge carrier balance within a device is of great importance for the OMR effect and that different cathode materials lead to different OMR values. In the hole-dominated device in figure 3.7 the number of injected electrons and, as a consequence, the concentration of formed e-h pairs is significantly reduced compared to the bipolar device. Since according to the e-h pair model the concentration of e-h pairs which are influenced by the magnetic field is related to the value of the OMR effect, this might explain why only small OMR values are detected in the hole-dominated device.

   In a similar way the observed reduction of the magnetoconductance in SY-PPV devices upon introducing PtOEP into the emission layer might be understood (see figure 3.6). Due to the efficient trapping of electrons the number of formed e-h pairs is expected to be smaller in SY-PPV:PtOEP devices compared to pure SY-PPV devices. In addition, the reduced OMR values in these devices might be caused by the fact that the lifetime of e-h pairs involving a deeply trapped electron can become larger than the spin-lattice relaxation time. However, in section 2.4 it was shown that magnetic field effects on the spin states of e-h pairs in general can only be expected under the condition that the lifetime of the e-h pairs is shorter than the spin-lattice relaxation time.

6. In the context of the e-h pair model it is also possible to understand the temperature dependence of $\Delta I/I(\mathrm{U})$. Figure 3.14a shows a slightly different way of presenting the

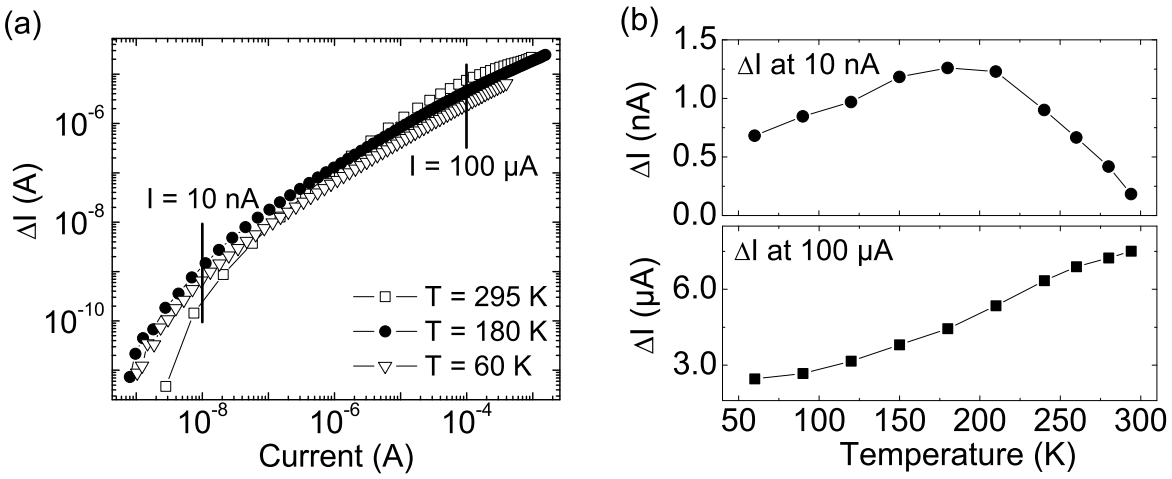

Figure 3.14: (a) Absolute change ΔI in current at a magnetic field of 30 mT as a function of current for a conditioned SY-PPV device at different temperatures. (b) Absolute change ΔI in current at a magnetic field of 30 mT for two selected currents as a function of temperature.

data from figure 3.9 by plotting the change in current ΔI due to the magnetic field as a function of current for different temperatures.

Two distinct current regimes can be identified in which ΔI demonstrates different temperature dependencies. Figure 3.14b demonstrates that for a small current of 10 nA ΔI first increases as temperature is reduced, followed by a slight decrease at low temperatures. With decreasing temperature the charge carrier mobility is reduced and the lifetime of the e-h pairs is increased. Consequently, the number of e-h pairs that are affected by the magnetic field is assumed to increase, which presumably causes the increasing change ΔI in current with decreasing temperature down to 180 K. A comparison with the voltage dependence of $\Delta I/I$ in figure 3.9c shows that the regime of small currents on the order of 10 nA is in a voltage range below U_{max} for each temperature. At high temperatures the corresponding electric field in this voltage range is small and the influence of the electric field on the lifetime of the e-h pairs is not assumed to be significant. As temperature is decreased, the $\Delta I/I(U)$ curves are shifted to higher voltages. In addition, larger voltages and larger electric fields are necessary to maintain a certain current density at lower temperatures. As a consequence, the proposed influence of the electric field becomes stronger at lower temperatures and is considered to be responsible for the slight decrease of the value of ΔI with decreasing temperature below 180 K. The regime of high currents (on the order of 100 μA) in figure 3.14b corresponds to the voltage regime above U_{max} in the curves from figure 3.9c. Here, the influence of the electric field is assumed to dominate the dependence of ΔI on the temperature and might be an explanation for the reduction of ΔI at fixed current as temperature is decreased.

A closer look at figure 3.9c might furthermore allow to solve the discrepancies regarding different temperature dependencies that have been reported for the OMR effect in literature. In references [Fra04, Mer05a] the magnetoresistance values in PFO and Alq_3 are claimed to be insensitive to temperature changes in the range from 10 K to 300 K. However, in both studies the magnetoresistance was only investigated in a small voltage range which was shifted to higher voltage values as temperature was reduced. It is apparent from figure 3.9c that by choosing selected voltage values it is possible to obtain a constant magnetoconductance value (e.g., $\Delta I/I = 10\,\%$ in figure 3.9c) over a large temperature range. Hence, analyzing the OMR effect only for selected voltages provides an incomplete picture.
In a different study the magnetoconductance in a small molecule device with 100 nm Alq_3 as emitting layer was shown to monotonically decrease at a constant voltage of 10 V as temperature is decreased from room temperature to 130 K [Blo08a]. Since the applied voltage was significantly higher than the voltages that were applied to the SY-PPV devices of similar thickness in section 3.3, the internal electric fields were obviously higher in the Alq_3 device. Hence, the proposed influence of the electric field on the lifetime of e-h pairs might have governed the OMR effect in the investigated Alq_3 device even at room temperature. Therefore, the observed reduction of the magnetoconductance might be explained by a reduced number of formed e-h pairs as a consequence of a lower current density at fixed voltage at lower temperatures.

7. The results on magnetoconductance in SY-PPV devices under illumination from figure 3.11 can also be interpreted on the basis of the e-h pair model. At a low voltage of 2 V only very few e-h pairs are formed after electrical injection. An illumination with highly energetic light leads to the photogeneration of free charge carriers which can form e-h pairs under the influence of the applied voltage. The increased magnetoconductance as a consequence of the increased concentration of e-h pairs in the device during illumination can be understood in the framework of proposed explanations for the magnetic field effect on photocurrents as discussed in section 2.3.2. At a voltage of 4 V a large number of e-h pairs are formed after electrical injection, and large magnetoconductance values are observed in the dark. Illuminating the device is again supposed to result in a creation of additional e-h pairs. However, the illumination also provides an additional source of energy for the electrically injected e-h pairs and might facilitate their dissociation. In total, the number of dissociated e-h pairs might even be larger than the number of additionally created e-h pairs. Hence, the reduced magnetoconductance during the illumination periods could be explained assuming that the highly energetic illumination reduces the number of e-h pairs which can possibly be influenced by the magnetic field.

In summary, it can be stated that the e-h pair model provides a suitable basis for a qualitative explanation of experimental results concerning magnetic field effects in OLED devices. The fact that the e-h pair model is the only concept which is in line with all experimental results obtained in this thesis certainly favors this model for the general description of the OMR effect. Nevertheless, it should be mentioned that to a certain extent the presented interpretation of experimental data in the framework of the e-h pair model is rather speculative and needs to be confirmed in future studies. In addition, it is worth noting that even though the evaluation of previously proposed OMR models revealed several deficiencies, each of the models can be brought in line with some of the experimental results that were obtained in SY-PPV devices. Therefore, it can not be excluded at the moment that future investigations might even identify ways of explaining the OMR effect on the basis of a combination of different models.

4 Enhancement of the OMR effect by device conditioning

In order to make the organic magnetoresistance effect suitable for potential applications, it is desirable to obtain large magnetoconductance values. Hence, it is important to either find appropriate materials and device structures which exhibit particularly large OMR values or to identify ways of controlling the OMR values in a given device. In literature a controlled tuning of the magnetoconductance values was shown to be achievable by influencing the charge carrier balance in polymer- and small molecule-based devices via the introduction of appropriate interlayers [Hu07]. However, the OMR values reported in this study were in the range of only several percent at weak magnetic fields. In the course of this thesis it was discovered that exposing OLED devices to electrical stress can be used as an easy method to significantly increase the OMR values without changing the device architecture [Nie08a, Nie08b, Nie09, Bag09a]. In the following this procedure of electrically stressing a device at a constant current density will be called “electrical conditioning”.

4.1 Basic features of electrical conditioning

Figures 4.1a and 4.1b show $\Delta I/I$ and $\Delta EL/EL$ of a bipolar SY-PPV device (with 100 nm emitter thickness) as a function of applied voltage at constant magnetic field before and after a conditioning procedure during which the device was stressed at a current density of 180 mA/cm^2 for 2 hours [Nie09]. The small values of magnetoconductance and magnetoelectroluminescence in the pristine SY-PPV device are significantly enhanced after the conditioning process. The maximum magnetoconductance $\Delta I/I$ is increased from 1 % at 2.5 V to 25 % at 3.9 V and a magnetic field of 40 mT. At the same time, the maximum magnetoelectroluminescence $\Delta EL/EL$ is increased from 4 % at 2.2 V to 50 % at 3.9 V and a magnetic field of 40 mT after conditioning. These values are the largest values achieved so far for the organic magnetoresistance in polymer-based devices with similar emitter thickness in the voltage range below 5 V. Comparable values have only been reported by Nguyen *et al.* for Alq_3-based devices with an emitter thickness of 150 nm at much higher voltages around 13 V [Ngu08].

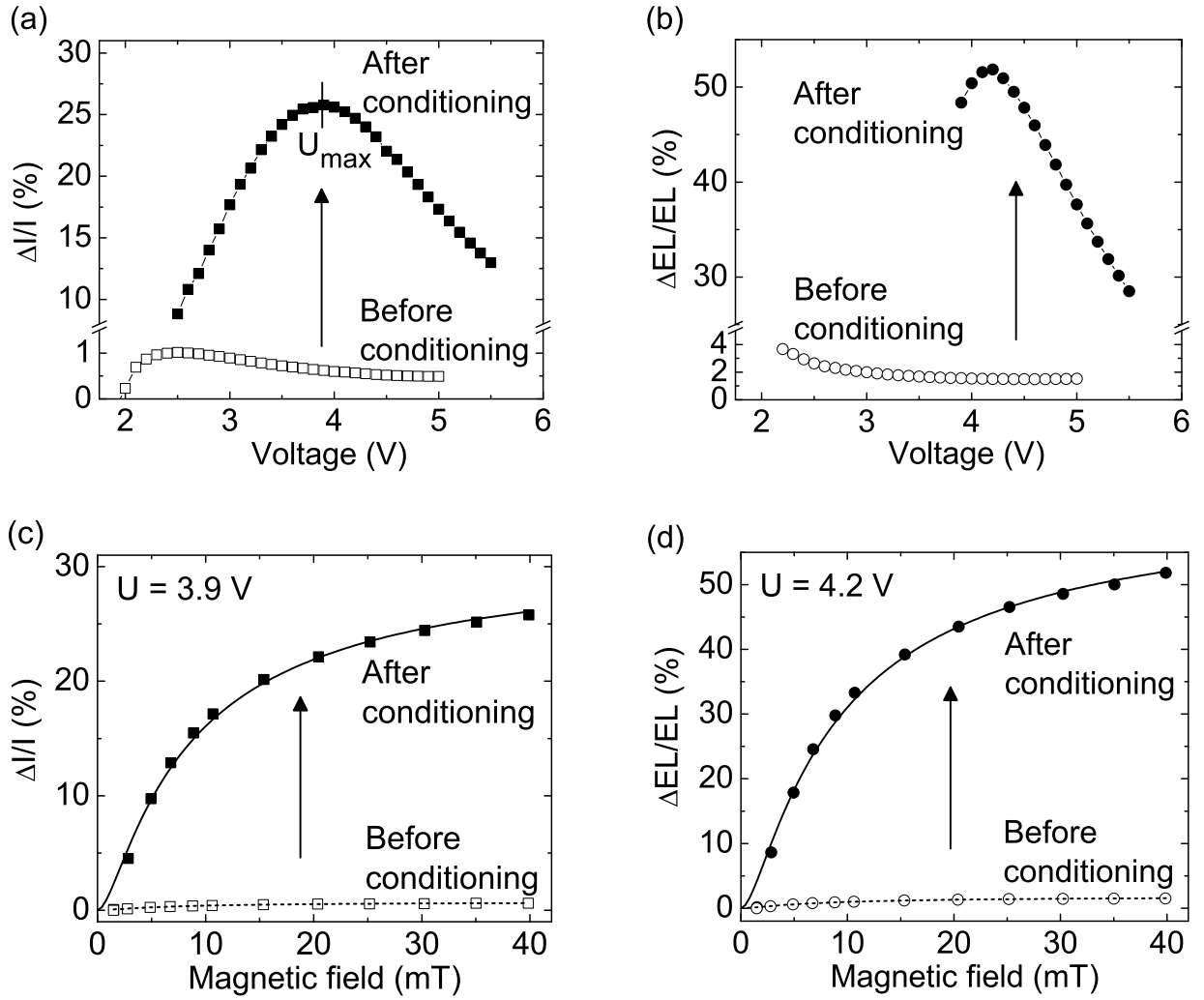

Figure 4.1: (a) Percentage change of current and (b) percentage change of electroluminescence at a magnetic field of 40 mT for a SY-PPV device as a function of voltage before and after electrical conditioning at a current density of 180 mA/cm^2 for 2 h. (c) Percentage change of current and (d) percentage change of electroluminescence at a magnetic field of 40 mT for a SY-PPV device as a function of magnetic field before and after electrical conditioning at a current density of 180 mA/cm^2 for 2 h.

$\Delta I/I$ and $\Delta EL/EL$ as a function of magnetic field before and after conditioning are plotted in figures 4.1c and 4.1d for voltages with maximum OMR effect after conditioning. The line shapes of the magnetic field dependent curves are not changed after the conditioning procedure and still follow the OMR characteristics according to equation (3.1) for $\Delta I/I$ and equation (3.2) for $\Delta EL/EL$. Furthermore, it is remarkable that the same value of the fitting parameter $B_0 = 3$ mT can be used to describe the corresponding curves of pristine and conditioned devices, respectively.

4.2 Variation of conditioning parameters

In order to investigate the influence of the conditioning time on the OMR effect, an OLED device was conditioned at a constant current density of 100 mA/cm^2 for 1 hour. After certain time intervals the conditioning procedure was interrupted and OMR measurements as a function of voltage were performed at a magnetic field of 40 mT.

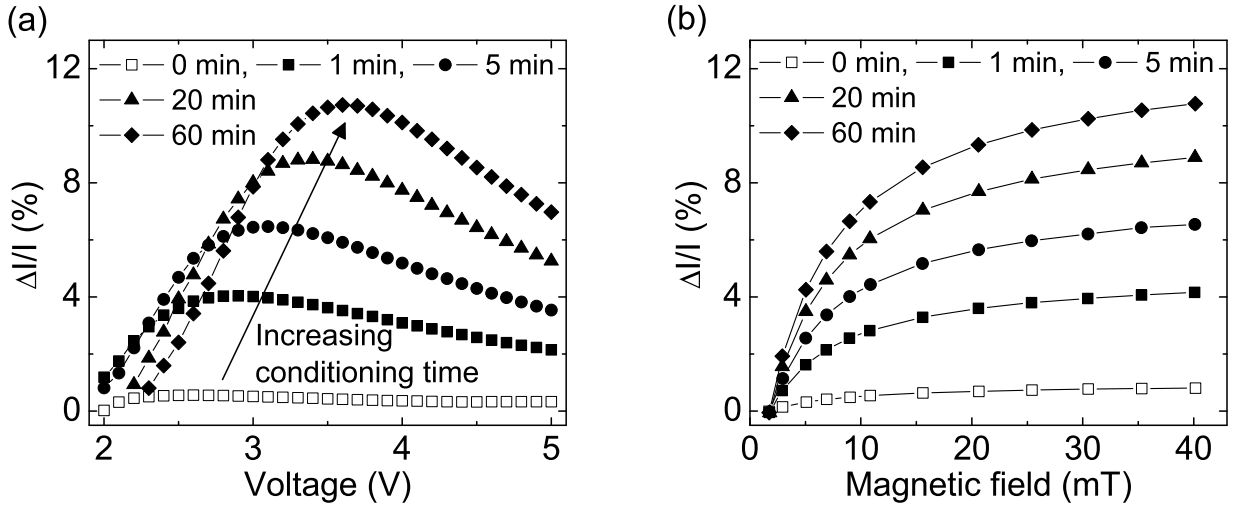

Figure 4.2: Percentage change of current (a) at a magnetic field of 40 mT as a function of voltage and (b) at the voltage U_{max} as a function of magnetic field for a SY-PPV device after electrical conditioning at a current density of 100 mA/cm^2 for different time intervals.

As illustrated in figure 4.2a a longer conditioning process leads to larger values of the magnetoconductance. Furthermore, the maximum of the $\Delta I/I(U)$ curve is shifted to higher voltages for longer conditioning times. The characteristic width of the magnetic field dependent curves in figure 4.2b remains unaffected by the conditioning procedure.

In a more comprehensive measurement the variation of both conditioning time and conditioning current was investigated. Five OLED devices were exposed to conditioning procedures at different current densities for 10 hours. Every 10 minutes the conditioning procedure was interrupted and a short OMR measurement at different voltages was performed in order to determine U_{max} and the corresponding value of $\Delta I/I$ at U_{max}. One additional device was used as a reference and was not conditioned between the OMR measurements. Figure 4.3a shows the obtained magnetoconductance values during the conditioning procedure at different current densities. It is clearly seen that after a fixed time the value of $\Delta I/I$ is larger in those devices that experienced a conditioning at higher current densities. The fact that the magnetoconductance of the reference device which was not conditioned does not show any remarkable changes over the entire investigated time range indicates that the intermediate OMR measurements by themselves do not cause an enhancement of

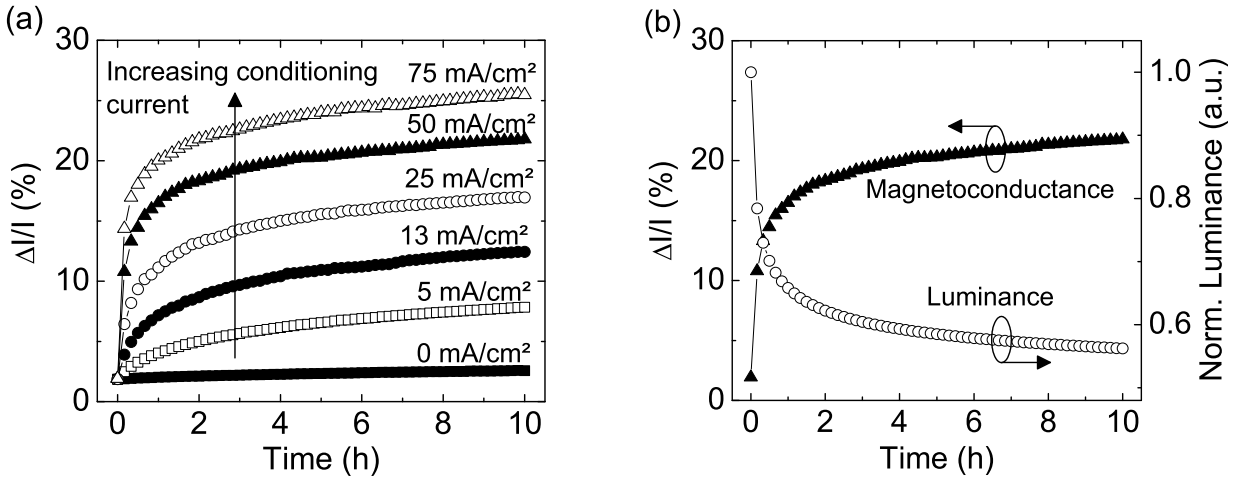

Figure 4.3: (a) Percentage change of current at a magnetic field of 40 mT and the voltage U_{max} as a function of conditioning time for a SY-PPV device after electrical conditioning at different current densities for 10 h. (b) Temporal evolution of magnetoconductance at a magnetic field of 40 mT and the voltage U_{max} as well as luminance (normalized to the start value) during conditioning at a current density of 50 mA/cm^2.

the OMR values. It should be emphasized that for large current densities even very short conditioning times in the range of a few minutes can have a significant impact on the OMR signal. On the other hand, driving a device at low current densities for several hours still yields magnetoconductance values that are lower compared to those that can be achieved after application of higher current densities for a short time. Hence, an efficient conditioning procedure requires current densities that are significantly higher than 0.1 mA/cm^2, which is a typical value of the current density at the voltage U_{max} in SY-PPV devices.
However, it should be noted that the conditioning process only works in a limited parameter range since an exposure to extremely high current densities ultimately leads to a destruction of the device. In additional control experiments it furthermore turned out that applying a reverse bias to a device for several hours does not change the magnetoconductance values.

4.3 Influence of electrical conditioning on electro-optical device parameters

Electrical device stressing not only changes the OMR performance of a device but naturally has an impact on the IV and LV characteristics [Par99, Sil01]. This is demonstrated in figure 4.4 where the device characteristics of the devices from figure 4.3a are plotted before and after conditioning. A clear reduction of current density and electroluminescence intensity at fixed voltage can be observed after conditioning. The reduction is more pronounced for devices that were conditioned at higher current densities. It should be noted in this context that during a conditioning procedure at a selected current density

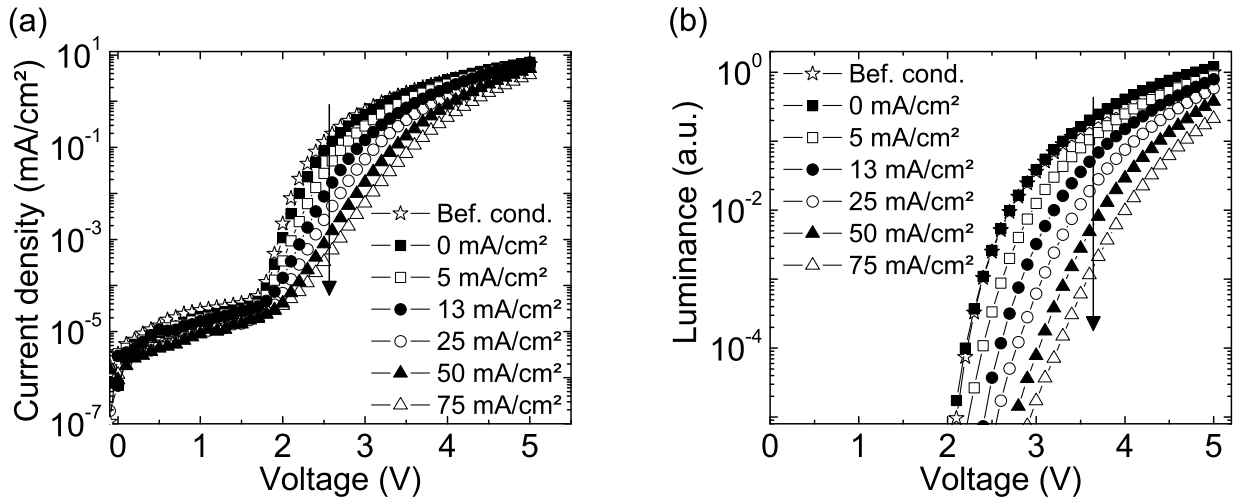

Figure 4.4: (a) IV characteristics and (b) LV characteristics of SY-PPV devices before and after electrical conditioning at different current densities for 10 h.

the voltage which is necessary to keep this constant current level monotonically increases over time.

An interesting feature becomes apparent when the temporal evolutions of luminance and magnetoconductance of a device during conditioning are compared. Figure 4.3b illustrates that the enhancement of $\Delta I/I$ during conditioning is accompanied by a decrease in EL. Even though magnetoconductance and luminance are not correlated in a quantitative way, it is remarkable that both quantities show pronounced changes during the first few hours of conditioning while only small additional changes are observed on a longer timescale.

From the results presented so far it is not yet clear whether the reduction in IV and LV performance is caused by a modification of an interface or by a modification within the bulk material of the emitter layer. To clarify this issue the photoluminescence (PL) signal of a SY-PPV device was recorded during conditioning using a Perkin Elmer Luminescence spectrometer LS 50B.

Figure 4.5 clearly illustrates that the PL signal is monotonically reduced during conditioning. A similar trend for the evolution of the PL signal during electrical stressing was also reported in references [Pop01, Fer05]. Since PL spectroscopy probes the bulk properties of the active material this indicates that the conditioning procedure indeed causes modifications within the bulk emitter material. During conditioning the spectral position of the PL signal remains unchanged which indicates that no additional emitting species is created within the active layer in the course of the conditioning procedure. As a general tendency, it appears that a stronger reduction in PL during conditioning goes along with a larger increase in magnetoconductance.

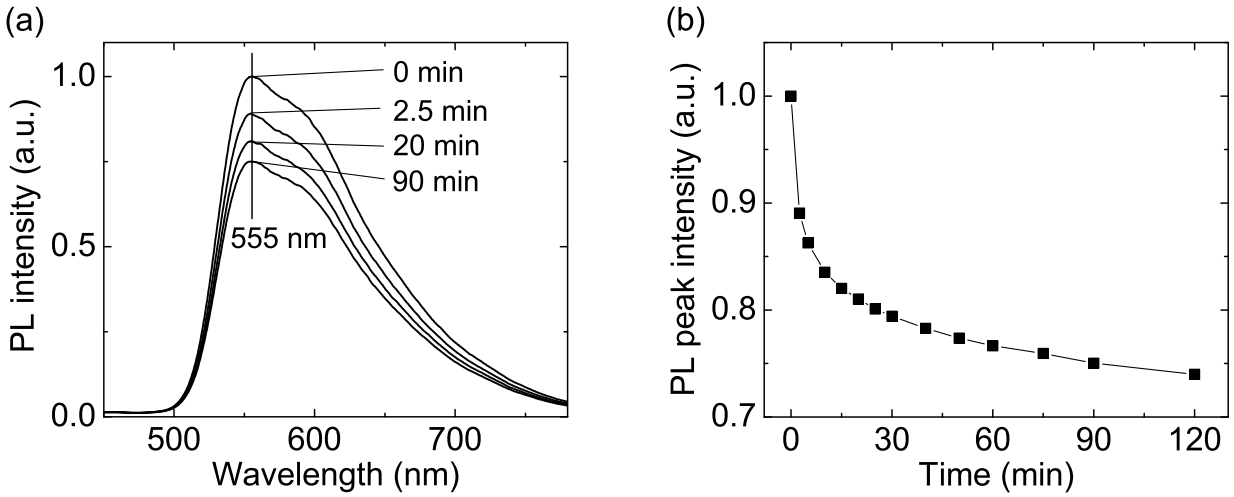

Figure 4.5: (a) PL spectra of a SY-PPV device after conditioning at a current density of 75 mA/cm^2 for different time intervals. (b) PL peak intensity at a wavelength of 555 nm for the device from part (a) as a function of conditioning time. All data are normalized to the corresponding data before conditioning.

4.4 Electrical conditioning of Alq_3 devices

One of the reasons why SY-PPV was chosen as material system for the comprehensive investigations in this thesis was the fact that large magnetoconductance values could be achieved in SY-PPV devices after electrical conditioning. Most of the OMR investigations published in literature, however, are performed on OLED devices using the small molecule material Alq_3 as emitter material [Kal03a, Pri06, Blo07, Des07a, Ngu08]. In the course of this thesis it was tested whether the literature results can be verified in own measurements and whether the electrical conditioning procedure can also be applied to small molecule devices. The Alq_3 was purchased from the same supplier that provided the Alq_3 for the PEDOT / 150 nm Alq_3 / Ca devices in reference [Ngu08] where Nguyen *et al.* obtained large magnetoconductance values of up to 21 % at 40 mT. As in the case of the literature report the Alq_3 was used as received without any further purification. In this thesis devices comprising 120 nm ITO / 40 nm NPB / 100 nm Alq_3 / 0.7 nm LiF / 150 nm Al were fabricated and investigated with respect to their OMR performance.

Figure 4.6a shows OMR measurements of Alq_3 devices in the pristine state and after exposure to electrical conditioning procedures at different current densities for 10 hours. In the pristine devices very small magnetoconductance values of about 0.1 % at 40 mT were detected over the entire voltage range that was investigated. Only after extensive conditioning at 100 mA/cm^2 for 10 hours it was possible to increase the maximum magnetoconductance to values around 3 % at 40 mT. The line shape of the $\Delta I/I(B)$ curves in figure 4.6b can also be described by relation (3.1) which was used to fit the corresponding

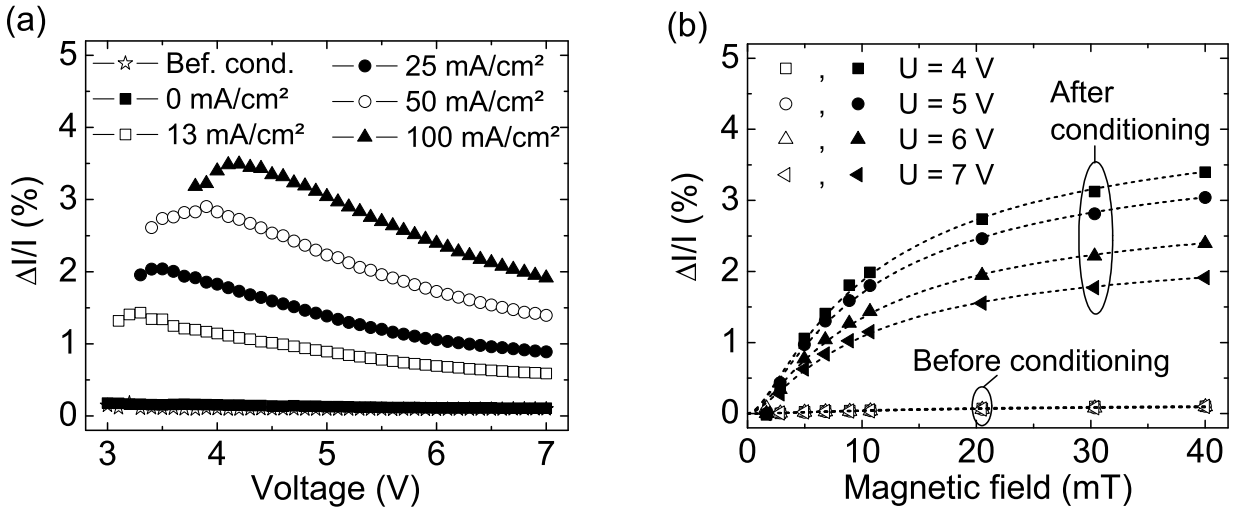

Figure 4.6: (a) Percentage change of current at a magnetic field of 40 mT as a function of voltage for Alq_3 devices before and after electrical conditioning at different current densities for 10 h. (b) Percentage change of current as a function of magnetic field before and after conditioning at a current density of 100 mA/cm^2 for 10 h. The dashed lines are fits according to equation (3.1).

curves obtained for SY-PPV devices. The fitting parameter $B_0 \approx 5$ mT for the magnetic field dependent magnetoconductance curves of the investigated Alq_3 devices is in good agreement with a reported value of $B_0 = 5.4$ mT for Alq_3 devices in literature [She06]. Like in the case of SY-PPV devices it was also observed for the Alq_3 devices that after conditioning at higher current densities the voltage U_{max} with the maximum $\Delta I/I$ is shifted to higher voltages.

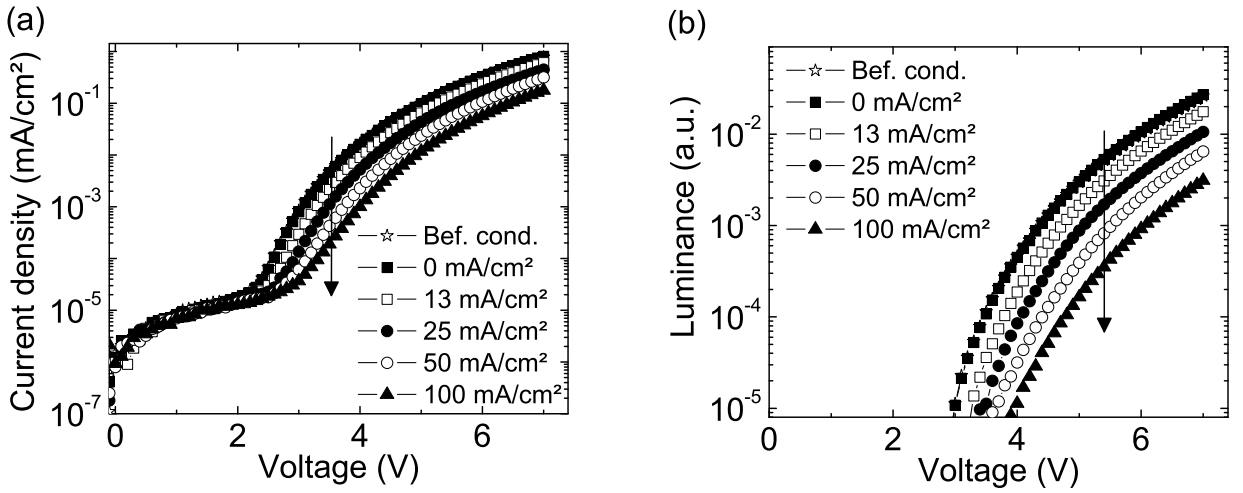

Figure 4.7: (a) IV characteristics and (b) LV characteristics of Alq_3 devices before and after electrical conditioning at different current densities for 10 h.

An analysis of the *IV* and *LV* characteristics before and after conditioning in figure 4.7 shows that also in Alq_3 devices the electro-optical device performance is reduced after conditioning and that higher conditioning currents lead to more pronounced changes of the device characteristics.

In summary, this investigation demonstrates that the conditioning procedure can successfully be applied to Alq_3 devices as well. Nevertheless, the large magnetoconductance values which were reported in reference [Ngu08] could not be verified in own measurements. At this point it can only be speculated that special features in the device fabrication process used by Nguyen *et al.* might have caused a modification of the active layer which is responsible for the large values of the OMR effect in their devices.

4.5 Optical conditioning

In addition to the electrical way of device conditioning it was also discovered in the course of this thesis that a purely optical device conditioning can be used to increase the OMR values in SY-PPV devices. During this optical conditioning procedure the OLED device is not electrically connected and is simply illuminated with highly intense light at wavelengths in the absorption range of the SY-PPV. For the following investigations the same light source was employed that was also used for the measurements presented in section 3.4. However, the distance between the lamp and the OLED chip was now fixed in such a way that the chip was illuminated with a much higher power density of about 80 mW/cm^2.

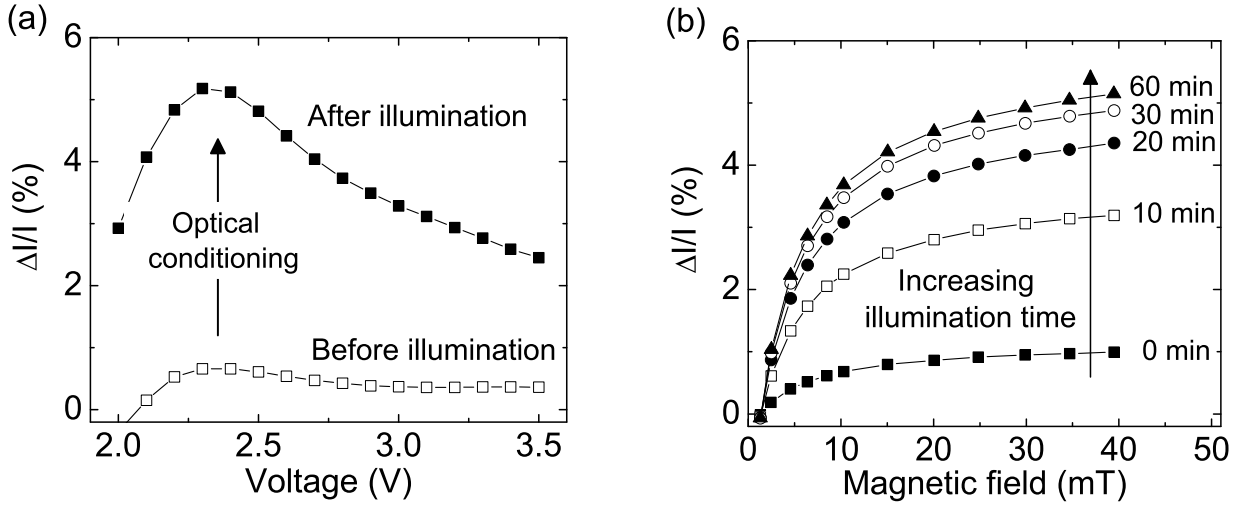

Figure 4.8: (a) Percentage change of current at a magnetic field of 40 mT as a function of voltage for a SY-PPV device before and after optical conditioning for 1 h. (b) Percentage change of current at a voltage of 2.4 V as a function of magnetic field for a SY-PPV device before and after optical conditioning for different time intervals.

Figure 4.8a shows magnetoconductance curves of a SY-PPV device as a function of voltage before and after optical conditioning. Illuminating the device for 1 hour enhances the magnetoconductance $\Delta I/I$ from 1 % up to 5 % at a magnetic field of 40 mT and a voltage of 2.4 V. Figure 4.8b demonstrates that similar to the case of electrical conditioning a longer time interval of optical conditioning leads to a larger increase of the OMR values. However, the achieved values of $\Delta I/I$ stayed well below 10 % in all measurements, which indicates that optical conditioning is not as effective as electrical conditioning. In additional experiments it was found that the effects of electrical and optical conditioning can even be combined. Electrically stressing devices and simultaneously exposing them to highly intense light yields better OMR results compared to a situation where only one type of conditioning is applied.

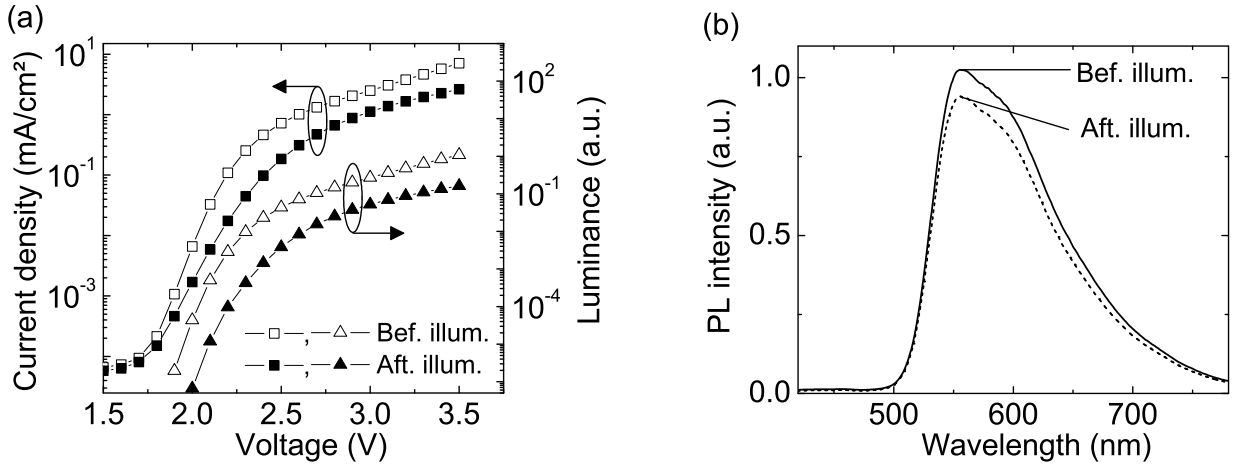

Figure 4.9: (a) IV and LV characteristics and (b) photoluminescence signal of a SY-PPV device before and after optical conditioning for 1 h.

An analysis of the IV and LV characteristics in figure 4.9a shows that they are affected by the illumination procedure in a similar way to what has been observed in the case of electrical conditioning. After optical conditioning a lower current density and a lower luminance are measured at fixed voltage. In addition, figure 4.9b illustrates that optical conditioning reduces the PL signal of the device without changing the spectral position of the emission peak.

4.6 Discussion of conditioning mechanism

In summary, several important features of the conditioning procedure have been observed in experiment:

1. Electrical conditioning significantly increases the magnetoconductance $\Delta I/I$ and the magnetoelectroluminescence $\Delta EL/EL$. The voltage $U_{\max}$ with the maximum of $\Delta I/I$ is shifted to higher voltages after electrical conditioning.
2. Optical conditioning also increases the OMR values but is less efficient than electrical conditioning.
3. Both types of conditioning reduce the current density and the EL intensity at fixed voltage and cause a reduction of the photoluminescence signal.

These results suggest that electrical and optical conditioning modify the bulk material of a device in a way that is favorable for the OMR effect but unfavorable for the charge carrier transport. For a better understanding it is beneficial to replot the data from figures 4.1 and 4.4 in a different way in order to analyze the magnetic field dependent changes of current and electroluminescence as a function of current.

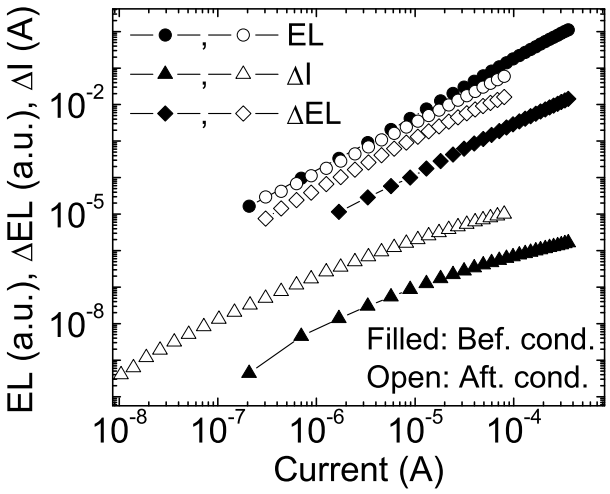

Figure 4.10:
Electroluminescence (EL) at zero magnetic field as well as absolute changes ΔI in current and ΔEL in electroluminescence at a magnetic field of 40 mT as a function of current in a SY-PPV device. Filled symbols indicate results in the pristine device, open symbols represent results after conditioning at a current density of 180 mA/cm^2 for 2 h.

Figure 4.10 demonstrates that the relative change of $EL(I)$ due to the conditioning procedure is only small, whereas $\Delta I(I)$ and $\Delta EL(I)$ are significantly enhanced after conditioning relative to the situation before conditioning.
These results can also be interpreted on the basis of the e-h pair model. It has been proposed in literature that a spin mixing of e-h pairs can only occur if the lifetime τ of the e-h pairs is longer than the time τ_{evo} of spin evolution due to the hyperfine interaction [Sok74, Zel88]. Only those e-h pairs which fulfill this condition are assumed to participate

in the mechanism which causes the OMR effect according to the e-h pair model. Hence, the observed increase of ΔI and ΔEL at fixed current suggests that after conditioning a larger fraction of the formed e-h pairs fulfills the criterion $\tau > \tau_{\mathrm{evo}}$ and contributes to the OMR effect.

From the IV curves in figure 4.4a it can be seen that after conditioning a higher voltage than before conditioning is necessary in order to reach a certain current density. Taking into account the proposed influence of the electric field on the lifetime of e-h pairs a higher voltage is expected to reduce the lifetime and should result in a smaller ΔI at fixed current after conditioning. At first glance, this seems to be in contradiction to the experimental results. In order to solve this discrepancy, another mechanism is suggested which is assumed to increase the e-h pair lifetime after conditioning and which might be superimposed on the electric field influence. In the following chapter strong evidence will be provided that this mechanism is related to the formation of charge carrier traps within the emitter layer of the OLED device.

Slowing down the charge carrier transport by an increase of energetic disorder and a creation of additional trap states might be an explanation for the reduction of current density and electroluminescence at fixed voltage that can be observed after conditioning. Furthermore, it can be argued that an increase in the lifetime of e-h pairs due to a reduced charge carrier mobility might account for the increase of ΔI and ΔEL after conditioning (see figure 4.10) as well as for the enhancement of $\Delta I/I$ and $\Delta EL/EL$ after conditioning (see figure 4.1). Moreover, in a system with reduced charge carrier mobility larger electric fields are necessary to reach charge carrier velocities so that the lifetime of an e-h pair is in the range of the spin evolution time. This could explain the shift of the voltage U_{max} to higher values after conditioning, which was observed in figure 4.1a. In addition, trap states can act as nonradiative recombination centers [Pop01, Sil01], which would be in line with the reduced electroluminescence at fixed voltage in figure 4.4b and the observed quenching of the photoluminescence signal in figure 4.5 after conditioning.
It is worth mentioning that an enhancement of the OMR values due to an increased number of trap states in the active material would even be in line with other models proposed for the OMR effect in literature [Nie09]. Finally, the fact that the observed magnetoconductance values in a given device structure critically depend on the device history might be an explanation for the large variations of the OMR values that have been reported for identical device structures in literature [Fra04, Hu07, Blo08b].

5 Material modification during device conditioning

This chapter presents strong indications that the presence of trap states is favorable for the OMR effect. It will be shown that the value of the magnetoconductance can be influenced by actively changing the number of trapped charge carriers. Moreover, it will be demonstrated by means of charge carrier extraction methods that electrical device conditioning increases the number of trap states and reduces the charge carrier mobility inside the active material.

5.1 OMR under infrared illumination

In order to prove the importance of charge carrier trapping for the OMR effect, the influence of infrared (IR) illumination on the magnetoconductance was investigated. By illuminating the device with IR light the number of trapped charges can actively be reduced since the absorption of IR radiation by molecules in the active material can lead to a release of charge carriers from their traps. In contrast to the conditioning process (which is assumed to change the number of available trap states) it is likely that the IR illumination only changes the probability for an occupation of existing trap states. As IR light source a 300 W xenon lamp with an edge filter was used to illuminate the sample in the spectral range from 700 nm to 1100 nm, which corresponds to photon energies between 1.1 eV and 1.8 eV. The illumination wavelengths were chosen to be well above the fundamental absorption of SY-PPV to ensure that no charge carriers are photogenerated in direct transitions from the HOMO to the LUMO.

Figure 5.1 shows measurements of the magnetoconductance and the IV characteristics of electrically conditioned SY-PPV devices before, during and immediately after the IR illumination. Using the same measurement principle similar curves were also obtained for OLED devices comprising a different PPV derivative [Bag09a]. It is clearly seen that the magnetoconductance decreases considerably upon IR illumination. In contrast, the current flow through the device at fixed voltage shows an increase which is especially pronounced in the low voltage regime between 2 V and 3 V. This voltage region closely above the threshold voltage of substantial charge carrier injection corresponds to the trap filling regime where the influence of trap states on the IV characteristics is assumed to be most relevant [Yan99]. It is important to note that immediately after switching off the IR

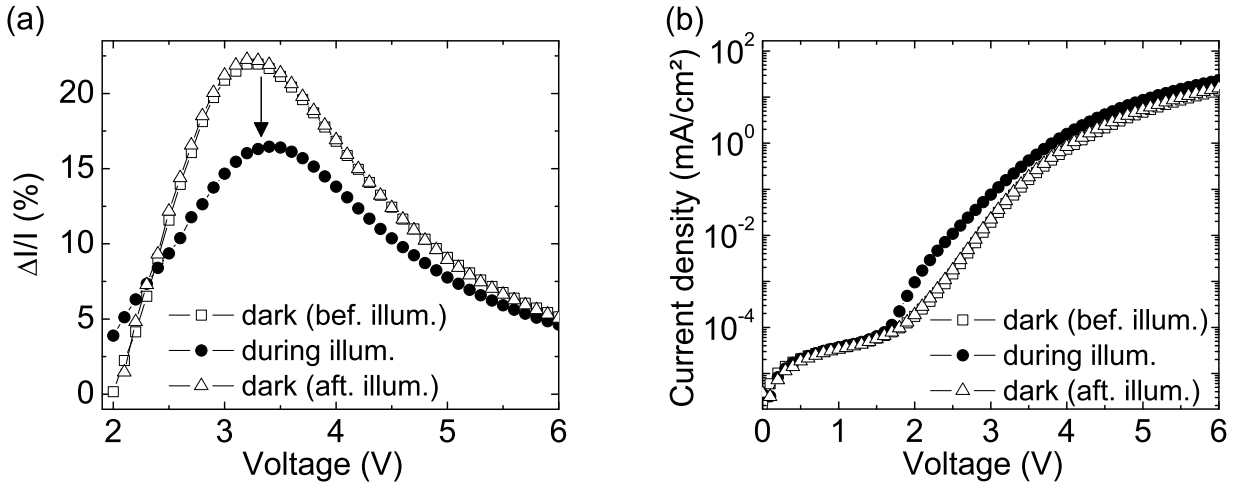

Figure 5.1: (a) Percentage change of current at a magnetic field of 30 mT as a function of voltage and (b) IV characteristics of a conditioned SY-PPV device in the dark and under illumination with IR light.

illumination the initial curves for magnetoconductance and current as a function of voltage are restored, which excludes any effects due to heating of the device by the IR light.

At first glance, the decrease of $\Delta I/I$ might appear to be a simple consequence of the increased current upon illumination, which reduces the ratio $\Delta I/I$. However, an analysis of ΔI at fixed magnetic field as a function of current shows that this conclusion is insufficient. From figure 5.2 it is apparent that the IR illumination affects the change ΔI in current due to the magnetic field, which is even more important than the influence of the IR light on the current. Especially in the range of low currents the difference between ΔI in the dark and under illumination is pronounced. A possible interpretation of this phenomenon is that the IR illumination leads to an optical depletion of trap states and reduces the number of e-h pairs which involve a trapped charge carrier. This would be in line with the

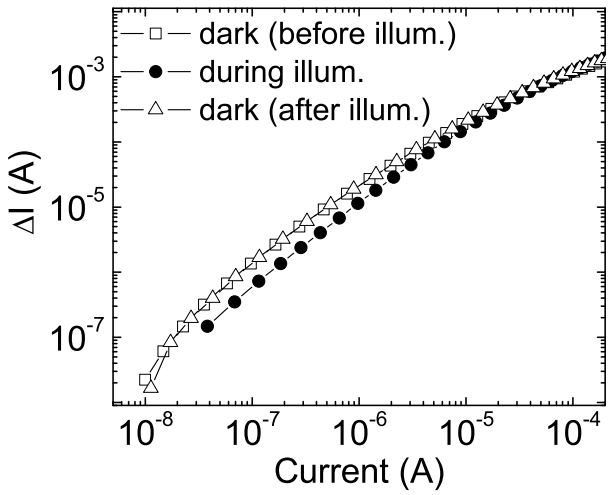

Figure 5.2:
Absolute change ΔI in current at a magnetic field of 30 mT as a function of current for a conditioned SY-PPV device in the dark and under illumination with IR light.

assumption that during the IR illumination fewer e-h pairs have a lifetime long enough to be influenced by the magnetic field and to contribute to the OMR effect.

Even though an optical depletion of trap states nicely explains the obtained results for the magnetoconductance, it might not be the only mechanism that can cause an increase in current density upon IR illumination. All investigated SY-PPV devices also contained a layer of PEDOT:PSS which is known to absorb in the infrared spectral range [Mes03]. Hence, the illumination with IR light causes interband transitions in the PEDOT:PSS and results in a photogeneration of free charge carriers which might also contribute to the overall current. Yet another possible explanation for the change in current due to the IR illumination might be an enhanced efficiency of charge carrier injection from the electrodes into the organic materials. However, a plain increase in current due to a photogeneration of charges or due to an enhanced injection can not explain the decrease in ΔI at fixed current upon IR illumination, which was observed in figure 5.2.

In order to further distinguish between the contribution of detrapped charges in the SY-PPV and possible other contributions to the overall current, an additional experiment involving IR illumination at low temperatures was carried out. A conditioned device with a maximum magnetoconductance of 15 % at 40 mT was cooled down to 81 K and electrically loaded by applying a current density of 75 mA/cm^2 for 1 min. After completion of the loading procedure a voltage of 0 V was applied to the device, and the extraction current driven by the built-in potential was monitored over a time period of 15 min (see figure 5.3).
In a first measurement the device was kept in the dark all the time. Due to the low thermal energy at 81 K only very shallow traps could be depleted and few charges were extracted from the device, resulting in a small, monotonically decreasing current. It should be noted that the resulting extraction current has to be analyzed with respect to a baseline which is indicated in figure 5.3 and which was obtained by measuring the extraction current

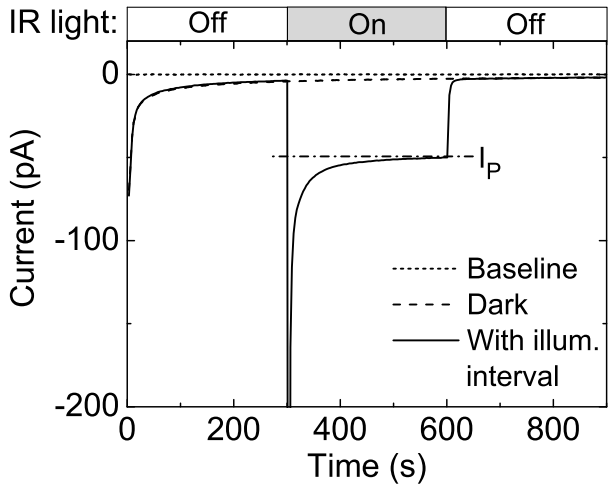

Figure 5.3:
Temporal evolution of the current through a SY-PPV device at an externally applied voltage of 0 V during the thermalization period after electrical loading at a temperature of 81 K. See text for details.

without previously loading the device. After heating up the device to room temperature, cooling it down again and repeating the electrical loading a second measurement of the extraction current at 0 V was performed. In contrast to the first measurement, the device was now kept in the dark for 5 min, then exposed to IR illumination for 5 min, and finally kept in the dark for another 5 min. Initially, the extraction current was found to be identical to the one observed in the first measurement.
During the illumination interval the situation changed and two important observations could be made: The first point to notice was that upon IR illumination the current immediately showed a rapid increase followed by a monotonic decrease. During the entire illumination period the extraction current was higher compared to the first measurement in the dark. A second important point was the saturation of the extraction current at a value I_P towards the end of the illumination period. Only after switching off the IR light the extraction current fully returned to the values that had been observed in the first measurement.
These results suggest that the large spike followed by the monotonic decrease of the extraction current during the IR illumination interval results from a detrapping of charges in the SY-PPV. The saturation current I_P might be attributed to additional free charge carriers that have been photogenerated in the PEDOT:PSS layer.

5.2 Thermally stimulated current measurements

In order to explicitely show that electrical conditioning increases the number of trap states in SY-PPV devices, thermally stimulated current (TSC) measurements were performed with a device in the pristine state ($\Delta I/I = 1\,\%$ at 40 mT and U_{max}) and after electrical conditioning ($\Delta I/I = 15\,\%$ at 40 mT at U_{max}). In both cases the device was electrically loaded at a temperature of 81 K by applying a current density of 75 mA/cm^2 for 1 min. After a thermalization period of 15 min the device was heated with a rate of 10 K/min, and the extraction current at 0 V external bias was recorded in order to obtain a TSC spectrum.

Figure 5.4a shows the TSC spectra before and after conditioning together with a baseline that was recorded in a TSC scan without previously loading the device. The area under a TSC curve with respect to this baseline indicates the amount of thermally released charges during the scan. The TSC spectrum of the pristine device shows a pronounced peak at 100 K and a shoulder at 120 K. Compared to this spectrum the extraction current after conditioning shows a slight increase at 100 K and a considerable increase in the entire range from 125 K to 190 K. This observation indicates that more charge carriers are trapped in low energetic states after conditioning. Hence, the result serves as direct evidence that during the conditioning procedure additional electronic trap states are created in the device.

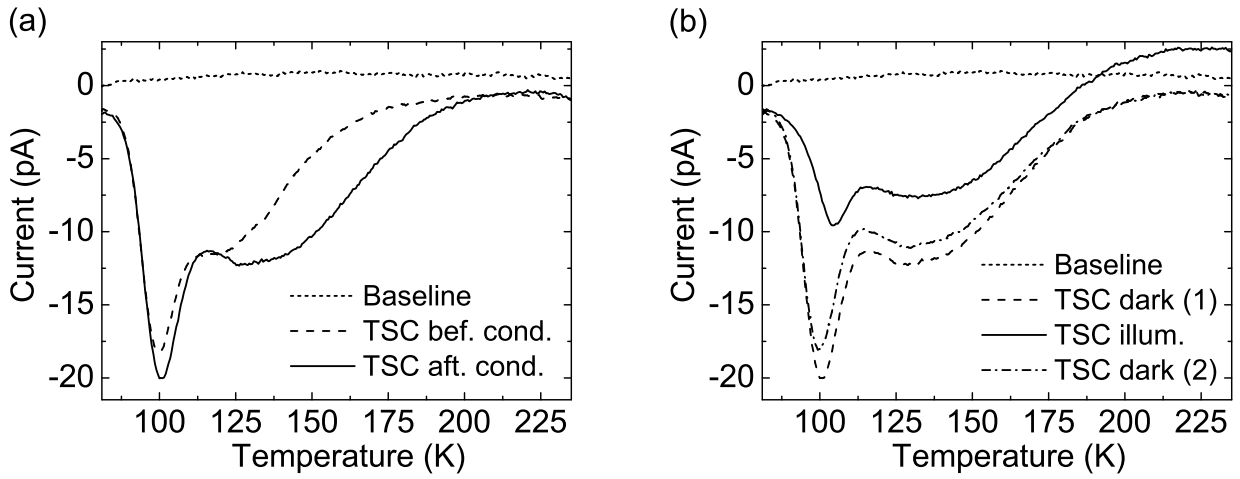

Figure 5.4: (a) TSC signals of a SY-PPV device before and after electrical conditioning at a current density of 100 mA/cm^2 for 1 h. The baseline indicates the TSC signal without previously loading the device. (b) TSC signals of a conditioned SY-PPV device without IR illumination (TSC dark (1) and TSC dark (2)) and with IR illumination (TSC illum.) during the thermalization period.

It should be mentioned that the recorded TSC spectra (which indicate rather shallow traps) do not necessarily reflect the entire number of trap states inside the SY-PPV. It is possible that deep traps exist in the material which could not be investigated due to limitations in the temperature range of the experimental setup. In addition, it is likely that not all available trap states in the active material were filled with charges during the loading procedure. Nevertheless, the presented results in figure 5.4a demonstrate the general tendency that device conditioning increases the number of trap states.

The influence of pre-illumination with IR light on the TSC spectra was also investigated. Three consecutive TSC scans were performed in the dark which only differed in the illumination conditions during the thermalization period after the electrical loading. For the first and the third TSC scan the device was kept in the dark during the thermalization period while for the second TSC scan the device was illuminated with IR light for 5 min similarly to the procedure that was described in the context of figure 5.3. The results in figure 5.4b show that the pre-illumination with IR light changes the TSC spectrum in the entire temperature range under investigation. Despite the presence of a positive TSC signal at high temperatures (the nature of which is still unclear) it is apparent that the TSC signal after illumination is reduced compared to the signals that were obtained without previous illumination. This indicates that a number of initially trapped charges can be released during the illumination period and do not contribute to the TSC signal any more.

5.3 Photo-CELIV measurements

A different approach to investigate the influence of conditioning on the electronic structure of SY-PPV is to determine the charge carrier mobility in the material before and after conditioning. Since electronic trap states slow down the charge carrier transport it is expected that the charge carrier mobility in SY-PPV is also reduced after electrical conditioning. A convenient way to prove this hypothesis is the photo-CELIV technique which was introduced in section 2.6.2. The voltage ramp and typical extraction current transients obtained in a photo-CELIV measurement using a pristine SY-PPV device are illustrated in figure 5.5 for the case of a delay time $t_{\mathrm{del}} = 5\,\mu s$ between the laser pulse and the start of the voltage ramp. During and immediately after the laser pulse an offset voltage of 2 V was applied to the device in order to compensate the built-in potential of the device. After the delay time the voltage (in reverse direction) was linearly increased with a voltage rise speed of $0.8\,\mathrm{V}/\mu s$, the duration of the voltage ramp was $15\,\mu s$.

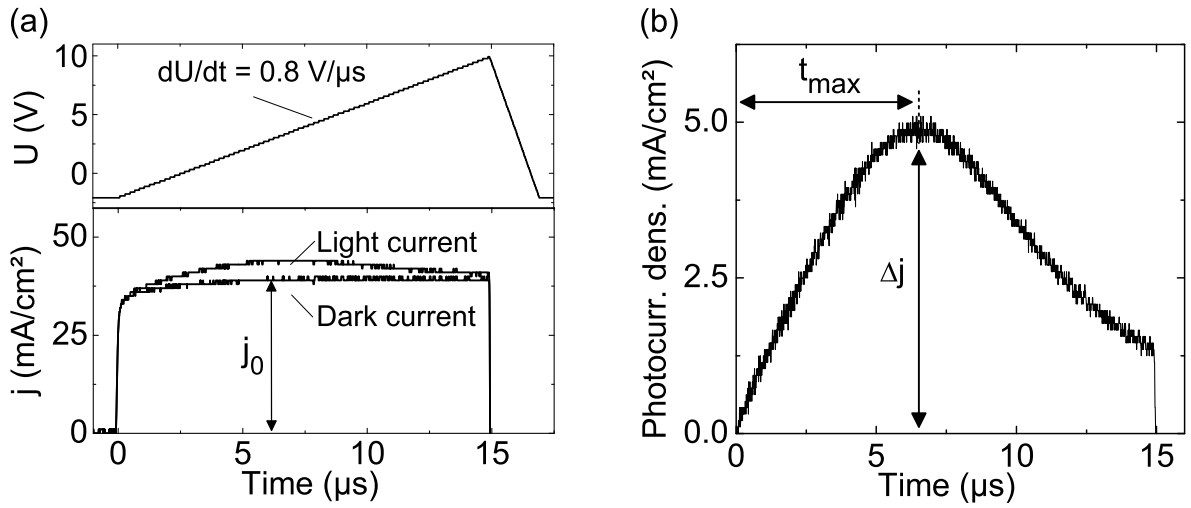

Figure 5.5: (a) Voltage ramp applied during a photo-CELIV measurement and resulting extraction currents without illumination (dark current) and with previous laser illumination (light current) of a SY-PPV device. The capacitive displacement current j_0 is indicated. (b) Extracted photocurrent, calculated as difference between light current and dark current. The maximum value Δj is reached after a time t_{max}.

The two current transients in figure 5.5a were obtained with and without pre-illumination by the laser pulse, respectively. As expected, the dark transient shows a plateau at a current density j_0 which is related to the geometrical capacitance of the device. After illumination, an additional photocurrent is observed on top of the dark transient. For the quantitative evaluation of the photocurrent both the dark transient and the transient after laser excitation were averaged over 512 voltage pulses before calculating the difference between the two transients. Figure 5.5b shows the extracted photocurrent which reaches its maximum Δj after a certain time t_{max}.

In a series of photo-CELIV measurements with variable delay times SY-PPV devices were investigated in the pristine state with a maximum $\Delta I/I$ of 1 % at 40 mT and in the conditioned state with a maximum $\Delta I/I$ of 17 % at 40 mT. Figure 5.6 shows the recorded photocurrent curves for three different delay times ranging from 1 μs to 50 μs before and after conditioning.

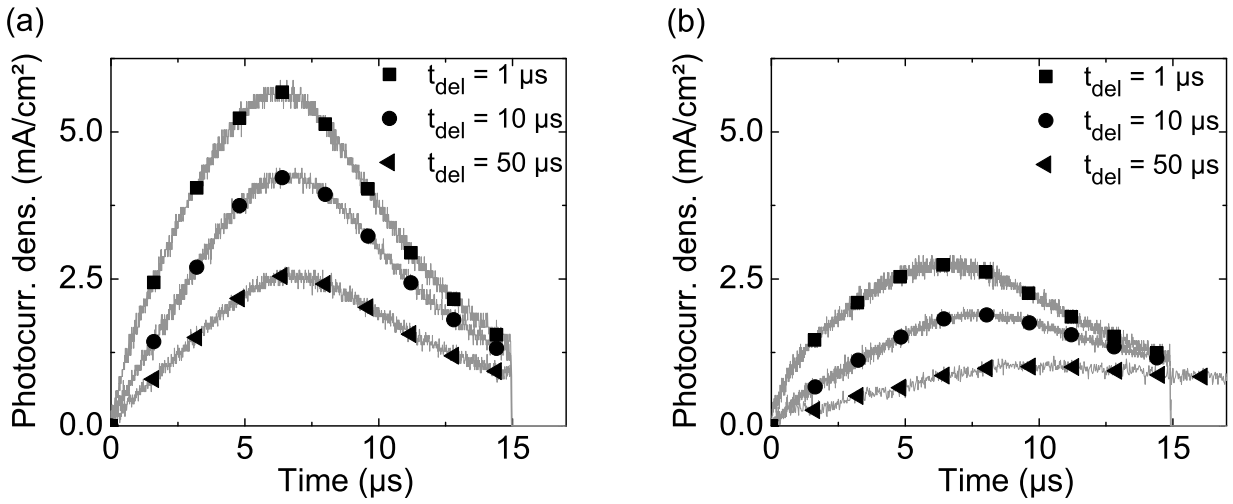

Figure 5.6: Photocurrent transients after different delay times for a SY-PPV device (a) before conditioning and (b) after conditioning at a current density of 100 mA/cm^2 for 1 h.

In both cases it is clearly seen that the maximum value Δj of the photocurrent decreases with increasing delay time. This indicates that a recombination of photogenerated charge carriers takes place during the delay time and fewer charge carriers are available for extraction after a longer delay time. It is noticeable that for identical delay times the extracted photocurrents are smaller after conditioning compared to the situation before conditioning. A possible explanation for this observation might be an increased number of trap states after conditioning which serve as quenching centers and facilitate charge carrier recombination during the delay time [Pop01, Sil01]. An analysis of the photocurrent transients furthermore shows that the maximum of the photocurrent shifts to longer times t_{max} as the delay time is increased. Before conditioning only a small shift is detected which becomes more pronounced after conditioning.

In figure 5.7 the mobility values calculated according to equation (2.12) are plotted as a function of $t_{\mathrm{del}} + t_{\mathrm{max}}$. Since holes are known to dominate the charge carrier transport in PPV [Blo01, Man07] the mobility values in figure 5.7 are related to hole transport. Moreover, values on the order of 10^{-6} cm^2/Vs were also reported in literature for the hole mobility in PPV [Blo01]. It is clearly seen that for all delay times the charge carrier mobility is reduced after conditioning. Hence, the photo-CELIV measurements provide a further indication that additional trap states have been created during conditioning.

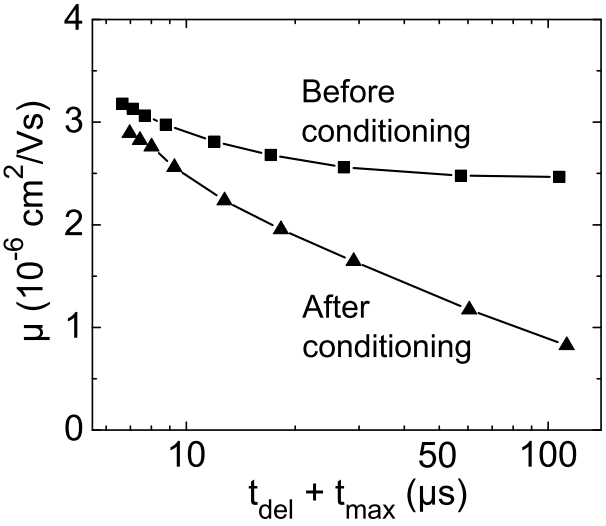

Figure 5.7:
Calculated mobility values as a function of the time $t_{\mathrm{del}} + t_{\mathrm{max}}$ for a SY-PPV device before conditioning and after conditioning at a current density of 100 mA/cm^2 for 1 h.

It should be noted in the context of figure 5.7 that no consistent interpretation regarding the functional dependence of the mobility on the delay time exists up to now. In literature an initial decay followed by a saturation of the mobility as a function of delay time (as observed in the SY-PPV devices before conditioning) has been interpreted as an energy relaxation of the photogenerated charge carriers towards low-energy states of the DOS distribution where a dynamic equilibrium is attained [Öst04, Moz05a, Moz05b]. According to this interpretation all photogenerated charge carriers in the pristine SY-PPV devices would reach the dynamic equilibrium within 30 μs. After conditioning the mobility values in figure 5.7 do not saturate even at the longest delay times where a reasonable photocurrent could be measured. Following the interpretation from literature this would mean that the dynamic equilibrium has not been reached within the accessible time range because the relaxation to thermal equilibrium presumably takes longer with more low-energy states being present in the device. However, even though it is claimed in literature on photo-CELIV measurements that the thermalization of charge carriers in polymer materials occurs on a μs timescale [Öst04, Moz05a, Moz05b] this scenario seems very unlikely. In fact, it was shown by means of ultrafast spectroscopy that relaxation times below 1 ns can be observed in conjugated polymers [Ker93]. Moreover, it was suggested very recently that the presence of high charge carrier densities in the devices during photo-CELIV measurements might lead to an artificial time dependence of the obtained mobility values [Ban09].

6 Reduction of the OMR effect by thermal activation

Even though it has become clear that device conditioning leads to the formation of additional trap states, the nature of the traps, however, has still remained obscure. Therefore, additional measurements were carried out which provide information about material modifications which are likely to cause the formation of the trap states.

6.1 OMR reduction by relaxation at room temperature

In the course of investigating the electrical conditioning procedure it was found that the material modifications during conditioning are non-permanent and can partially be reversed. Figure 6.1a shows the temporal evolution of the magnetoconductance once the conditioning procedure has been turned off. For this measurement a SY-PPV device was initially conditioned at a current density of 100 mA/cm^2 for 1 h and then kept in the experimental setup for 100 h. Every 10 min short voltage scans (< 1 min) with magnetocon-

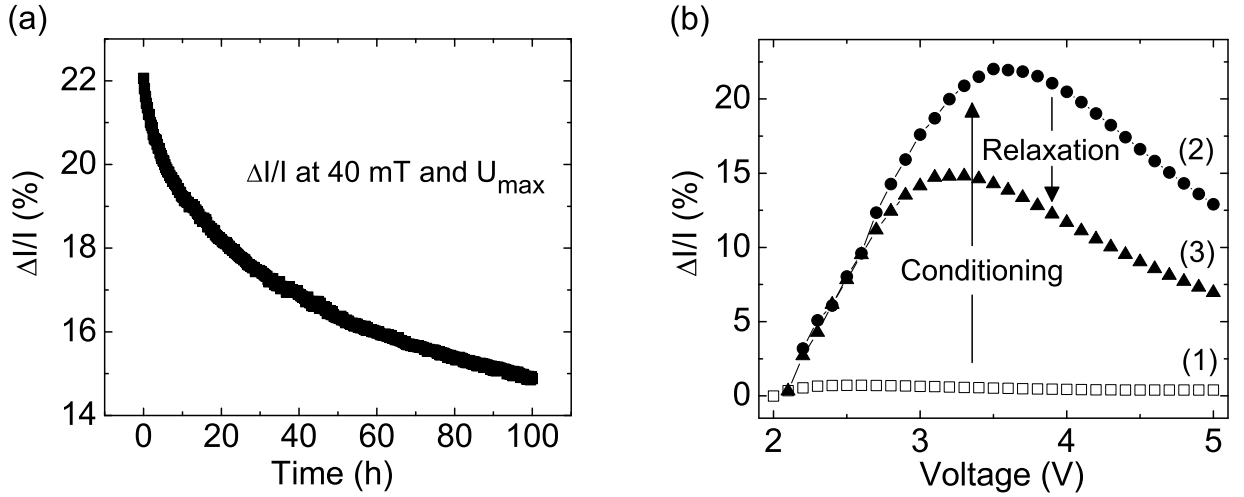

Figure 6.1: (a) Percentage change of current at a magnetic field of 40 mT and the voltage U_{max} for a SY-PPV device as a function of relaxation time after conditioning at a current density of 100 mA/cm^2 for 1 h. (b) Magnetoconductance at a magnetic field of 40 mT as a function of voltage for a SY-PPV device before conditioning (1), after conditioning at a current density of 100 mA/cm^2 for 1 h (2), and after subsequent relaxation for 100 h (3).

ductance measurements at fixed magnetic field were performed and the maximum $\Delta I/I$ was determined for each scan. Between the measurements no voltage was applied to the device and the contacts were floating. It should be noted that during the measurement scans the current densities were below 0.1 mA/cm^2 which was small enough not to cause any additional conditioning. After 100 h of room temperature storage the maximum magnetoconductance at 40 mT was reduced from initially 22 % (after conditioning) to only 16 %. Figure 6.1b demonstrates that after the relaxation time interval the voltage $U_{\max}$ to reach the maximum magnetoconductance decreased from 3.5 V to 3.2 V, thus approaching $U_{\max}$ of the pristine device.

6.2 OMR reduction by thermal annealing

6.2.1 Annealing after electrical conditioning

To further investigate the non-permanent material modification during conditioning additional measurements were performed where conditioned devices were subjected to thermal annealing (see figure 6.2). For these measurements a set of five individual devices was used which were simultaneously processed on the same substrate. All devices were conditioned at 100 mA/cm^2 for 30 min at room temperature. Subsequently, each device was placed on a hotplate for 15 min and annealed at different temperatures in the range

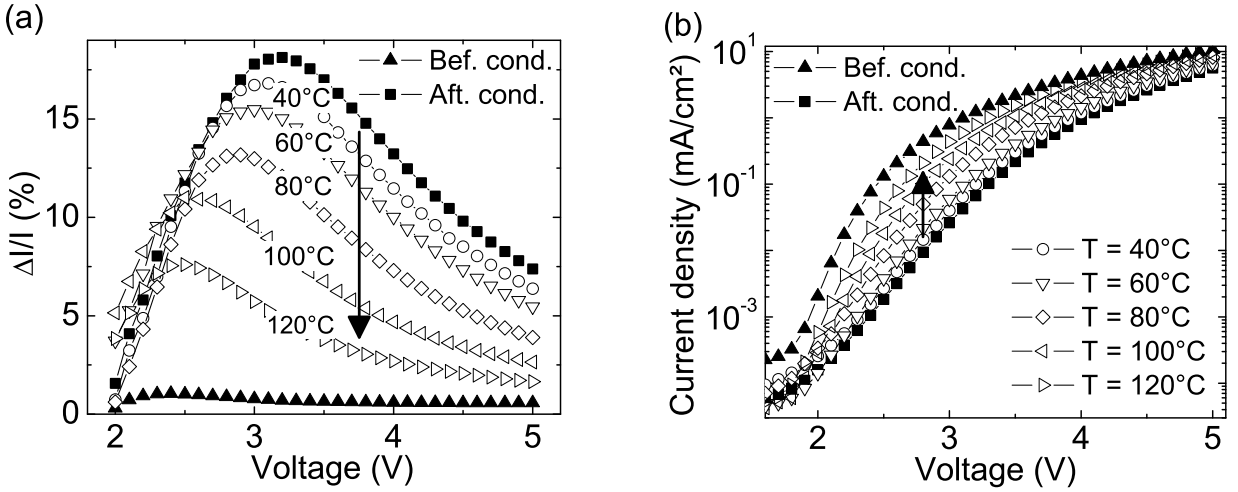

Figure 6.2: (a) Percentage change of current through a SY-PPV device as a function of voltage at a magnetic field of 40 mT. Filled triangles show $\Delta I/I$ before conditioning, filled squares show $\Delta I/I$ after conditioning at a current density of 100 mA/cm^2 for 30 min. Open symbols show $\Delta I/I$ after conditioning and subsequent annealing for 15 min at different temperatures. (b) Corresponding IV characteristics of the devices from part (a).

from 40 °C to 120 °C. It should be noted that these temperatures are still below the glass transition temperature of SY-PPV (≈ 150 °C [Edm04]). During the annealing procedure the devices were not electrically contacted. After annealing the devices were actively cooled down to room temperature using a Peltier element before the electro-optical parameters and the magnetoconductance values were determined.

In the pristine state all devices demonstrated an equal behavior in IV and LV performance and showed a magnetoconductance of 1 % at a magnetic field of 40 mT and a voltage of 2.5 V. After conditioning the magnetoconductance was increased to 18 % at 40 mT and 3.2 V in all devices whereas current density and luminance at fixed voltage were reduced. Figure 6.2a clearly demonstrates that the annealing procedure leads to significant changes in the OMR performance. For higher annealing temperatures a more pronounced reduction of the magnetoconductance can be observed. After annealing for 15 min at 120 °C the magnetoconductance at $U_{\max}$ is drastically decreased from 18 % to 8 % at 40 mT. Furthermore, the value of $U_{\max}$ strongly shifts towards the voltage where the maximum $\Delta I/I$ was obtained in the pristine devices.
Remarkable changes can also be observed when analyzing the IV characteristics before and after annealing, which are shown in figure 6.2b. Higher annealing temperatures lead to a more pronounced healing of the device and an increase of the previously reduced current density at fixed voltage. In control experiments it was found that in pristine devices with low magnetoconductance comparable annealing steps do not significantly change the maximum magnetoconductance value.

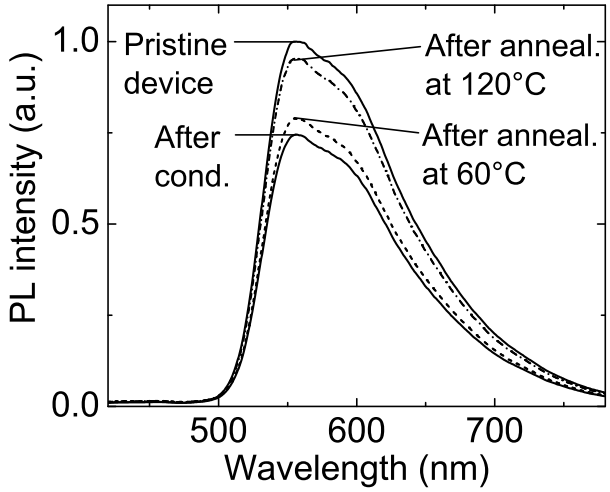

Figure 6.3:
PL spectra of a SY-PPV device in the pristine state, after conditioning at a current density of 100 mA/cm^2 for 30 min, and after subsequent annealing for 15 min at 60 °C and 120 °C, respectively. All spectra are normalized to the spectrum in the pristine state.

Figure 6.3 illustrates the PL signals before conditioning, after conditioning, and after subsequent annealing at two different temperatures. Again, individual devices have been used for each annealing temperature. In both cases the PL signal is reduced in intensity without changing its spectral position after conditioning. Thermal annealing partially restores the original PL intensity. It is clearly seen that annealing at 120 °C is more efficient in restoring

the PL signal of the pristine device than annealing at 60 °C. This is further evidence that a thermal treatment causes a healing of the stressed bulk material. In addition, it should be mentioned that the annealing procedure did not cause any permanent damage to the device. By repeating the conditioning procedure after the annealing step it was possible to increase the magnetoconductance again.

6.2.2 Annealing after optical conditioning

The reduction of magnetoconductance by thermal annealing not only works for devices that have been electrically conditioned but can as well be applied to devices that have been exposed to optical conditioning.

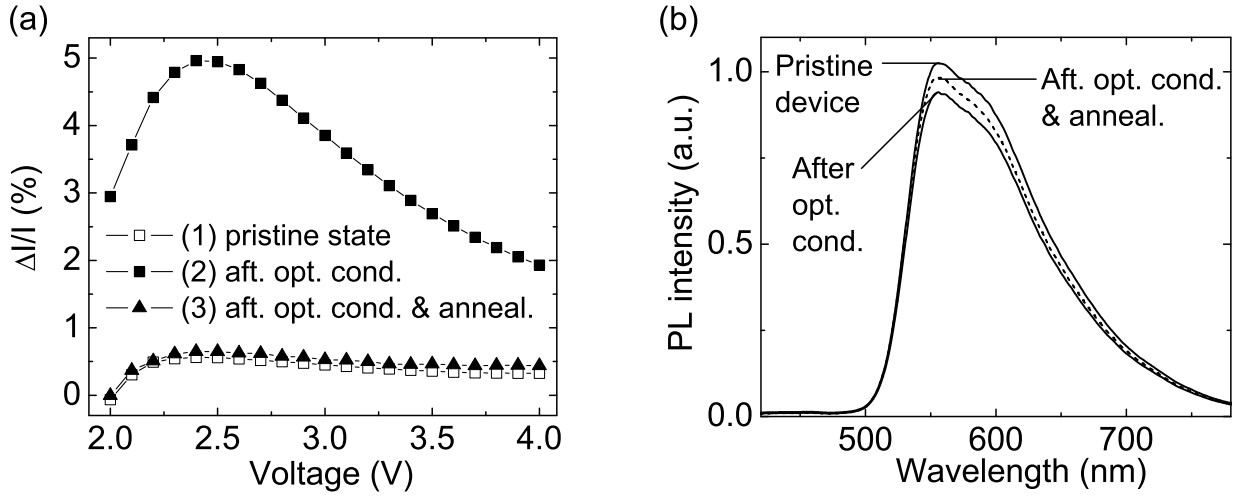

Figure 6.4: (a) Magnetoconductance at a magnetic field of 40 mT as a function of voltage for a SY-PPV device in the pristine state, after optical conditioning for 1 h, and after subsequent annealing at 130 °C for 20 min. (b) Corresponding PL spectra (normalized to the spectrum in the pristine state) for the device from part (a).

Figure 6.4a shows an OMR measurement where the maximum magnetoconductance was increased from initially 1 % to 5 % at 40 mT after optical conditioning for 1 hour. Subsequent annealing at 130 °C for 20 min reduced the magnetoconductance to its initial value. The corresponding PL signals in figure 6.4b showed variations similar to what has been observed in the case of annealing after electrical conditioning. The modification of the emitter material during conditioning caused a reduction of the PL signal, whereas the healing of the material due to annealing partially restored the original PL signal. Finally, it should be noted that after the annealing step it was possible to increase the magnetoconductance again by illuminating the device at room temperature a second time.

In summary, it can be concluded that thermally activated processes can partially reverse the material modifications that are induced by device conditioning.

6.3 Electrical conditioning at low temperatures

In case the conditioning mechanism itself is a thermally activated process the conditioning procedure is expected to be less efficient at lower temperatures. In order to check this issue, two devices on the same OLED chip with a maximum magnetoconductance of 1 % at 40 mT were electrically conditioned at different temperatures.

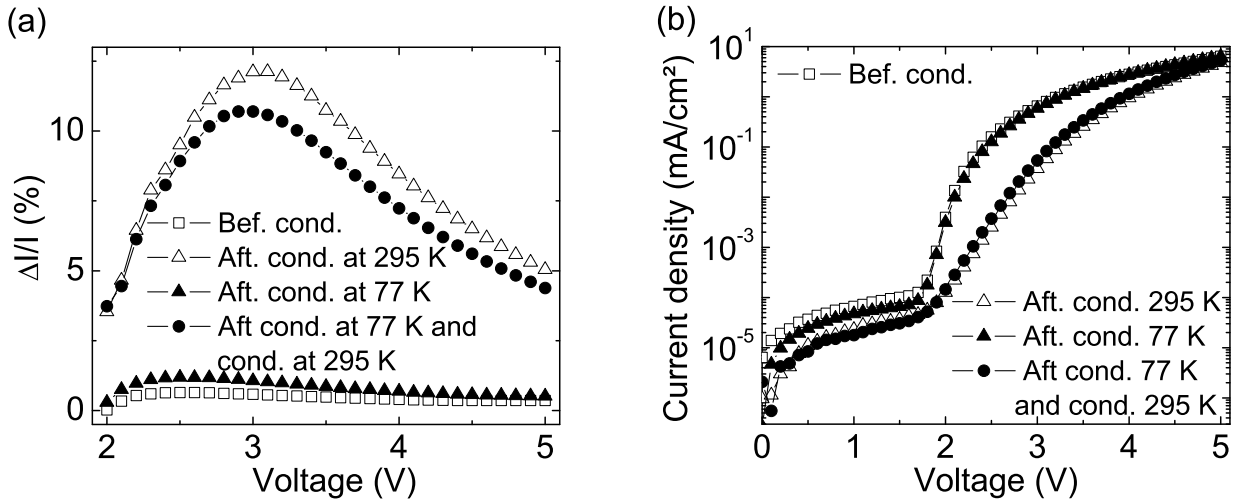

Figure 6.5: (a) Percentage change in current at a magnetic field of 40 mT as a function of voltage and (b) IV characteristics of a SY-PPV device before conditioning and after electrical conditioning at a current density of 100 mA/cm^2 for 30 min at different temperatures.

One device on the chip was used as a reference and was conditioned at 100 mA/cm^2 for 30 min at room temperature. It is shown in figure 6.5a that the magnetoconductance was increased as expected and reached a value of $\Delta I/I = 12\,\%$ at a magnetic field of 40 mT and a voltage of 3 V. Subsequently, the chip was dipped into liquid nitrogen and was cooled down to 77 K. After cooling down, a second device on the chip was conditioned at 100 mA/cm^2 for 30 min. At 77 K the necessary voltage to achieve the selected current density during conditioning was more than twice as high compared to the corresponding voltage at room temperature. After the low temperature conditioning procedure the device was heated up and the OMR effect was measured at room temperature. The maximum magnetoconductance was only slightly increased from 1 % to 1.5 % at 40 mT, which clearly differed from the large enhancement that had been observed after room temperature conditioning. In order to confirm that the device has not been damaged during the temperature changes, an additional conditioning procedure at room temperature was applied to the same device and a maximum magnetoconductance of 10 % at 40 mT was measured afterwards. The previously observed tendency that a better OMR performance after conditioning is accompanied by a poorer IV performance was also confirmed in this mea-

surement. Figure 6.5b shows that the low temperature conditioning with a small change in magnetoconductance only slightly influenced the IV characteristics, whereas the room temperature conditioning with a pronounced enhancement of the magnetoconductance led to a significant reduction of the IV performance.

6.4 Discussion of results

The results presented above demonstrate that the proposed material modifications which lead to the OMR enhancement during electrical or optical conditioning are non-permanent. Since the modifications can partially be reversed by an appropriate thermal treatment it is possible to exclude any permanent device degradation due to oxygen [Bur94, Sco96, Lin01] or due to photochemical reactions [Hei05, Zyu95] within the active material. However, it is known from literature that a thermal treatment can have a significant influence on the morphology of the polymer layer and therefore can affect the device performance [Ngu00, Liu02]. Hence, the increase of the number of trap states in SY-PPV during device conditioning might possibly be explained by morphological or conformational changes of the polymer layer. This would also be in line with a literature report where it was suggested that in electrically stressed PPV-based OLEDs structural modifications of the polymer are responsible for a decrease of the PL signal [Ke02].
A possible interpretation of the results on conditioning and annealing involves the idea that charge carrier transport in disordered materials does not occur homogeneously inside the bulk material. Previous experimental and theoretical studies suggested that one-dimensional percolation paths through the organic material carry the entire current during device operation [Mal02, Hol09].

On this background the tunability of both the OMR effect and the electro-optical device performance of SY-PPV devices by conditioning and annealing can be interpreted in the following way: In pristine devices the main current flow through the polymer is assumed to be restricted to only a few percolation paths. Since in pristine devices the density of trap states along these paths is expected to be low only a small OMR values can be observed in this case. During the conditioning procedure high local current densities occur and it can be assumed that power dissipation along the percolation paths leads to strong temperature gradients within the material. These gradients might cause mechanical stress inside the material and could be a possible origin of material modifications which create additional trap states along the paths or in the vicinity of the paths. These traps potentially lead to an enhancement of the OMR values by slowing down the charge carrier transport and by increasing the lifetime of e-h pairs in the material.
During the annealing procedure the polymer film is assumed to relax to a more homogeneous equilibrium morphology, thus containing fewer or less efficient traps. This could

explain the reduction of magnetoconductance as well as the increase in current density and electroluminescence after annealing. A reduction of the number of traps which serve as potential quenching centers might be the reason for the increased photoluminescence signal that was obtained after annealing [Pop01, Sil01].
The observation that conditioning at low temperatures is not very efficient also supports the idea that the film morphology plays a role for the OMR effect. Due to the good thermal contact with the nitrogen bath no local heating could occur inside the device during conditioning at 77 K. Hence, it seems reasonable that no significant changes of the morphology could be achieved during the low temperature conditioning, which resulted in an almost unchanged magnetoconductance. The fact that only during the subsequent conditioning at room temperature it was possible to increase the magnetoconductance suggests thermally activated processes as the reason for the OMR enhancement.

Finally, the effect of optical conditioning can also be interpreted assuming morphological changes inside the active material. At first glance, a reduction of the electro-optical performance after illumination in the near-UV and UV range might be attributed to irreversible photochemical reactions which have been studied in literature. It was shown that absorption of UV light can lead to a breaking up of C=C double bonds in polymers [Zyu95]. Oxygen atoms can afterwards attach to the free bonds and create carbonyl groups (C=O) which are known to serve as trapping and quenching centers [Zyu95]. However, photochemical reactions can be excluded as major source of the OMR enhancement in the case of optical conditioning since annealing can partially reverse the material modifications which were caused by the illumination. Hence, it is likely that also in the case of optical conditioning modifications of morphological nature are induced in the material. After absorption of the externally provided, highly intense light not all excited molecules return to the ground state via a radiative decay of excitons. In fact, nonradiative decay processes also take place and lead to the generation of high frequency vibrations inside the material. Assuming that these nonradiative decay processes occur inhomogeneously on a microscopic scale a local generation of vibrations might be expected. Similar to the case of electrical conditioning these vibrations potentially lead to mechanical stress inside the material and might result in morphological modifications which cause the formation of additional trap states in the material. Electrical conditioning is assumed to only affect the regions on or close to the percolation paths which are considered to be important for the charge carrier transport. In contrast, it is supposed that optical conditioning creates trap states throughout the polymer. Hence, the concentration of traps in the vicinity of percolation paths could be expected to be smaller compared to the situation after electrical conditioning. This might explain why only a moderate enhancement of the magnetoconductance values is achieved after optical conditioning, whereas a large enhancement of $\Delta I/I$ can be obtained after electrical conditioning.

7 Conclusion and outlook

7.1 Conclusion

Magnetic field effects in OLED devices have received an increasing amount of attention in recent years. Triggered by the discovery of the organic magnetoresistance (OMR) effect in the year 2003 both scientific and industrial research groups have started to investigate the phenomenon that external magnetic fields can have an impact on current flow and light output in OLED devices. On the one hand, studies of the OMR effect are expected to improve the general understanding of spin dynamics in OLEDs, on the other hand they might be a useful basis for the development of novel magnetic field sensor applications in the future. However, even though the OMR effect has been observed in a number of devices based on different fluorescent organic materials a fully consistent description of the underlying mechanism is still missing.
Motivated by these issues, a comprehensive characterization of the OMR effect in OLED devices based on the commercially available polymer “Super-Yellow” poly(paraphenylene vinylene) (SY-PPV) was performed in this thesis. In a first step, the influence of operating parameters and device architecture on the OMR effect was investigated and analyzed in the scope of different theoretical models. In a second step, a tunability of the OMR effect in SY-PPV devices was explored and potential explanations for this behavior were discussed.

Basic measurements showed that in bipolar SY-PPV devices both the current flow and the corresponding light output at fixed voltage can be increased when the devices are subjected to a moderate magnetic field of arbitrary orientation. In spectral measurements it was found that the application of a magnetic field only increases the intensity of the electroluminescence spectrum whereas the photoluminescence spectrum remains unchanged. A significant reduction of the OMR values in SY-PPV devices was observed when the concentration of electrons contributing to the current was lowered by varying the cathode material and by introducing deep traps for electrons in the emitter layer, respectively. Temperature dependent investigations and OMR measurements under constant current operation furthermore indicated that strong electric fields inside the emitter layer of bipolar SY-PPV devices are disadvantageous for the OMR effect.
On the basis of these fundamental results previously published theoretical models for the OMR effect were evaluated. In the currently most discussed models the mechanisms causing the OMR effect are proposed to be magnetic field dependent changes in the formation rate of bipolarons (bipolaron model), in the exciton formation rate (exciton model) and

in the intersystem crossing rate from triplet excitons to singlet excitons (exciton polaron interaction model), respectively. A comparison with own experimental data revealed that each of these models is in contradiction with selected results obtained in SY-PPV devices in the course of this thesis. However, a suitable explanation for all experimental findings in SY-PPV devices could be obtained by analyzing the obtained results in the scope of an e-h pair model which is based on the previously published assumption that the mixing between different spin states of e-h pairs with sufficiently long lifetime can be influenced by a magnetic field. According to this model the application of a magnetic field results in a larger concentration of e-h pairs in an OLED device in the steady state. A possible increase in the concentration of secondary charge carriers from e-h pair dissociation is assumed to result in a reduction of space charge effects, thus enhancing the current flow and causing a positive magnetoconductance at constant voltage. In addition, a possible increase in the concentration of formed singlet excitons from e-h pair recombination is supposed to produce a positive change in electroluminescence when a magnetic field is applied.

An important observation made in this thesis was that electrical stressing of OLED devices serves as an excellent way of device conditioning to enhance the OMR effect. In a systematic investigation of SY-PPV devices the qualitative dependence of the OMR values on the duration and the intensity of the conditioning procedure was shown and magnetoconductance values up to 25 % at a magnetic field of 40 mT were achieved. Illuminating SY-PPV devices with highly intense light in the absorption range of the active material was found to be an alternative but less efficient way to increase the OMR values without electrically contacting the devices. Both types of conditioning have in common that the investigated devices showed a reduced current density and luminance at fixed voltage as well as a reduced photoluminescence signal after conditioning. A possible reason for these changes in device performance was provided by additional results from charge carrier extraction measurements which indicated that electrical conditioning increases the number of available trap states and reduces the hole mobility inside the emitter layer of SY-PPV devices. Assuming that a slower charge carrier transport results in an increased number of e-h pairs which can potentially be influenced by a magnetic field a possible explanation of the enhanced OMR effect after conditioning in the framework of the e-h pair model was discussed.

Furthermore, it was found that both the enhancement of the OMR effect and the reduction of the electro-optical device performance after conditioning can partially be reversed by appropriate thermal annealing procedures. Based on these results it was suggested that morphological or conformational changes inside the emitter material might be responsible for the formation of additional trap states in SY-PPV devices during the conditioning procedure.

7.2 Outlook

The systematic investigations presented in this thesis extended the knowledge about the OMR effect in polymer-based devices and revealed some features that had not been discussed before in this context. Nevertheless, the OMR effect is still far from being completely understood and will certainly be subject to further research with the goal of clarifying speculative assumptions that have been made in potential explanations for the OMR effect in the past.

Up to now all theoretical models for the OMR effect rely on the microscopic mechanism of spin conversion due to the hyperfine interaction. However, no direct experimental evidence for the existence of this mechanism in materials typically used in OLED devices has been provided so far. The proposed relevance of the hyperfine interaction for the OMR effect might be checked by investigating the magnetoconductance in organic materials in which the hydrogen atoms have been replaced by atoms with a different strength of the hyperfine interaction.

Another task for future research is the ultimate decision whether a single-carrier mechanism, a double-carrier mechanism or a combination of both is the correct way of describing the OMR effect. Even though most publications (including this thesis) are in favor of a double-carrier mechanism, they can not exclude all other possible options with certainty. In this context it might be advisable to perform charge carrier transport studies on truly unipolar devices in order to find out whether or not magnetic fields can have an influence on the mobility of charge carriers.

Moreover, future studies could be devoted to a further exploration of the OMR enhancement due to device conditioning. On the one hand, it might be interesting to learn more about the material modifications during conditioning, for instance by employing structural analysis techniques or more sophisticated optical measurement methods. On the other hand, efforts should be made to find alternative ways to obtain large magnetoconductance values even in pristine devices. According to the e-h pair model an improvement of the OMR values might be achieved by artificially slowing down the charge carrier transport in the active material.

Finally, further efforts might be devoted to investigations of the OMR effect from a technological point of view. The results presented in this thesis demonstrate the high potential of organic electronics because the OMR values achieved in conditioned devices are comparable in magnitude to values caused by conventional magnetoresistance effects which are used in commercially available sensors based on inorganic materials. However, the rather poor stability of the OMR signal over time and the pronounced temperature dependence of both the zero-field conductance and the magnetoconductance in organic materials are serious challenges that have to be either overcome or compensated by appropriate electronic circuits before the OMR effect can be brought into practical application.

A Calculations within the electron-hole pair model

In the following sections a derivation of expressions for magnetic field effects on the concentration of singlet and triplet excitons as well as on the concentration of secondary charge carriers from dissociation in the framework of the e-h pair model will be given. As in the case of the derivation of the magnetic field effect on the concentration of e-h pairs in section 3.6 the two limiting cases of zero magnetic field and large magnetic field (compared to the hyperfine interaction strength) will be evaluated in order to calculate the corresponding expressions. All constants in the calculations are used according to their definitions in section 3.6. It is furthermore assumed that only the lifetime of e-h pairs depends on the magnetic field whereas the relevant times for the depopulation of excitonic states are considered to be independent of the magnetic field.

Magnetic field effect on the concentration of singlet excitons

- Generation rate S_0 of singlet excitons in zero magnetic field:

$$S_0 = G\tau_0 k_{\mathrm{r}}^{\mathrm{S}} = \frac{G k_{\mathrm{r}}^{\mathrm{S}}}{(k_{\mathrm{r}}^{\mathrm{S}} + k_{\mathrm{d}}^{\mathrm{S}}) + 3(k_{\mathrm{r}}^{\mathrm{T}} + k_{\mathrm{d}}^{\mathrm{T}})}. \tag{A.1}$$

- Generation rate S_B of singlet excitons with applied magnetic field:

$$S_B = (G/2)\tau_{\mathrm{ST}} k_{\mathrm{r}}^{\mathrm{S}} = \frac{(G/2) k_{\mathrm{r}}^{\mathrm{S}}}{\left(k_{\mathrm{r}}^{\mathrm{S}} + k_{\mathrm{d}}^{\mathrm{S}} + k_{\mathrm{r}}^{\mathrm{T}} + k_{\mathrm{d}}^{\mathrm{T}}\right)}. \tag{A.2}$$

- Relative change in concentration of singlet excitons due to a magnetic field:

$$\frac{\Delta S}{S} = \frac{S_B - S_0}{S_0} = \frac{\tau_{\mathrm{S}}/\tau_{\mathrm{T}} - 1}{2\left(1 + \tau_{\mathrm{S}}/\tau_{\mathrm{T}}\right)}. \tag{A.3}$$

  Expression (A.3) is equivalent to expression (3.11) and is plotted in figure 3.13a in section 3.6.

Magnetic field effect on the concentration of triplet excitons

- Generation rate T_0 of triplet excitons in zero magnetic field:

$$T_0 = G\tau_0 3k_r^T = \frac{G\,3k_r^T}{(k_r^S + k_d^S) + 3(k_r^T + k_d^T)}. \tag{A.4}$$

- Generation rate T_B of triplet excitons with applied magnetic field:

$$T_B = (G/2)\tau_{ST}k_r^T + 2(G/4)\tau_T k_r^T = \frac{(G/2)k_r^T}{\left(k_r^S + k_d^S + k_r^T + k_d^T\right)} + \frac{(G/2)k_r^T}{k_r^T + k_d^T}. \tag{A.5}$$

- Relative change in concentration of triplet excitons due to a magnetic field:

$$\frac{\Delta T}{T} = \frac{T_B - T_0}{T_0} = \frac{1 - \tau_S/\tau_T}{6\left(1 + \tau_S/\tau_T\right)\tau_S/\tau_T}. \tag{A.6}$$

Expression (A.6) is equivalent to expression (3.12) and is plotted in figure 3.13a in section 3.6.

Magnetic field effect on the concentration of secondary charge carriers

- Generation rate Q_0 of secondary charge carriers in zero magnetic field:

$$Q_0 = G\tau_0\left(k_d^S + 3k_d^T\right) = \frac{G\left(k_d^S + 3k_d^T\right)}{(k_r^S + k_d^S) + 3(k_r^T + k_d^T)}. \tag{A.7}$$

- Generation rate Q_B of secondary charge carriers with applied magnetic field:

$$Q_B = (G/2)\tau_{ST}\left(k_d^S + k_d^T\right) + 2(G/4)\tau_T k_d^T = \frac{(G/2)k_r^T}{\left(k_r^S + k_d^S + k_r^T + k_d^T\right)} + \frac{(G/2)k_r^T}{k_r^T + k_d^T}. \tag{A.8}$$

- Relative change in concentration of secondary charge carriers due to a magnetic field:

$$\frac{\Delta Q}{Q} = \frac{Q_B - Q_0}{Q_0} = \frac{\left(\tau_S/\tau_T - 1\right)\left(\tau_S/\tau_T - k_d^T/k_d^S\right)}{2\left(1 + \tau_S/\tau_T\right)\tau_S/\tau_T\left(1 + 3k_d^T/k_d^S\right)}. \tag{A.9}$$

Expression (A.9) is equivalent to expression (3.13) in section 3.6.

Depending on the value of $b = k_{\mathrm{d}}^{\mathrm{T}}/k_{\mathrm{d}}^{\mathrm{S}}$ expression (A.9) can be simplified in the following ways:

$$b = 1 \implies \frac{\Delta Q}{Q} = \frac{\left(\tau_{\mathrm{S}}/\tau_{\mathrm{T}} - 1\right)^2}{8\left(1 + \tau_{\mathrm{S}}/\tau_{\mathrm{T}}\right)\tau_{\mathrm{S}}/\tau_{\mathrm{T}}}, \tag{A.10}$$

$$b << 1 \implies \frac{\Delta Q}{Q} = \frac{\tau_{\mathrm{S}}/\tau_{\mathrm{T}} - 1}{2\left(1 + \tau_{\mathrm{S}}/\tau_{\mathrm{T}}\right)}. \tag{A.11}$$

Expressions (A.10) and (A.11) are plotted in figure 3.13b in section 3.6.

List of Abbreviations and Symbols

Abbreviations

a.u.	Arbitrary units
Alq_3	Aluminum tris(8-hydroxyquinoline)
DF	Delayed fluorescence
DOS	Density of states
E-h pair	Electron-hole pair
EL	Electroluminescence
EPI	Exciton polaron interaction
HF	Hyperfine
HOMO	Highest occupied molecular orbital
ISC	Intersystem crossing
IR	Infrared
$Ir(ppy)_3$	Tris(2-phenylpyridyl)iridium (III)
ITO	Indium tin oxide
IV	Current-voltage
LUMO	Lowest unoccupied molecular orbital
LV	Luminance-voltage
NPB	N,N'-bis(naphthalen-1-yl)-N,N'-bis(phenyl)-benzidine
OLED	Organic light emitting diode
OMR	Organic magnetoresistance
P	Polaron
P3HT	Poly-3-hexylthiophene
PCBM	[6,6]-phenyl C61-butyric acid methyl ester
PEDOT:PSS	Poly(3,4-ethylenedioxythiophene):poly(styrenesulfonate)
PFO	Polyfluorene
Photo-CELIV	Photogenerated charge carrier extraction by linearly increasing voltage
PL	Photoluminescence
PPV	Poly(paraphenylene vinylene)
PtOEP	Platinum octaethylporphyrin
S	Singlet
SY-PPV	"Super yellow"-PPV
T	Triplet
TSC	Thermally stimulated current

Symbols

a	Hyperfine coupling constant
β	Exciton formation rate
$\mathbf{B}$	Magnetic field
$\mathbf{B}_{\mathrm{HF}}$	Hyperfine interaction field
d	Layer thickness
$\Delta EL/EL$	Magnetoelectroluminescence
$\Delta I/I$	Magnetoconductance
$\Delta R/R$	Magnetoresistance
$\Delta S/S$	Change in concentration of singlet excitons
$\Delta T/T$	Change in concentration of triplet excitons
$\Delta Q/Q$	Change in concentration of secondary charge carriers
E	Energy, Electric field
E_{F}	Fermi energy level
EL	Electroluminescence intensity
Φ	Work function
g	g-factor
G	Creation rate of e-h pairs
H	Hamiltonian
I	Current
$\mathbf{I}$	Nuclear spin
j	Extraction current density
J	Exchange interaction parameter
k_{B}	Boltzmann constant
k_{d}	Dissociation rate constant
k_{r}	Recombination rate constant
μ	Charge carrier mobility
μ_{B}	Bohr magneton
N	Concentration of e-h pairs
Q	Generation rate of secondary charge carriers, Electric charge
r	Distance
R	Resistance
σ	Formation cross section of e-h pair formation
S	Generation rate of singlet excitons
$\mathbf{S}$	Spin of charge carrier
t	Time
τ	Lifetime of e-h pair
τ_{rel}	Spin-lattice relaxation time
τ_{evo}	Spin evolution time
T	Temperature; Generation rate of triplet excitons
t_{del}	Delay time
t_{max}	Time of maximum extraction current
U	Voltage
U_{max}	Voltage with maximum OMR effect
U_{th}	Threshold voltage

List of Figures

2.1 Typical device structure of an OLED 7
2.2 Energy level diagram and working principle of a two-layer OLED 8
2.3 Density of states for HOMO and LUMO in an organic semiconductor 9
2.4 Possible spin states of an e-h pair 10
2.5 Energy levels of excitonic states and possible transitions between them 11
2.6 Magnetoresistance curves for an ITO/PEDOT/PFO/Ca device 15
2.7 Spin-flip of a charge carrier due to the hyperfine interaction 18
2.8 Possible spin conversion events for e-h pairs with and without applied magnetic field 20
2.9 Processes in an OLED with a potential magnetic field dependence 22
2.10 Hopping transport according to the bipolaron model 24
2.11 Charge carrier density in an OLED according to the exciton model 25
2.12 Charge carrier transport with scattering events at triplet excitons 27
2.13 Current-voltage and luminance-voltage characteristics of a SY-PPV device . . 29
2.14 Experimental setup for LIV and OMR measurements 30
2.15 Exemplary measurement to determine the magnetoconductance 31
2.16 Pulse sequence and typical current transients of a photo-CELIV measurement 33
3.1 Influence of a magnetic field on the current flow through a SY-PPV device . . 38
3.2 Magnetoconductance of a SY-PPV device as a function of magnetic field and voltage 39
3.3 Magnetoelectroluminescence of a SY-PPV device as a function of magnetic field and voltage 40
3.4 Magnetic field effect on voltage and *EL* at constant current in a SY-PPV device 41
3.5 *IV* characteristics and magnetoconductance of SY-PPV devices with different emitter thicknesses 43
3.6 *LIV* characteristics and magnetoconductance of SY-PPV:PtOEP devices with different PtOEP concentrations 44
3.7 *LIV* characteristics and magnetoconductance of SY-PPV devices with different cathodes 46
3.8 *LIV* characteristics and magnetoconductance of SY-PPV devices with and without hole injection layer 47
3.9 *IV* characteristics and magnetoconductance of a SY-PPV device at different temperatures 48

3.10 Emission spectrum of an external light source and absorption spectrum of a SY-PPV film 49
3.11 Current and magnetoconductance in a SY-PPV device during illumination intervals 50
3.12 Energy level diagram and transition rate constants for free charges, e-h pairs and excitons 57
3.13 Calculated magnetic field effects for $\Delta N/N$, $\Delta S/S$, $\Delta T/T$ and $\Delta Q/Q$ 60
3.14 Absolute change in current at constant magnetic field as a function of current and temperature for a SY-PPV device 64
4.1 Magnetoconductance and magnetoelectroluminescence of a SY-PPV device as a function of voltage and magnetic field before and after electrical conditioning 68
4.2 Magnetoconductance of a SY-PPV device as a function of voltage and magnetic field after electrical conditioning for different time intervals 69
4.3 Magnetoconductance and luminance of a SY-PPV device as a function of conditioning time after conditioning at different currents 70
4.4 LIV characteristics of SY-PPV devices before and after electrical conditioning at different currents 71
4.5 PL spectra of a SY-PPV device after conditioning for different time intervals . 72
4.6 Magnetoconductance of Alq_3 devices as a function of voltage and magnetic field before and after electrical conditioning at different current densities . . 73
4.7 LIV characteristics of Alq_3 devices before and after electrical conditioning at different current densities 73
4.8 Magnetoconductance of a SY-PPV device as a function of voltage and magnetic field before and after optical conditioning 74
4.9 LIV characteristics and PL signal of a SY-PPV device before and after optical conditioning 75
4.10 *EL* and absolute changes in current and in *EL* at constant magnetic field as a function of current in a SY-PPV device 76
5.1 Magnetoconductance of a SY-PPV device as a function of voltage and IV characteristics in the dark and under illumination with IR light 80
5.2 Absolute change ΔI in current at constant magnetic field as a function of current for a SY-PPV device in the dark and under illumination with IR light 80
5.3 Temporal evolution of extraction current through a SY-PPV device with and without IR illumination during thermalization period 81
5.4 TSC signals for a SY-PPV device before and after electrical conditioning . . . 83
5.5 Voltage ramp and typical extraction currents during a photo-CELIV measurement 84

5.6 Photocurrent transients after different delay times for a SY-PPV device before and after conditioning 85
5.7 Calculated mobility values as a function of time for a SY-PPV device before and after conditioning 86
6.1 Magnetoconductance of a conditioned SY-PPV device during and after a relaxation time interval 87
6.2 Magnetoconductance and IV characteristics of a conditioned SY-PPV device after annealing at different temperatures 88
6.3 PL spectra of a SY-PPV device in the pristine state, after conditioning, and after subsequent annealing 89
6.4 Magnetoconductance and PL spectra of a SY-PPV device in the pristine state, after optical conditioning, and after subsequent annealing 90
6.5 Magnetoconductance and IV characteristics of a SY-PPV device before and after electrical conditioning at different temperatures 91

Bibliography

[Abk95] M. A. Abkowitz, H. A. Mizes and J. S. Facci, Appl. Phys. Lett. **66** (10), 1288 (1995).

[Ark98] V. I. Arkhipov, E. V. Emelianova, Y. H. Tak, and H. Bässler, J. Appl. Phys. **84**, 848 (1998).

[Bag03] S. A. Bagnich and H. Bässler, Chem. Phys. Lett. **381**, 464 (2003).

[Bag09a] S. A. Bagnich, U. Niedermeier, C. Melzer, W. Sarfert, and H. von Seggern, J. Appl. Phys. **105**, 123706 (2009).

[Bag09b] S. A. Bagnich, U. Niedermeier, C. Melzer, W. Sarfert, and H. von Seggern, J. Appl. Phys. **106**, 113702 (2009).

[Bai88] M. N. Baibich, J. M. Broto, A. Fert, F. Nguyen van Dau, F. Petroff, P. Eitenne, G. Creuzet, A. Friederich, and J. Chazelas, Phys. Rev. Lett. **61**, 2472 (1988).

[Bal99] M. A. Baldo, D. F. O'Brien, M. E. Thompson, and S. R. Forrest, Phys. Rev. B **60**, 14422 (1999).

[Ban09] S. Bange, PhD thesis, Universität Potsdam (2009).

[Bäs93] H. Bässler, Phys. Stat. Sol. (b) **175**, 15 (1993).

[Bin89] G. Binasch, P. Grünberg, F. Saurenbach, and W. Zinn, Phys. Rev. B **39**, 4828 (1989).

[Blo00] P. W. M. Blom and M. C. J. M. Vissenberg, Mat. Sci. Eng. **27**, 53 (2000).

[Blo01] P. W. Blom, H. C. F. Martens, and J. N. Huiberts, Synth. Met. **121**, 1621 (2001).

[Blo07] F. L. Bloom, W. Wagemans, M. Kemerink, and B. Koopmans, Phys. Rev. Lett. **99**, 257201 (2007).

[Blo08a] F. L. Bloom, W. Wagemans, and B. Koopmans, J. Appl. Phys **103**, 07F320 (2008).

[Blo08b] F. L. Bloom, W. Wagemans, M. Kemerink, and B. Koopmans, Appl. Phys. Lett. **93**, 263302 (2008).

[Bob07] P. A. Bobbert, T. D. Nguyen, F. W. A. van Oost, B. Koopmans, and M. Wohlgenannt, Phys. Rev. Lett. **99**, 216801 (2007).

[Bol08] H. J. Bolink, E. Coronado, J. Orozco, and M. Sessolo, Adv. Mater. **20**, 1 (2008).

[Bra01] C. J. Brabec, N. S. Sariciftci, and J. C. Hummelen, Adv. Funct. Mater. **11**, 15 (2001).

[Bra08] S. E. Braslavsky, E. Fron, H. B. Rodriguez, E. S. Roman, G. D. Scholes, G. Schweitzer, B. Valeur, and J. Wirz, Photochem. Photobiol. Sci. **7**, 1444 (2008).

[Bur90] J. H. Burroughes, D. D. C. Bradley, A. R. Brown, R. N. Marks, K. Mackay, R. H. Friend, P. L. Burns, and A. B. H. Holmes, Nature **347**, 539 (1990).

[Bur94] P. E. Burrows, V. Bulovic, S. R. Forrest, L. S. Sapochak, D. M. McCarty, and M. E. Thompson, Appl. Phys. Lett. **65**, 2922 (1994).

[Che06] L. Chen, L. Zhu, and Z. Shuai, J. Phys. Chem. A **110**, 13349 (2006).

[Cöl04] M. Cölle and C. Gärditz, Appl. Phys. Lett. **84**, 3160 (2004).

[De99] R. De, Y. Fujiwara, T. Haino, and Y. Tanimoto, Chem. Phys. Lett. **315**, 383 (1999).

[Ded09] V. A. Dediu, L. E. Hueso, I. Bergenti, and C. Taliani, Nat. Mater. **8**, 707 (2009).

[Des07a] P. Desai, P. Shakya, T. Kreouzis, W. P. Gillin, N. A. Morley, and M. R. J. Gibbs, Phys. Rev. B **75**, 094423 (2007).

[Des07b] P. Desai, P. Shakya, T. Kreouzis, and W. P. Gillin, J. Appl. Phys. **102**, 073710 (2007).

[Dex53] D. L. Dexter, J. Chem. Phys. **21**, 836 (1953).

[Dho02] A. S. Dhoot, D. S. Ginger, D. Beljonne, Z. Shuai, and N. C. Greenham, Chem. Phys. Lett. **360**, 195 (2002).

[Din00] X. Ding, L. Hung, L. Cheng, Z. Deng, X. Hou, C. Lee, and S. Lee, Appl. Phys. Lett. **76**, 2704 (2000).

[Dya98] V. Dyakonov and E. Frankevich, Chem. Phys. **227**, 203 (1998).

[Edm04] L. Edman, M. Pauchard, D. Moses, and A. J. Heeger, J. Appl. Phys. **95**, 4357 (2004).

[Ern68] V. Ern and R. E. Merrifield, Phys. Rev. Lett. **21**, 609 (1968).

[Fer05] C. Fery, B. Racine, D. Vaufrey, H. Doyeux, and S. Cina, Appl. Phys. Lett. **87**, 213502 (2005).

[För48] T. Förster, Ann. Phys. **2**, 55 (1948).

[Fra92a] E. Frankevich, A. Lymarev, I. Sokolik, F. Karasz, S. Blumstengel, R. Baughman, and H. Hörhold, Phys. Rev. B **46**, 9320 (1992).

[Fra92b] E. L. Frankevich, A. A. Lymarev, and I. A. Sokolik, Chem. Phys. **162**, 1 (1992).

[Fra04] T. L. Francis, Ö. Mermer, G. Veeraraghavan, and M. Wohlgenannt, New J. Phys. **6**, 185 (2004).

[Fri99] R. H. Friend, R. W. Gymer, A. B. Holmes, J. H. Burroughes, R. N. Marks, C. Taliani, D. D. C. Bradley, D. A. Dos Santos, J. L. Bredas, M. Logdlund, and W. R. Salaneck, Nature **397**, 121 (1999).

[Gär05] C. Gärditz, A. Mückl, and M. Cölle, J. Appl. Phys. **98**, 104507 (2005).

[Hei05] H. Heil, G. Andress, R. Schmechel, H. von Seggern, J. Steiger, K. Bonrad, and R. Sprengard, J. Appl. Phys. **97**, 124501 (2005).

[Her07] D. Hertel and K. Meerholz, J. Phys. Chem. B **111**, 12075 (2007).

[Hol09] J. J. M. van der Holst, M. A. Uijttewaal, B. Ramachandhran, R. Coehoorn, P. A. Bobbert, G. A. de Wijs, and R. A. de Groot, Phys. Rev. B **79**, 085203 (2009).

[Hu07] B. Hu and Y. Wu, Nat. Mater. **6**, 985 (2007).

[Hu09] B. Hu, L. Yan, and M. Shao, Adv. Mater. **21**, 1500 (2009).

[Hun03] A. Hunze, PhD thesis, Universität Erlangen-Nürnberg (2003).

[Joh70] R. C. Johnson and R. E. Merrifield, Phys. Rev. B **1**, 896 (1970).

[Jul75] M. Julliere, Phys. Lett. A **54**, 225 (1975).

[Jus00a] G. Juska, K. Arlauskas, M. Viliunas, and J. Kocka, Phys. Rev. Lett. **84**, 4946 (2000).

[Jus00b] G. Juska, K. Arlauskas, M. Viliunas, K. Genevicius, R. Österbacka, and H. Stubb, Phys. Rev. B **62**, R16235 (2000).

[Kal03a] J. Kalinowski, M. Cocchi, D. Virgili, P. di Marco, and V. Fattori, Chem. Phys. Lett. **380**, 710 (2003).

[Kal03b] J. Kalinowski, J. Szmytkowski, and W. Stampor, Chem. Phys. Lett. **378**, 380 (2003).

[Ke02] L. Ke, P. Chen, and S. J. Chua, Appl. Phys. Lett. **80**, 697 (2002).

[Ker93] R. Kersting, U. Lemmer, R. F. Mahrt, K. Leo, H. Kurz, H. Bässler, and E. O. Göbel, Phys. Rev. Lett. **70**, 3820 (1993).

[Ker94] R. Kersting, U. Lemmer, M. Deussen, H. J. Bakker, R. F. Mahrt, H. Kurz, V. I. Arkhipov, H. Bässler and E. O. Göbel, Phys. Rev. Lett. **73**, 1440 (1994).

[Kod08] Eastman Kodak Company, Press release, www.kodak.com (2008).

[Köh02] A. Köhler, J. S. Wilson, and R. H. Friend, Adv. Mater. **14**, 701 (2002).

[Kug99] T. Kugler, W. Salaneck, H. Rost, and A. Holmes, Chem. Phys. Lett. **310**, 391 (1999).

[Lid99] D. R. Lide (Ed.), CRC Handbook of Chemistry and Physics, CRC Press, Boca Raton (1999).

[Lin01] K. K. Lin, S. J. Chua, and S. F. Lim, J. Appl. Phys. **90**, 976 (2001).

[Liu02] J. Liu, T. F. Guo, and Y. Yang, J. Appl. Phys. **91**, 1595 (2002).

[Ma05] M. Ma, P. Iyer, X. Gong, B. Liu, D. Moses, G. Bazn, and A. Heeger, Adv. Mater. **17**, 274 (2005).

[Maj09] S. Majumdar, H. S. Majumdar, H. Aarnio, D. Vanderzande, R. Laiho, and R. Österbacka, Phys. Rev. B **79**, 201202(R) (2009).

[Mäk02] A. J. Mäkinen, I. G. Hill, and Z. H. Kafafi, J. Appl. Phys. **92**, 1598 (2002).

[Mal02] N. von Malm, J. Steiger, H. Heil, R. Schmechel, and H. von Seggern, J. Appl. Phys. **92**, 7564 (2002).

[Mal03] N. von Malm, PhD thesis, Technische Universität Darmstadt (2003).

[Man07] M. M. Mandoc, B. de Boer, G. Paasch, and P. W. M. Blom, Phys. Rev. B **75**, 193202 (2007).

[Mar01] H. C. F. Martens, W. F. Pasveer, H. B. Brom, J. N. Huiberts, and P. W. M. Blom, Phys. Rev. B **63**, 125328 (2001).

[Mer68] R. E. Merrifield, J. Chem. Phys. **48**, 4318 (1968).

[Mer05a] Ö. Mermer, G. Veeraraghavan, T. Francis, and M. Wohlgenannt, Solid State Commun. **134**, 631 (2005).

[Mer05b] Ö. Mermer, G. Veeraraghavan, T. Francis, Y. Sheng, T. D. Nguyen, M. Wohlgenannt, A. Köhler, M. K. Al-Suti, and M. S. Khan, Phys. Rev. B **72**, 205202 (2005).

[Mes03] S. C. J. Meskers, J. K. J. van Duren, and R. A. J. Janssen, Adv. Funct. Mater. **13**, 805 (2003).

[Moz05a] A. J. Mozer, N. S. Sariciftci, L. Lutsen, D. Vanderzande, R. Österbacka, M. Westerling, and G. Juska, Appl. Phys. Lett. **86**, 112104 (2005).

[Moz05b] A. J. Mozer, G. Dennler, N. S. Sariciftci, M. Westerling, A. Pivrikas, R. Österbacka, and G. Juska, Phys. Rev. B **72**, 035217 (2005).

[Nab07] W. J. M. Naber, S. Faez, and W. G. van der Wiel, J. Phys. D: Appl. Phys. **40**, R205 (2007).

[Neu05] F. Neumann, Y. A. Genenko, R. Schmechel, and H. von Seggern, Synth. Met. **150**, 291 (2005).

[Ngu00] T. Q. Nguyen, R. C. Kwong, M. E. Thompson, and B. J. Schwartz, Appl. Phys. Lett. **76**, 2454 (2000).

[Ngu07a] T. D. Nguyen, Y. Sheng, J. Rybicki, G. Veeraraghavan, and M. Wohlgenannt, J. Mater. Chem. **17**, 1995 (2007).

[Ngu07b] T. D. Nguyen, Y. Sheng, M. Wohlgenannt, and T. D. Anthopoulos, Synth. Met. **157**, 930 (2007).

[Ngu08] T. D. Nguyen, Y. Sheng, J. E. Rybicki, and M. Wohlgenannt, Phys. Rev. B **77**, 235209 (2008).

[Nie08a] U. Niedermeier, M. Vieth, R. Pätzold, W. Sarfert, and H. von Seggern, Appl. Phys. Lett. **92**, 93309 (2008).

[Nie08b] U. Niedermeier, W. Sarfert, and H. von Seggern, Proc. of SPIE Vol. **6999**, 699913 (2008).

[Nie09] U. Niedermeier, S. A. Bagnich, C. Melzer, W. Sarfert, and H. von Seggern, Synth. Met., doi: 10.1016/j.synthmet.2009.06.012, in press (2009).

[Oda06] H. Odaka, Y. Okimoto, T. Yamada, H. Okamoto, M. Kawasaki, and Y. Tokura, Appl. Phys. Lett. **88**, 123501 (2006).

[Osr08] OSRAM GmbH, Press release, www.osram.de (2008).

[Öst99] R. Österbacka, M. Wohlgenannt, D. Chinn, and Z. V. Vardeny, Phys. Rev. B **60**, R 11 253 (1999).

[Öst04] R. Österbacka, A. Pivrikas, G. Juska, K. Genevicius, K. Arlauskas, and H. Stubb, Curr. Appl. Phys. **4**, 534 (2004).

[Par59] R. H. Parmenter and W. Ruppel, J. Appl. Phys. **30**, 1548 (1959).

[Par99] I. D. Parker, Y. Cao, and C. Y. Yang, J. Appl. Phys. **85**, 4 (1999).

[Pas05] W. F. Pasveer, J. Cottaar, C. Tanase, R. Coehoorn, P. A. Bobbert, P. W. M. Blom, D. M. de Leeuw, and M. A. J. Michels, Phys. Rev. Lett. **94**, 206601 (2005).

[Pop01] Z. D. Popovic, H. Aziz, N. X. Hu, A. Ioannidis, and P. N. M. dos Anjos, J. Appl. Phys. **89**, 4673 (2001).

[Pop82] M. Pope and C. Swenberg, Electronic Processes in Organic Crystals, Oxford University Press, (1982).

[Pri06] V. N. Prigodin, J. D. Bergeson, D. M. Lincoln, and A. J. Epstein, Synth. Met. **156**, 757 (2006).

[Ran09] B. P. Rand, S. Schols, D. Cheyns, H. Gommans, C. Girotto, J. Genoe, P. Heremans, and J. Poortmans, Org. Electron. **10**, 1015 (2009).

[Rei09] S. Reineke, F. Lindner, G. Schwartz, N. Seidler, K. Walzer, B. Lüssem, and K. Leo, Nature **459**, 234 (2009).

[Reu05] M. Reufer, M. J. Walter, P. G. Lagoudakis, B. Hummel, J. S. Kolb, H. G. Roskos, U. Scherf, and J. M. Lupton, Nat. Mater. **4**, 340 (2005).

[Roc82] K. D. Rockwitz and H. Bässler, Chem. Phys. **70**, 307 (1982).

[Roh99] M. Rohlfing and S. G. Louie, Phys. Rev. Lett. **82**, 1959 (1999).

[Rot96] L. Rothberg and A. Lovinger, J. Mat. Res. **11**, 3174 (1996).

[Sch78] K. Schulten and P. G. Wolynes, J. Chem. Phys. **68**, 3292 (1978).

[Sch04] R. Schmechel and H. von Seggern, Phys. Stat. Sol. (a) **201**, 1215 (2004).

[Sco03] J. C. Scott and J. Vac. Sci. Technol. A **21**, 521 (2003).

[Sco96] J. C. Scott, J. H. Kaufman, P. J. Brock, R. DiPietro, J. Salem, and J. A. Goitia, J. Appl. Phys. **79**, 2745 (1996).

[Sha07] Y. Shao, G. C. Bazan, and A. J. Heeger, Adv. Mater. **19**, 365 (2007).

[Sha08] P. Shakya, P. Desai, T. Kreouzis, W. P. Gillin, S. M. Tuladhar, A. M. Ballantyne, and J. Nelson, J. Phys.: Condens. Matter **20**, 452203 (2008).

[She06] Y. Sheng, T. D. Nguyen, G. Veeraraghavan, Ö. Mermer, M. Wohlgenannt, S. Qiu, and U. Scherf, Phys. Rev. B **74**, 045213 (2006).

[She07] Y. Sheng, T. D. Nguyen, G. Veeraraghavan, Ö. Mermer, and M. Wohlgenannt, Phys. Rev. B **75**, 035202 (2007).

[Sil01] G. C. M. Silvestre, M. T. Johnson, A. Giraldo, and J. M. Shannon, Appl. Phys. Lett. **78**, 11 (2001).

[Sir99] H. Sirringhaus, P. J. Brown, R. H. Friend, M. M. Nielsen, K. Bechgaard, B. M. W. Langeveld-Voss, A. J. H. Spiering, R. A. J. Janssen, E. W. Meijer, P. Herwig, and D. M. de Leeuw, Nature **401**, 685 (1999).

[Sok74] I. A. Sokolik and E. L. Frankevich, Sov. Phys.-Usp. **16**, 687 (1974).

[Son07] SONY Corp., Press release, www.sony.net (2007).

[Spr03] H. Spreitzer, H. Becker, E. Breuning, A. Falcou, K. Treacher, A. Büsing, A. Parham, P. Stößel, S. Heun, and J. Steiger, Proc. of SPIE Vol. **4800**, 16 (2003).

[Ste89] U. E. Steiner and T. Ulrich, Chem. Rev. **89**, 51 (1989).

[Tan87] C. W. Tang and S. A. van Slyke, Appl. Phys. Lett. **51**, 913 (1987).

[Tsu86] A. Tsumura, H. Koezuka, and T. Ando, Appl. Phys. Lett. **49**, 1210 (1986).

[Wag08] W. Wagemans, F. L. Bloom, P. A. Bobbert, M. Wohlgenannt, and B. Koopmans, J. Appl. Phys. **103**, 07F303 (2008).

[Wan08] F. J. Wang, H. Bässler, and Z. V. Vardeny, Phys. Rev. Lett. **101**, 236805 (2008).

[Wil01] J. S. Wilson, A. S. Dhoot, A. J. A. B. Seeley, M. S. Khan, A. Köhler, and R. H. Friend, Nature **413**, 828 (2001).

[Woh01] M. Wohlgenannt, K. Tandon, S. Mazumdar, S. Ramasesha, and Z. V. Vardeny, Nature **409**, 494 (2001).

[Woh02] M. Wohlgenannt, X. M. Jiang, Z. V. Vardeny, and R. A. J. Janssen, Phys. Rev. Lett. **88**, 197401 (2002).

[Woh03] M. Wohlgenannt and Z. V. Vardeny, J. Phys.: Condens. Matter **15** R83 (2003).

[Woh06] M. Wohlgenannt, arXiv:cond-mat/0609592, 1 (2006).

[Wu07] Y. Wu, Z. Xu, B. Hu, and J. Howe, Phys. Rev. B **75**, 035214 (2007).

[Xin09] L. Xin, C. Li, F. Li, S. Liu, and B. Hu, Appl. Phys. Lett. **95**, 123306 (2009).

[Xio04] Z. H. Xiong, D. Wu, Z. V. Vardeny, and J. Shi, Nature **427**, 821 (2004).

[Yan99] J. Yang and J. Shen, J. Appl. Phys. **85**, 2699 (1999).

[Yu94] G. Yu, K. Pakbaz, and A. J. Heeger, Appl. Phys. Lett. **64**, 3422 (1994).

[Zel88] Y. B. Zeldovich, A. L. Buchachenko, and E. L. Frankevich, Sov. Phys. Usp. **31**, 385 (1988).

[Zyu95] T. Zyung and J. J. Kim, Appl. Phys. Lett. **67**, 3420 (1995).

List of publications and conference contributions

Publications

- **U. Niedermeier**, M. Vieth, R. Pätzold, W. Sarfert, and H. von Seggern
  Enhancement of organic magnetoresistance by electrical conditioning
  Appl. Phys. Lett. **92**, 193309 (2008).

- **U. Niedermeier**, W. Sarfert, and H. von Seggern
  Influence of a magnetic field on the device performance of OLEDs
  Proc. of SPIE Vol. **6999**, 699913 (2008).

- S. Bagnich, **U. Niedermeier**, C. Melzer, W. Sarfert, and H. von Seggern
  Origin of magnetic field effect enhancement by electrical stress in organic light emitting diodes
  J. Appl. Phys. **105**, 123706 (2009).

- S. Bagnich, **U. Niedermeier**, C. Melzer, W. Sarfert, and H. von Seggern
  Electron-hole pair mechanism for the magnetic field effect in organic light emitting diodes based on poly(paraphenylene vinylene)
  J. Appl. Phys. **106**, 113702 (2009).

- **U. Niedermeier**, S. Bagnich, C. Melzer, W. Sarfert, and H. von Seggern
  Tuning of organic magnetoresistance by reversible modification of the active material
  Synth. Met., doi: 10.1016/j.synthmet.2009.06.012, in press (2009).

Conference contributions

- **U. Niedermeier**, M. Vieth, W. Sarfert, M. Rührig, R. Pätzold, and H. von Seggern
  Magnetoresistance in organic semiconductors
  DPG Spring Meeting 2007, Regensburg/Germany

- **U. Niedermeier**, W. Sarfert, and H. von Seggern
  Magnetic field effects on charge carriers in OLEDs
  DPG Spring Meeting 2008, Berlin/Germany

- **U. Niedermeier**, R. Pätzold, W. Sarfert, and H. von Seggern
  Influence of a magnetic field on the device performance of OLEDs
  SPIE Photonics Europe 2008, Strasbourg/France

- **U. Niedermeier**, W. Sarfert, S. Bagnich, C. Melzer, and H. von Seggern
  Enhancement of organic magnetoresistance through device conditioning
  SPINOS 2009, Salt Lake City/USA

- S. Bagnich, C. Melzer, **U. Niedermeier**, W. Sarfert, and H. von Seggern
  Mechanism of magnetoconductivity in OLEDs based on a PPV derivative
  SPINOS 2009, Salt Lake City/USA

- **U. Niedermeier**, W. Sarfert, S. Bagnich, C. Melzer, and H. von Seggern
  Enhanced magnetoresistance in organic light emitting diodes
  DPG Spring Meeting 2009, Dresden/Germany

Acknowledgements

At the end of my thesis I would like to thank all the people who supported me at Technische Universität Darmstadt and at Siemens AG, Corporate Technology (CT MM 1) in Erlangen over the course of the past three years.

- First of all, I would like to express my gratitude to **Prof. Dr. Heinz von Seggern** for being my academic supervisor and for giving me the opportunity to become an external member of his workgroup. I appreciate the time he spent on discussions about my results and on the review of my thesis. His constructive feedback with valuable suggestions led to a great improvement of this thesis.

- I would like to thank **Prof. Dr. Lambert Alff** who kindly agreed to review this thesis and to write the co-report.

- I am very much indebted to **PD Dr. Sergey Bagnich** who greatly supported me in many ways. He helped me overcome several experimental and theoretical issues and was available whenever I had questions. Throughout my thesis I benefitted a lot from the cooperation with him.

- **Dr. Christian Melzer** is greatly acknowledged for valuable discussions and for the careful and competent proofreading of previous publications and of this thesis.

- Many thanks go to all **members of the electronic materials research group** at TU Darmstadt for the nice atmosphere during my visits. **Katja Stegmaier** is especially acknowledged for her time and efforts before and during my TSC measurements.

- Within the Siemens AG my gratitude first of all goes to the project leaders **Dr. Ralph Pätzold**, **Dr. Wiebke Sarfert** and **Dr. Gotthard Rieger** who have consecutively been in charge of the research project on organic magnetoresistance. They gave me the opportunity to work on this very challenging topic and provided me with great support during the course of my entire thesis.

- I am very grateful to **Sabine Herder** for her immense help with device processing and to **Dr. Joachim Bangert**, **Michael Vieth** and **Frank Ulsenheimer** for valuable discussions about technical issues of experimental setups.

- Furthermore, I would like to thank all my previous and current officemates and colleagues **Chien-Shu Chiu**, **Dana Habich**, **Frank Steinbacher**, **Riikka Suhonen**, **Dan Taroata**, **Jan Hauke Wemken**, **Dr. Christoph Gärditz**, **Dr. Fryderyk Kozlowsky**, **Dr. Ralf Krause**, **Dr. Stefan Seidel** and **Dr. Oliver Weiss** for the pleasant working atmosphere.

- For the photo-CELIV measurements and valuable discussions on the results I would like to thank **Prof. Dr. Dieter Neher**, **Dr. Frank Jaiser** and **Dr. Sebastian Bange** from Universität Potsdam.

- Many thanks go to **Jörg Frischeisen** from Universität Augsburg for proofreading my thesis.

- Finally, I am greatly indebted to my **parents** for their support and their encouragement during the time of my thesis.

Curriculum Vitae

Personal data

Name: Ulrich Niedermeier
Date of birth: January 12, 1980
Place of birth: Landshut

University education

Since 10/2006	PhD thesis at **Technische Universität Darmstadt** Department of Materials Science Advisor: Prof. Dr. Heinz von Seggern Experimental work performed at **Siemens AG, CT MM 1, Erlangen** Topic: "Magnetic field effect in organic light emitting diodes"
07/2005 - 09/2006	Diploma thesis at **Universität Regensburg** Institute of Experimental and Applied Physics Advisor: Prof. Dr. Werner Wegscheider Topic: "Optical investigation of spin polarization in semiconductor heterostructures"
09/2003 - 06/2004	Study abroad at **Wesleyan University, Middletown, CT (USA)**
10/2000 - 09/2006	Studies of Physics at **Universität Regensburg** Degree: Dipl.-Phys.

Military service

07/1999 - 04/2000	Air Force, Pfullendorf and Rottenburg/Laaber

School education

09/1990 - 06/1999	High School, Straubing Degree: Abitur

Erklärung zur Dissertation

Hiermit versichere ich, die vorliegende Dissertation selbständig und nur mit den angegebenen Quellen und Hilfsmitteln angefertigt zu haben. Alle Stellen, die aus Quellen entnommen wurden, sind als solche kenntlich gemacht. Ich habe keinen vorhergehenden Promotionsversuch unternommen.

Darmstadt, den 08. Oktober 2009

_____

(U. Niedermeier)